Doctoral Thesis

Rheological control and characterization of crosslinked polymer networks

Tae Hee Lee

Department of Chemical Engineering

Graduate School of UNIST

2019

Rheological control and characterization of crosslinked polymer networks

Tae Hee Lee

Department of Chemical Engineering

Graduate School of UNIST

Rheological control and characterization of crosslinked polymer networks

A dissertation
submitted to the Graduate School of UNIST
in partial fulfillment of the
requirements for the degree of
Doctor of Philosophy

Tae Hee Lee

6. 14. 2019
Approved by

Advisor
Chunggi Baig

Rheological control and characterization of crosslinked polymer networks

Tae Hee Lee

This certifies that the thesis/dissertation of Tae Hee Lee is approved.

06/14/2019

Signature

Advisor: Chunggi Baig

signature

Hyunhyub Ko

signature

So Youn Kim

signature

Seung Man Noh

signature

Hyun Wook Jung

Abstract

Crosslinked polymer networks have applications in the coating, paints, and adhesive industries to protect the substrate and endow the specific functional properties on surface, as well as in biomedical applications, wearable sensors, and lithium ion batteries, thus the control of corsslinking is a very important research area.

The control of crosslinking also plays a crucial role in the maintenance of pipelines and chemical tanks. The majority of chemical spill accidents are caused by leaks from chemical transfer pipes or tanks, so the periodic maintenance of chemical facilities is vital. If cracks are found in transfer or storage units during such inspections, they must be blocked rapidly by using an emergency crack recovery process in order to prevent the further spread of toxic chemicals. The appropriate crosslinking mechanism should be selected for this purpose.

The diverse reaction pathways and mechanisms of thiol-X ‘click’ chemistry have received extensive attention from physicists, biologists, chemists, and chemical, biomedical, electrical, and mechanical engineers because of their convenience and wide range of applications. In particular, the rates of crosslinking reactions can easily be controlled by using thiol-X click chemistry. Therefore, this chemistry offers a basic mechanism for the use of temporary restoration materials in hazardous chemical control.

In this thesis, I used a visualization technique to monitor the reaction kinetics of thiol-epoxy polymer networks (TEPNs). In order to track the variations in pH during the thiol-epoxy click reactions, a small amount of the pH indicator thymol blue was added to the TEPN formulations. Secondly, I designed a dual-stimuli-responsive self-reporting coating that can sense both crack occurrence and pH variation in chemical reservoir coatings. Finally, I developed a novel UV-curable patch system with high chemical resistance and adhesion properties for the rapid blocking of cracks in chemical reservoirs.

Contents

List of Figures

[Chapter 1]

Figure 4. Variations with reaction time in the FT-IR spectra of the TEPNs at room temperature: (a) SH3-TEPN, (b) SH4-TEPN, and (c) SH6-TEPN. The data were collected at regular time intervals (180 s) after sample preparation and loading (150 s).

Figure 5. Isothermal DSC analyses for the thiol-epoxy click reactions of the TEPNs as functions of time at room temperature. The initial stages of the thiol-epoxy reactions up to 300 s (at the red dashed line) were not recorded because of sample preparation and the loading time. The dotted lines are predictions based on the auto-catalysis effect.

Figure 6. Thermal and viscoelastic properties of films of the TEPNs: (a) variations in G' with temperature, (b) plots of the calculated loss factors versus temperature obtained with DMA measurements, (c) heat flow curves, and (d) first derivative heat flow curves obtained from DSC measurements.

Figure 7. Tensile stress versus tensile strain plots for the TEPNs.

[Chapter 3]

Figure 1. Self-reporting mechanism of DSRTET coatings.

Figure 2. Schematic diagram and chemical structure of materials used in this study.

Figure 3. Effect of agitation rate on diameter and size distribution of the microcapsule: (a) size distribution, (b) mean diameter, and (c) optical microscope images of the synthesized microcapsules.

Figure 4. Confirmation of the microcapsule formation: (a) FT-IR spectra of core material, UF/PU shell,

and synthesized microcapsule and (b) optical microscope images of the undamaged and ruptured microcapsules obtained under white or UV light sources.

Figure 5. Curing behaviors of the DSRTETs: (a) time versus storage modulus plot of DSRTETs measured using the oscillatory rheometer and (b) time versus frequency plot of DSRTETs obtained from the RPT measurement.

Figure 6. The result of nano-indentation test of DSRTET coatings: (a) Load-displacement curve and (b) changes in HIT and EIT values according to microcapsule contents.

Figure 7. Tensile stress versus tensile strain plots for the DSRTET coatings.

Figure 8. Effect of microcapsule content on the crack sensitivity of DSRTET coatings subjected to step-wise-increasing deforming load from 250 mN to 1000 mN: (a) optical microscope image of the cracked surface of DSRTET coatings under UV light (365 nm) and (b) penetration depths profiles as a function of lateral position of a line of the DSRTET coatings.

Figure 9. Color transition of DSRTET coatings in response to acid or base solutions: (a) optical microscope images of DSRTET coatings and (b) the color transitions of the DSRTET coatings in CIE 1931 color space before/after solution drop test.

Figure 10. Application of the DSRTET coatings to the laboratory scale chemical reservoirs: (a) illustration of chemical reservoir design and dual stimuli responsive self-reporting mechanism and (b) actual crack test.

[Chapter 4]

Scheme 1. a) The synthesis of AESO-PSAs from renewable sources and b) the UV-radical initiators used in this study.

Figure 1. Schematic overview of the UV-curable crack repair patch system.

Figure 2. ^{1}H-NMR spectra of (a) acrylated epoxidized soybean oil (AESO), (b) epoxidized soybean oil (ESO) and (c) soybean oil (SO).

Figure 3. The FT-IR spectra of (a) AESO and (b) AESO-PSA1.

Figure 4. a) Variation in FT-IR C=C band of AESO-PSA1 as a function of UV curing time b) time versus conversion curve of UV curing reaction of AESO-PSA1.

Figure 5. a) Schematic diagram of a photo-curable device in an oscillatory rheometer; b) photograph of UV photo-curing within an oscillatory rheometer.

Figure 6. a) Schematic illustration of the lap shear test; b) photographs of a lap shear test specimen in the UTM.

Figure 7. Calculation of the pressure and force on a cracked area due to dichloromethane. The velocity of the flow through the cracked area was estimated with the Bernoulli equation.

Figure 8. Curing behaviors of the AESOs measured with an oscillatory rheometer: a) epoxy-amine curing behaviors of the AESO-PSAs at 80 ℃ and b) the UV-curing behaviors of the PC-PSAs.

Figure 9. Thermal properties of the AESOs: TGA pyrograms of a) the AESO-PSAs and b) the PC-PSAs,

and DSC thermograms of c) the AESO-PSAs and PC-PSAs.

Figure 10. Adhesion properties and viscoelastic responses of the AESO-PSAs: a) peel and tack strengths, b) frequency versus storage modulus plots, c) frequency versus loss modulus plots, and d) frequency versus tan δ plots.

Figure 11. Strength versus strain curves for the PC-PSAs and AESO-PSAs.

Figure 12. The variation with patch size in crack repair performance.

Figure 13. Application of repair patches to cracks in the surface of a laboratory scale chemical tank (contained chemical: chloroform).

List of Table

Chapter 1. Introduction

1.1.Motivation and background of this research

The properties of crosslinked polymer networks are significantly affected by the conditions of the crosslinking reactions used to generate them, such as the reaction rate, temperature, and degree of conversion. Therefore, with the aim of generating networks with storage moduli suitable for various applications (e.g., coatings, paints, adhesives, and sensors), my studies have concentrated on controlling the crosslinking behavior. In particular, I have focused on low temperature rapid crosslinking of reactive polymers that change from liquid to solid state. The findings of this research can be used to develop fast curing adhesives and protective coatings.

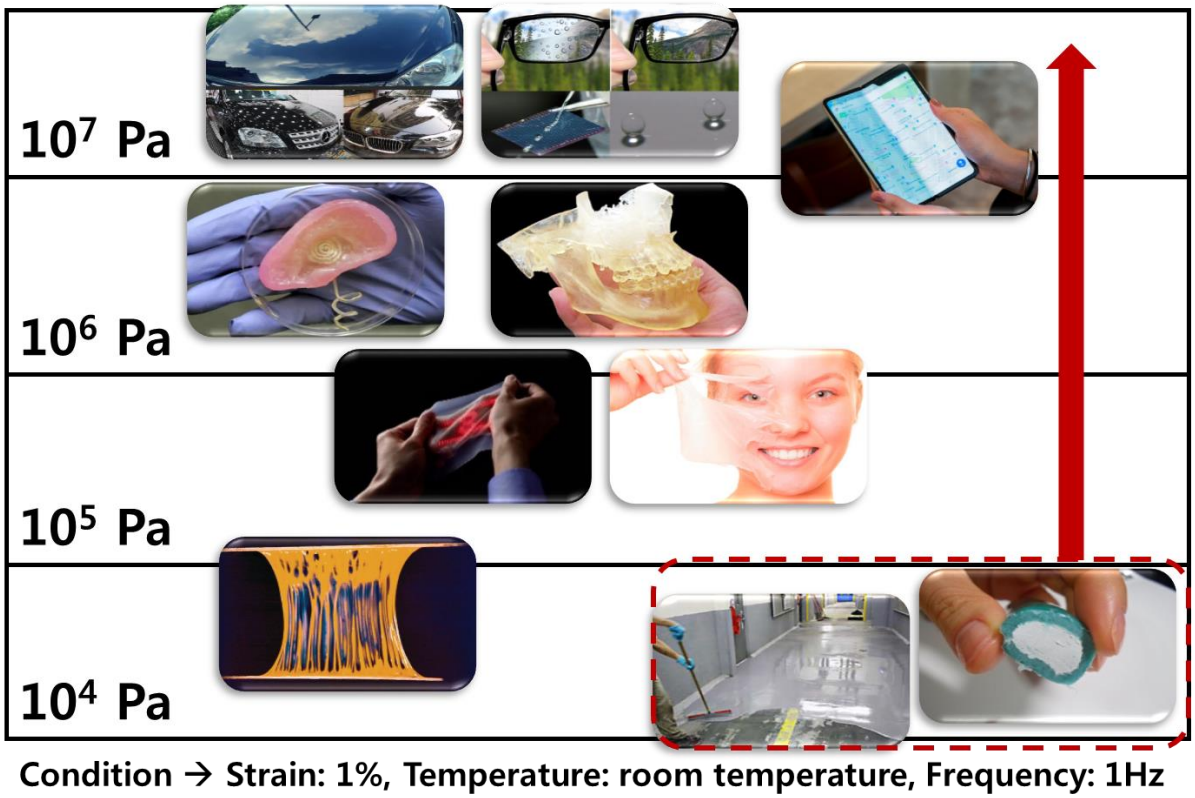

Figure 1. The usage of crosslinked polymer network according to storage modulus

Recently, accidents of toxic chemical spills are increasingly affecting large-scale and have a fatal impact of human ecosystem as shown in **Figure 2.** Developed countries devote to develop the technology that can cope with the toxic chemical spill within the golden time from the moment of recognition. Henkel, Germany, develops and supplies epoxy compounds in the Loctite series that can quickly cover cracks and leaks in metal and nonferrous metal materials. Devcon has developed and supplied a fast-curing epoxy putty approved by the U.S. Department of Defense for various emergency repairs. The heavy chemical industry accounts for a high proportion of industrial activity in Korea, and most of the infrastructure for this industry was built in the 1980s. As can be seen in **Figure 3**, the rate of accidents at these facilities has increased in the last 10 years as the infrastructure has aged.

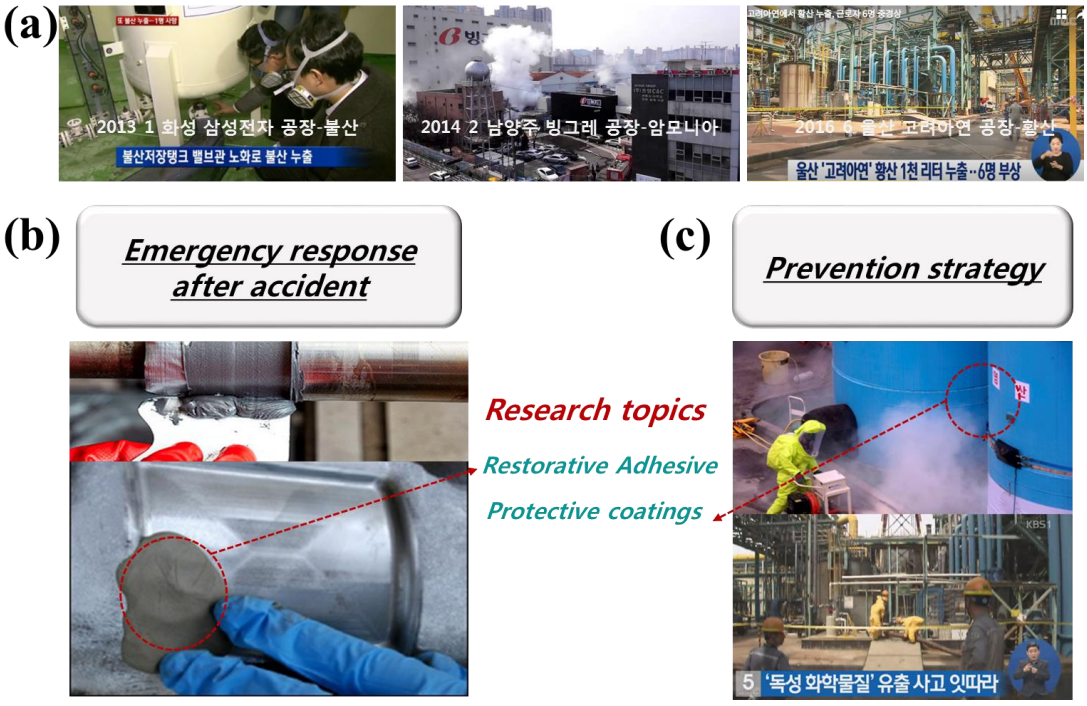

Figure 2. (a) Recently occurred chemical accidents (b) Temporary restorative materials (c) protective coatings

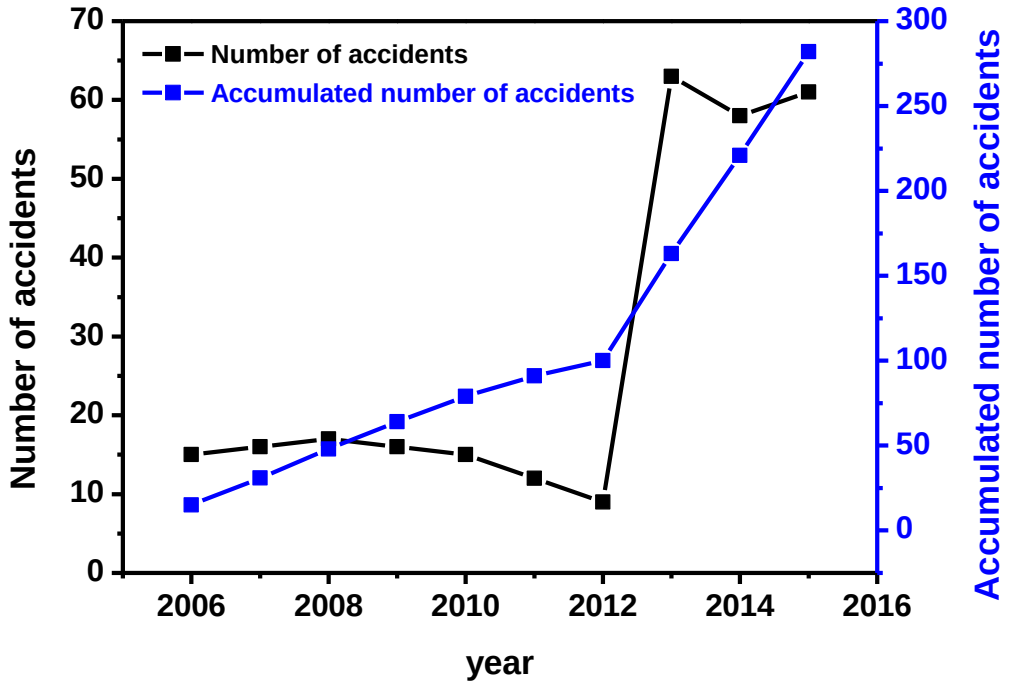

Figure 3. The number of accidents and accumulated number of accidents by years

In Korea, putty technology for emergency repair that exhibits rapid curing and chemical resistance against various hazardous chemical leaks has not yet been developed. An unsaturated polyester-based quick-drying putty capable of managing cracks or leaks in wood and cement, as well as repairing some damage to automotive steel sheets and steel sheets, has been developed and used in limited circumstances. However, the chemical resistance and durability of this putty are insufficient for managing chemical reservoir spills.

The development of temporary restorative materials that use new chemical reactions to address such spills is essential. I propose here a novel restorative material with a smart curing mechanism that can provide both rapid reactivity and storage stability. This material offers significant improvements over currently used temporary restorative materials. In addition, in order to prevent chemical accidents, a dual stimulus responsive coating was developed. This coating can changes color in response to physical stimuli through aggregation induced emission (AIE) phenomena and chemical stimuli through the pH-indicator thymol blue. Finally, to overcome the limitations in practical applications of previously developed temporary restorative materials, we developed a UV-photo curable pressure sensitive adhesive using chemically modified soybean oil.

1.1.1. Thiol-X 'Click' reactions

Thiol-X 'click' reactions have been used in various applications such as synthesis, polymerization, and functionalization. Thiols react in high yields under mild conditions with various other chemical functional groups, as shown in **Figure 4**.

Thiols are commonly referred to as mercaptans because of their original role in the scavenging of mercury and have been used in a wide range of chemical and material processes because of their high reactivity. Thiols are considered soft nucleophiles compared to their amine and alcohol counterparts because of their combination of inherent electron density and d-orbitals. Thiyl radicals and thiolate anions are more nucleophilic and thus have been used in a wide range of processes under benign conditions to produce high yields.

One of the most important features of thiol-X click chemistry is the facile control of its reactions. As a result, these click reactions are utilized across all of the basic disciplines of science and engineering. The thiol-X reaction was thus selected as an appropriate mechanism for the development of temporary restorative materials [1-3].

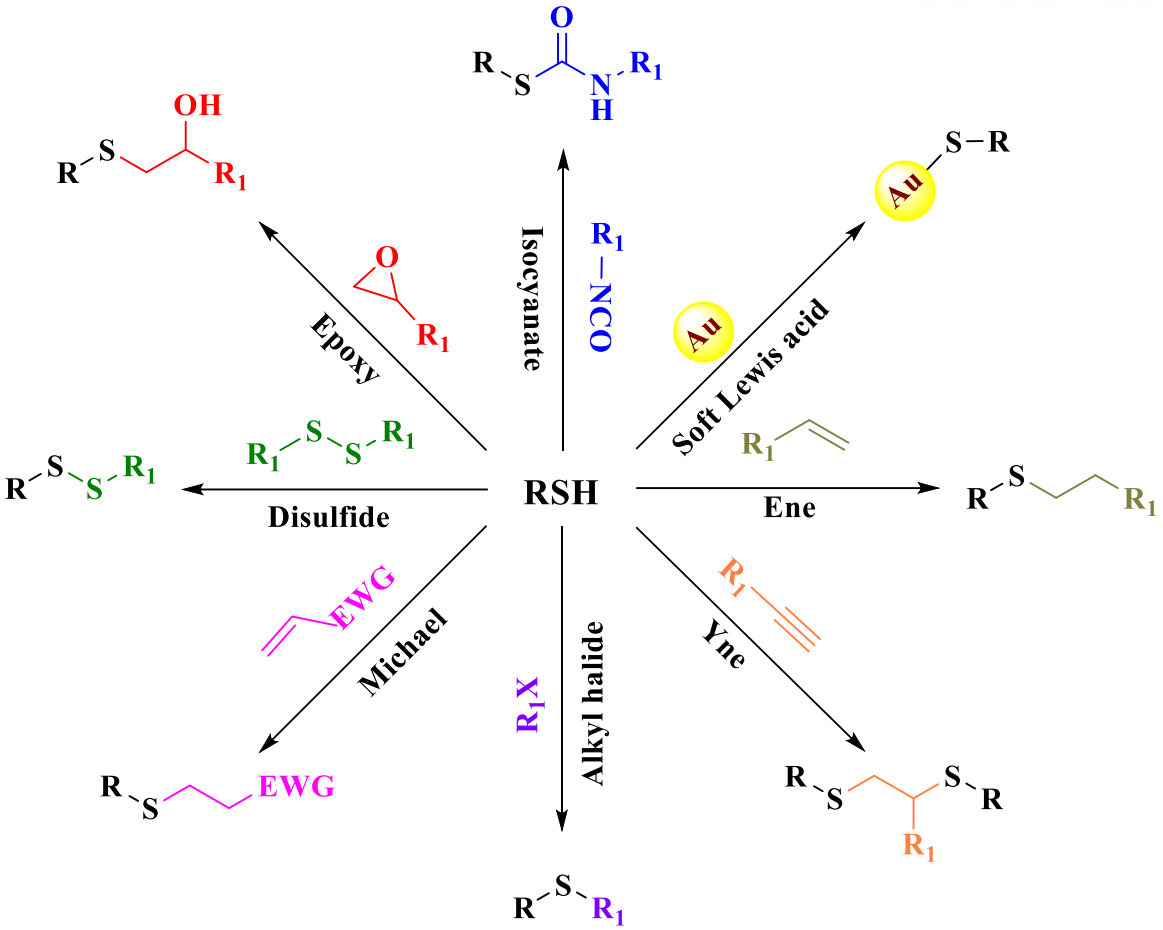

Figure 4. Various thiol-X click reactions (EWG = electron-withdrawing group; X = Br, I, and R_1 = aliphatic or aromatic organic groups).

1.1.2. Dual-crosslinking reactions

Dual-crosslinking reactions can be activated by stimuli such as UV irradiation and temperature, or through the control of reaction kinetics. Dual crosslinking is a methodology for obtaining polymer networks that combines two different and compatible crosslinking reactions that take place simultaneously or sequentially. Sequential dual crosslinking enables the preparation of an intermediate material arising from the first stage of crosslinking that, upon application of a second stimulus, can be further crosslinked to achieve an interpenetrating polymer network (IPN) that exhibits properties superior to those of the individual components.

In a dual-crosslinking polymer network system, the intermediate material can range from a viscoelastic liquid to a lightly crosslinked rubber or glassy crosslinked network and should have well-defined rheological, mechanical, and thermal properties. These intermediate materials become the desired polymer network after the second crosslinking. Therefore, careful consideration of the chemical structure, the composition of the monomer, the type of chemical reaction, and the stimulus conditions is required. Click-type reactions are especially suitable for dual crosslinking because of their selectivity, efficiency, and orthogonality [4-6].

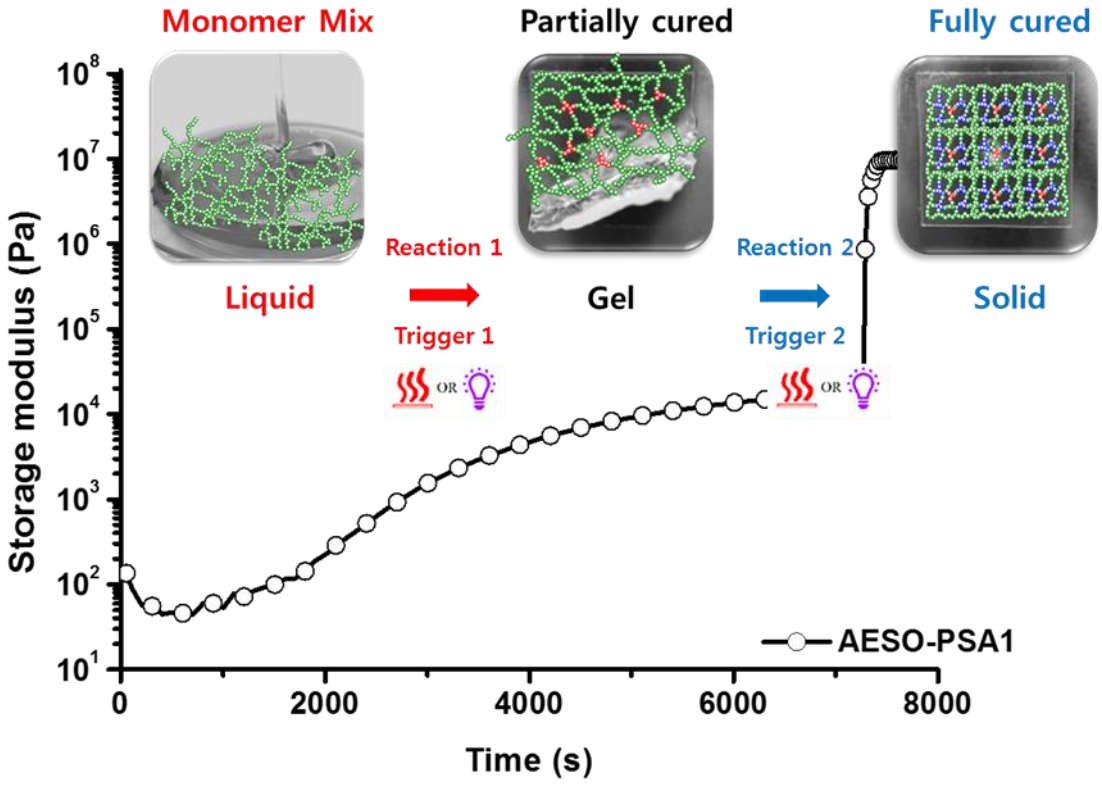

Figure 5. Schematic diagram of the sequential dual crosslinking of a polymer network system.

1.2.Objective of this thesis

In this thesis, various types of temporary restorative adhesives and coatings were developed and tested. The characterization of the crosslinking kinetics and mechanical properties of these systems was conducted with rheology, mechanical testing (RPT, UTM, NST, NI), DSC, DMA, and FT-IR. In addition, the developed materials were tested on laboratory scale chemical reservoirs in order to assess their potential uses.

In the first stage of this research, the kinetics of the crosslinking reactions of the model thiol-epoxy polymer networks (TEPNs) were visualized by tracking pH variation.as shown in **Figure 6.** The color transitions of the TEPNs were monitored in real-time and the results were correlated with those of Fourier transform infrared (FT-IR) spectroscopy, isothermal differential scanning calorimetry (DSC), and oscillatory rheology. The influences of the glass transition temperatures (T_g) of the TEPNs on the kinetics of the low temperature crosslinking reactions were investigated by employing various TEPNs with different crosslinker functionalities. The mechanical and chemical properties of the TEPNs were also determined, and the trends in the data were related to the crosslinking densities (ν_c) calculated from dynamic mechanical analysis (DMA) measurements.

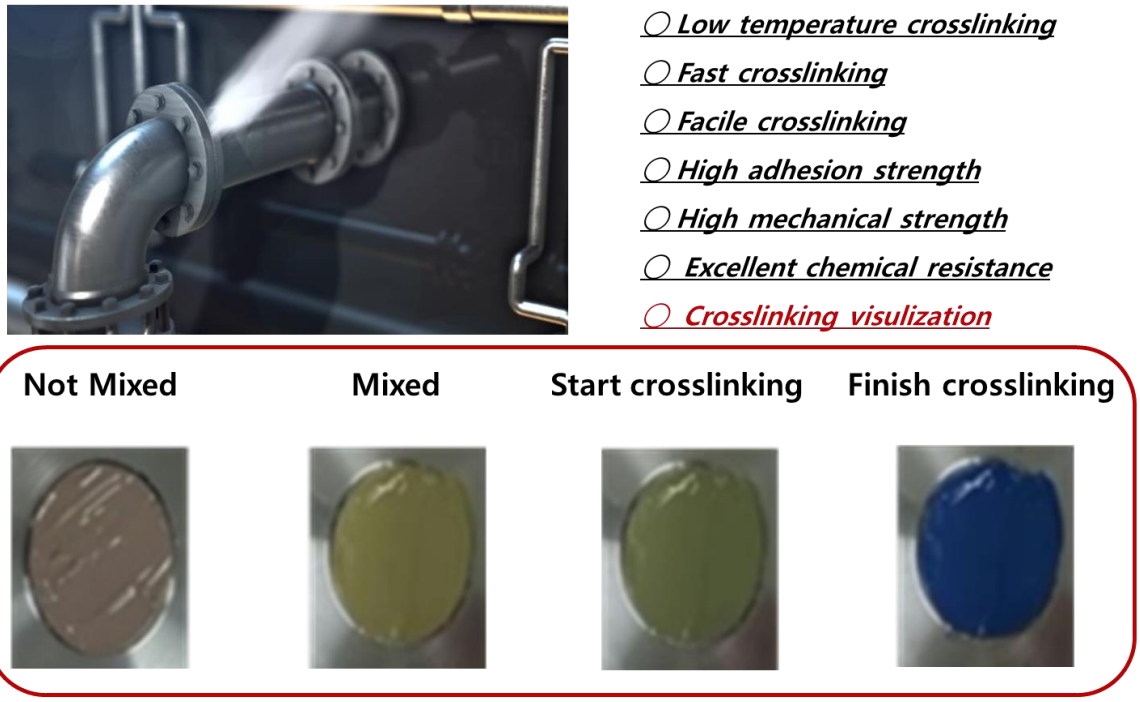

Figure 6. The concept summary of temporary restorative material that can visualize the crosslinking behaviors

In the second section of this thesis, I introduce a novel dual-stimuli-responsive self-reporting thiol-epoxy thermoset (DSRTET) coating that can detect both crack occurrence and pH variation. For crack detection, a microcapsule containing tetraphenylethylene (TPE) that exhibits the aggregation induced emission (AIE) effect was prepared via multi-step emulsion polymerization and dispersed in the DSRTET coatings. For pH variation detection, commercial thymol blue was added as a pH indicator into the polymer matrix. The effects of the microcapsules in the DSRTET coatings on their curing behavior, material properties, and crack sensitivity were characterized by using oscillatory rheology, the rigid body pendulum test (RPT), nanoindentation (NI), a universal test machine (UTM), and a scratch tester. It was found that the crack sensitivity of the DSRTET coatings is greatly influenced by their material properties as well as their microcapsule contents. The color transitions in the DSRTET coatings in response to acid or base solutions were quantitatively investigated by using a multi-angle spectrophotometer after simple acid and base solution drop tests. The color of the DSRTET coatings changes from a pale green to red for acidic solutions and to blue for basic solutions. Finally, the DSRTET selected according to the results of this study was applied to laboratory scale chemical reservoirs in order to assess its potential as a dual-stimuli-responsive self-reporting coating that can detect both cracks in coating materials and chemical spills caused by the leakage or breakage of reservoir components. **(Figure 7.)**

○ *High mechanical strength*

○ *Excellent chemical resistance*

○ *Mechanical damage reporting*

○ *Chemical damage reporting*

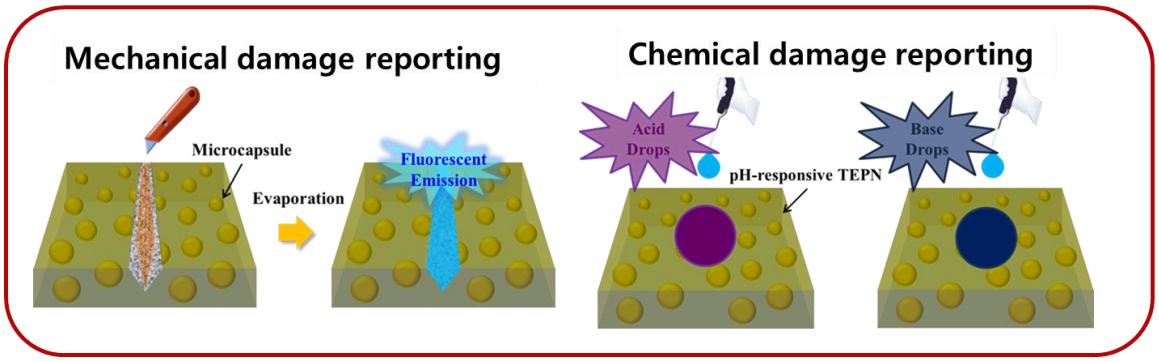

Figure 7. The concept summary of dual stimuli responsive coating that simultaneously respond to physical and chemical stimuli

In the last section, I present a novel UV-curable emergency patch system that can be used to repair the cracked surfaces of chemical reservoirs. When a crack occurs in a chemical reservoir, the patch can be quickly attached to the damaged area, and then cured with a portable UV source in order to prevent the further spread of toxic chemicals. Crosslinked acrylated epoxidized soy bean oil (AESO) materials with various compositions and crosslinking densities were prepared by reacting AESO with the triethylenetetramine (TETA) crosslinker and tested as UV-curable pressure sensitive adhesives (PSAs). The optimum curing behavior and adhesion performance of the UV-curable patch system were found by using various analytical methods, namely oscillatory rheology, and peel, tack strength, and tensile tests. Finally, an optimized patch was applied to a laboratory scale chemical reservoir in order to assess its performance as a UV-curable crack repairing patch system for the prevention of chemical spills from cracked reservoirs. **(Figure 8.)**

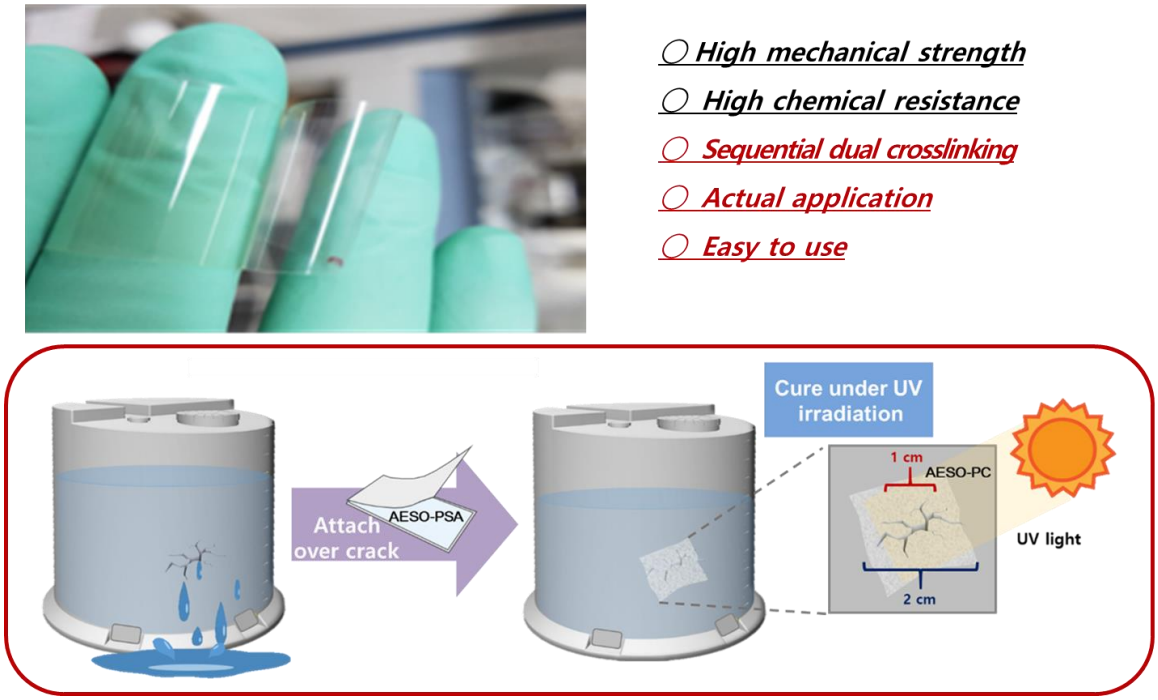

Figure 8. The concept summary of dual curable pressure sensitive adhesive that can be sequentially crosslinked by UV-light

1.3.Methods for the characterization of polymer networks

1.3.1. Oscillational rheometer

The crosslinking kinetics of the polymer network was correlated with its rheological properties as measured with an oscillational rheometer. As previously reported [4, 5, 7-9], it has been confirmed that rheological measurements offer well-correlated and reliable information that can be used to determine the in situ crosslinking kinetics of polymeric materials. Such results are in good agreement with those of other related techniques, e.g., differential thermal calorimetry [9-10] and real time FT-IR [9, 11]. A schematic diagram of the oscillational rheometer equipped with a UV/thermal dual-crosslinking system that played a key role in this research is shown in **Figure 9.**

The material functions for small amplitude oscillatory shear (SAOS) are the storage modulus $G^{'}(w)$ and the loss modulus $G^{''}(w)$; $G^{'}(w)$ and $G^{''}(w)$ are material functions of viscoelastic fluids that denote the energy storage and viscous dissipation respectively under an oscillatory shear strain, $\gamma_{21} = \gamma_0 \sin wt$. The numbers 1 and 2 in the subscript of the strain denote the x and y directions respectively.

$$\text{SAOS material functions: } \frac{-\tau_{21}}{\gamma_0} = G^{'} \sin wt + G^{''} \cos wt \quad \text{(eq. 1)}$$

$$\text{Storage modulus: } G^{'}(w) \equiv \frac{\tau_0}{\gamma_0} cos\delta \quad \text{(eq. 2)}$$

$$\text{Loss modulus: } G^{''}(w) \equiv \frac{\tau_0}{\gamma_0} sin\delta \quad \text{(eq. 3)}$$

For a Newtonian fluid in SAOS, the response is completely in phase with the strain rate: $G^{'} = 0$ and $G^{''} = \mu w$. For an elastic solid (Hookean solid) that follows Hooke's law, the shear-stress response in SAOS is completely in phase with the strain, i.e. $G^{'} = G$ and $G^{''} = 0$. The stress responses of viscoelastic fluids exhibit phase lags in the range $0° < \delta < 90°$.

The rheological properties measured under different crosslinking conditions quantitatively reflect the evolution of the polymer network structure. The modulus of the crosslinked polymer network are directly responsible for understanding the role of process, formulations, and controlling the final material properties.

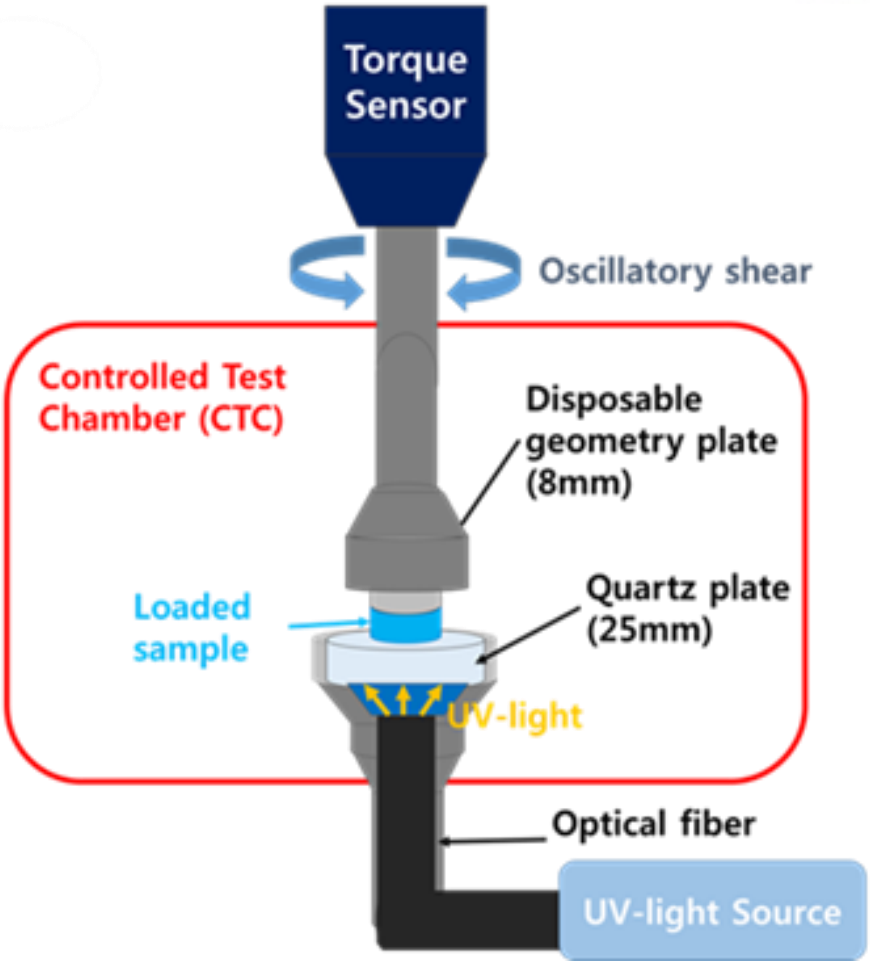

Figure 9. Schematic diagram of a UV/thermal oscillational rheometer.

1.3.2. Rigid-body pendulum test (RPT)

The rigid-body pendulum test (RPT) can be used to characterize the crosslinking and polymerization kinetics of organic coatings and thin films [4, 5, 9, 12]. A schematic diagram and the main features of RPT are shown in **Figure 10.** An aluminum plate is attached to the temperature control block and the edge of the pendulum is immersed in the coating sample. The pendulum is attached to an electro-magnet that provides the potential energy that is converted into the kinetic energy of swing motion. When the power to the electromagnet is cut off, the pendulum starts to swing. The motion sensor then measures the period and amplitude of the pendulum, and the free oscillating pattern is converted to the logarithmic damping ratio.

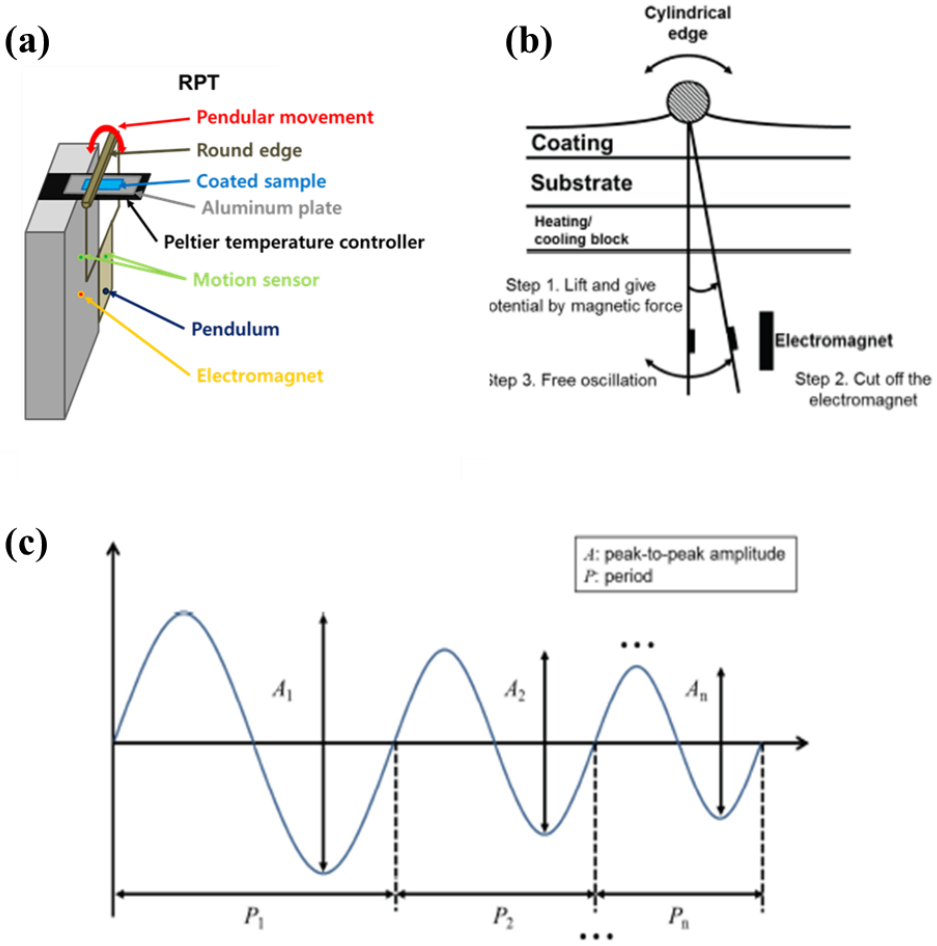

Figure 10. (a) Schematic diagram of the RPT 2000W; (b) principles of the rigid body pendulum test; (c) the wave function of the pendulum during a test.

1.3.3. Fourier transform infrared (FT-IR) spectroscopy

Fourier transform infrared spectroscopy (FT-IR) can be used to obtain the infrared absorption and emission spectra of a solid, liquid, or gas. We used FT-IR to examine the chemical structures of samples before, during, and after the crosslinking. Spectral data over a wide range of wavelengths were collected simultaneously during the crosslinking reactions with an FT-IR spectrometer. For example, in order to monitor the thiol-epoxy click reaction we recorded the intensities of the characteristic peaks of the hydroxyl group (-OH, 3300 cm-1), the thiol group (-SH, 2560 cm-1), and the epoxy group (C-O-C, 915 cm-1), and compared them to the intensity of the peak due to aromatic double bonds(C=C, 1608 cm-1)

1.3.4. Differential scanning calorimetery (DSC)

Differential scanning calorimetry (DSC) is a thermoanalytical technique that detects the exothermic/endothermic reactions of a sample by simultaneously heating/cooling the sample and reference pan. The temperatures of the furnace are controlled equally together but the temperature of the sample is different from that of the reference. We can use the difference in temperature which was converted to heat flux. The heat flux can be used for analysis of polymer thermodynamical properties.

DSC can be performed either with the power compensation method or the heat flux method. In this experiment, I carried out heat flux DSC. A schematic diagram of the procedure for heat flux DSC is shown in **Figure 11**. The results of these DSC experiments are curves of heat flux versus temperature. **Figure 12** shows a DSC curve typical of polymeric materials.

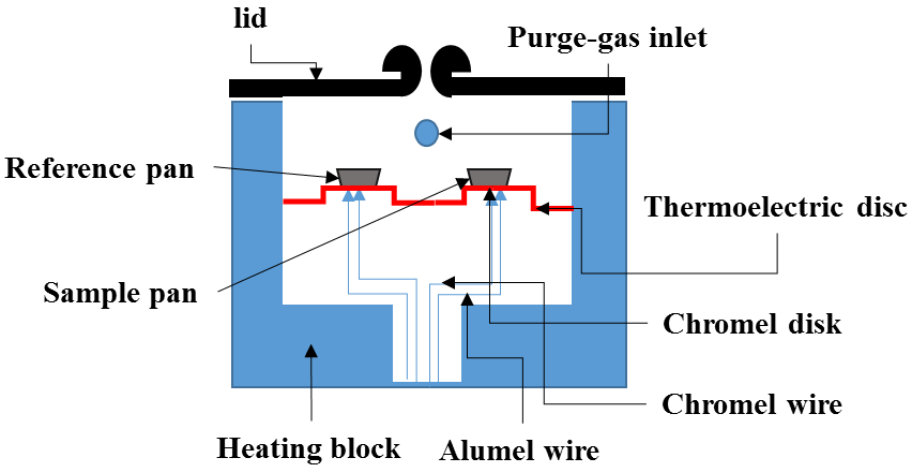

Figure 11. Schematic diagram of the heat flux DSC set-up.

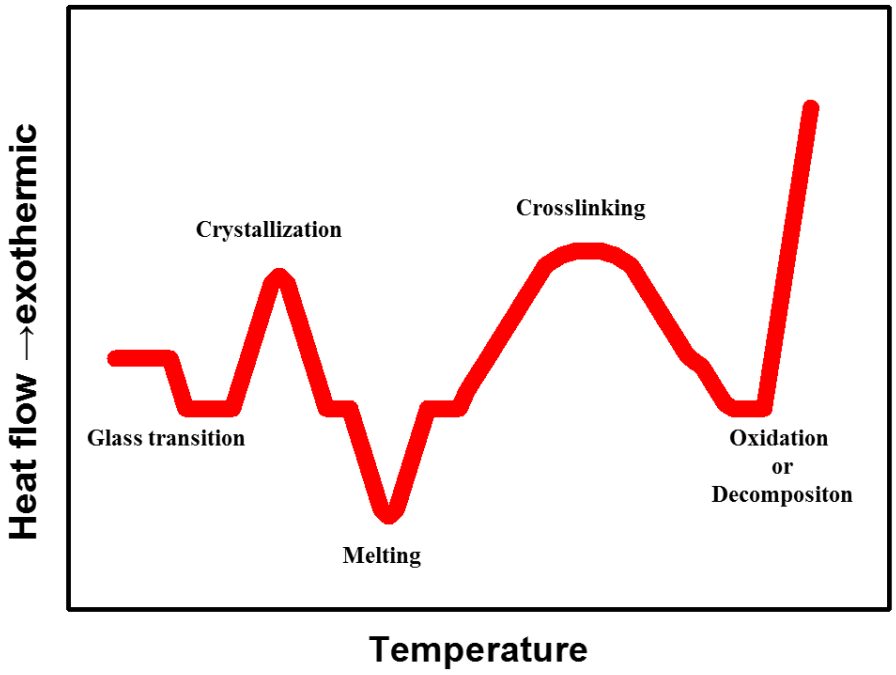

Figure 12. A DSC curve typical of polymeric materials.

1.3.5. Dynamic mechanical analysis (DMA)

Dynamic mechanical analysis (DMA) can be used to evaluate the thermal and mechanical properties of polymeric materials as functions of factors such as temperature, time, and frequency. The most commonly measured property for simple elastic materials is the stiffness or Young's modulus. However, more complex viscoelastic materials such as polymers and composites cannot be characterized with this value alone. The most commonly used test protocol for measuring viscoelastic properties is small amplitude oscillation. In this group of methods, the sample is deformed according to a sinusoidal deformation profile at a fixed frequency and amplitude (strain) while the force with which the sample resists deformation (stress) is measured, as shown in **Figure 13**(b). Oscillatory experiments are often used in conjunction with temperature profiles to characterize thermal events such as glass transitions, melting, crystallization, and curing. At small test amplitudes, the viscoelastic properties are independent of the strain. This region of deformation, known as the linear viscoelastic regime, most directly reflects molecular structure and is predictive of overall product performance. For some materials, this linear viscoelastic regime can be quite small, especially in the case of filled or crosslinked networks. For this reason, the control of very small deformations is critical to obtaining meaningful, reproducible, and actionable results.

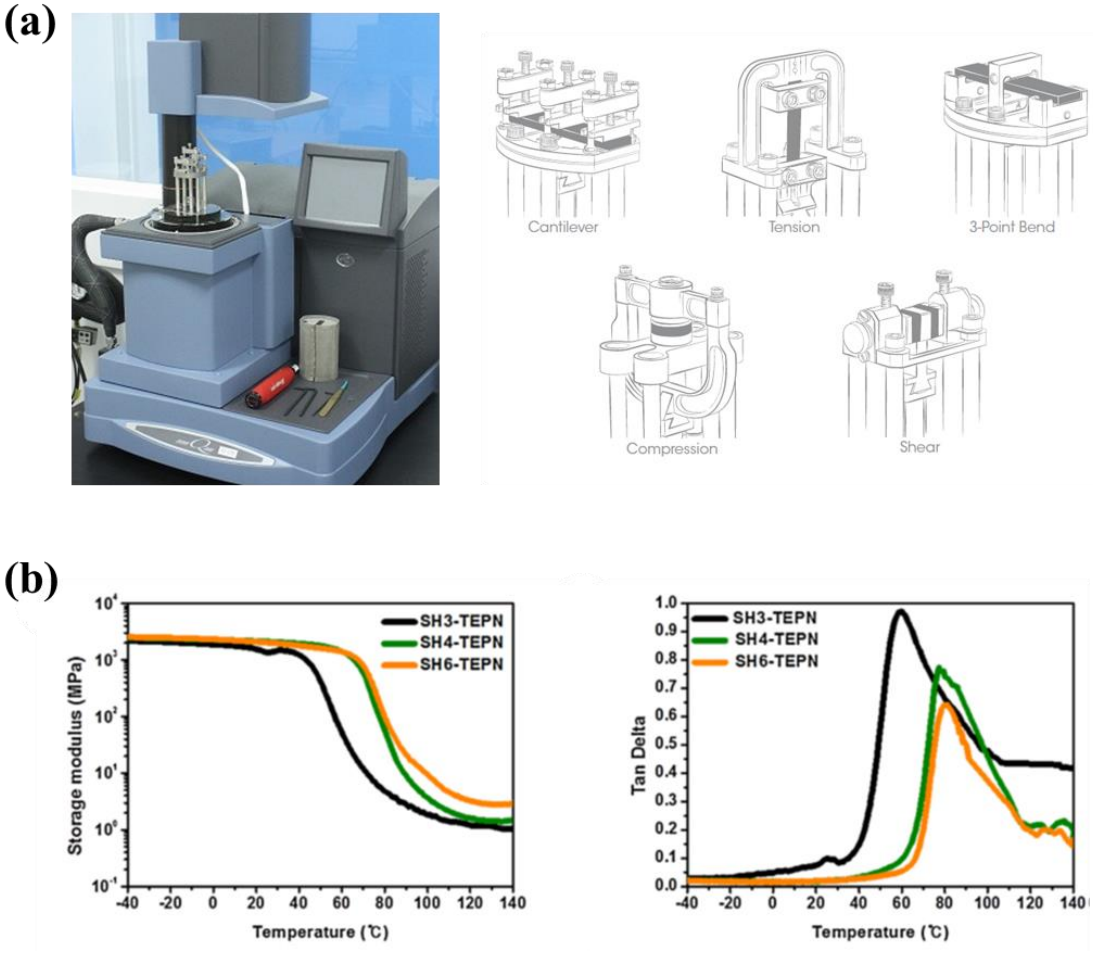

Figure 13. (a) Dynamic mechanical analysis (DMA, TA Instruments, U.S.A.) and the accessories required for various modes; (b) typical DMA curves for crosslinked polymer networks.

1.3.6. Universal testing machine (UTM)

A universal testing machine (UTM) is used to evaluate the tensile strength, lap shear strength, peel strength, and compressive strength of materials, and is the most commonly used equipment for measuring the mechanical properties of elastic or viscoelastic solids such as the stiffness or Young's modulus, *E*. The set-up and usage are detailed in a test method, often published by a standards organization. This method specifies the sample preparation, fixturing, gauge length (the length which is under study or observation), analysis, etc., as shown in **Figure 14**(a).

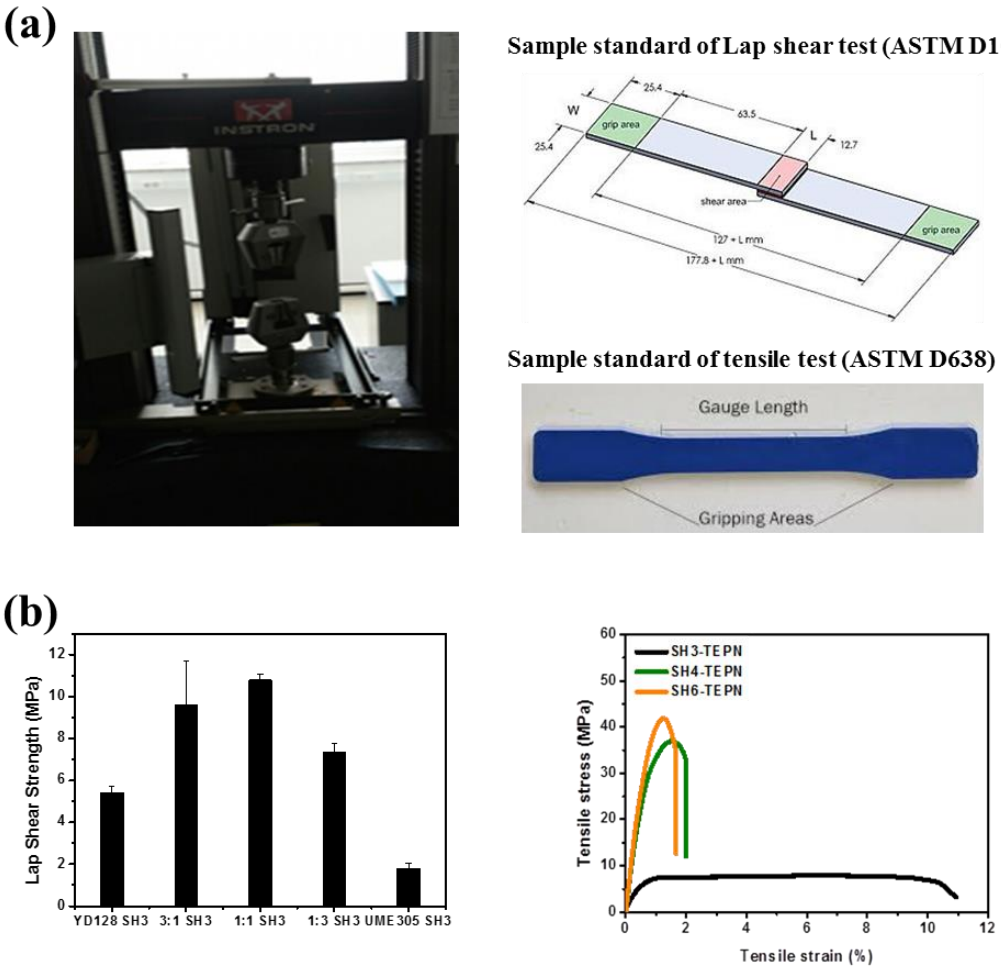

Figure 14. (a) Universal testing machine (UTM, Instron, U.S.A.) and test sample preparation standard; (b) typical UTM data for crosslinked polymer networks.

1.3.7. Nano indentation (NI)

Many materials exhibit different mechanical strengths and properties in their vertical and lateral displacements due to their internal structures [13-15]. Nanoindentation (NI) involves pressing an indenter of known geometry into the material surface while both penetration depth and normal load are monitored. The indentation hardness (HIT), elastic modulus (EIT), and other mechanical properties are then obtained from the load-displacement curve; typical indentation load-displacement data are depicted in **Figure 16.**

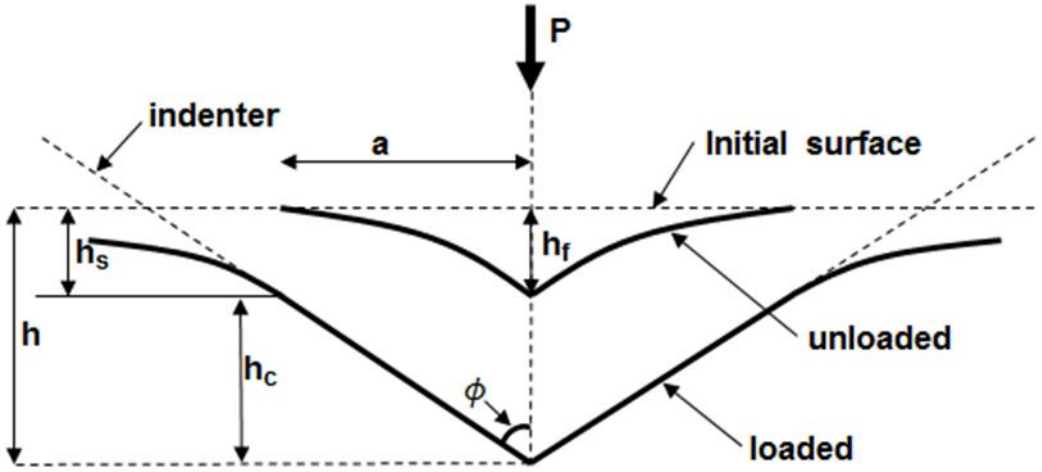

Figure 15. Schematic illustration of the unloading process showing the parameters characterizing the contact geometry.

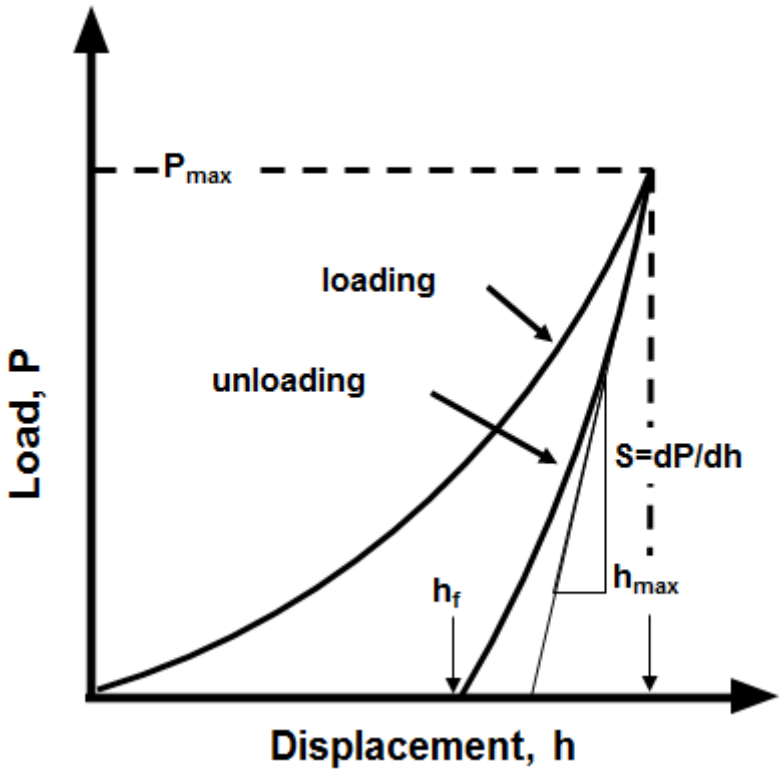

Figure 16. Schematic illustration of indentation load-displacement data showing the important measured parameters.

1.3.8. Nano scratch test (NST)

Nanoscratch testing (NST) is used to evaluate the mechanical resistance of a thin film or coating by imposing a progressive or stepwise deformation load on the film surface [13-15]. The ability of the scratch tester to characterize film-substrate systems and to quantify parameters such as the friction force and the adhesive strength with a variety of complementary methods makes it an invaluable tool for research, development, and quality control. This technique involves generating a controlled scratch with a diamond tip on the sample. The tip is drawn across the coated surface under constant, incremental, or progressive load. At a certain load, the coating will start to fail. Critical loads are very precisely detected by means of the tangential force, the penetration depth, and the acoustic emission sensors together with observations from a built-in optical microscope. **Figure 17**(c) shows the progressive deformation of a polymeric coating to measure its scratch resistance.

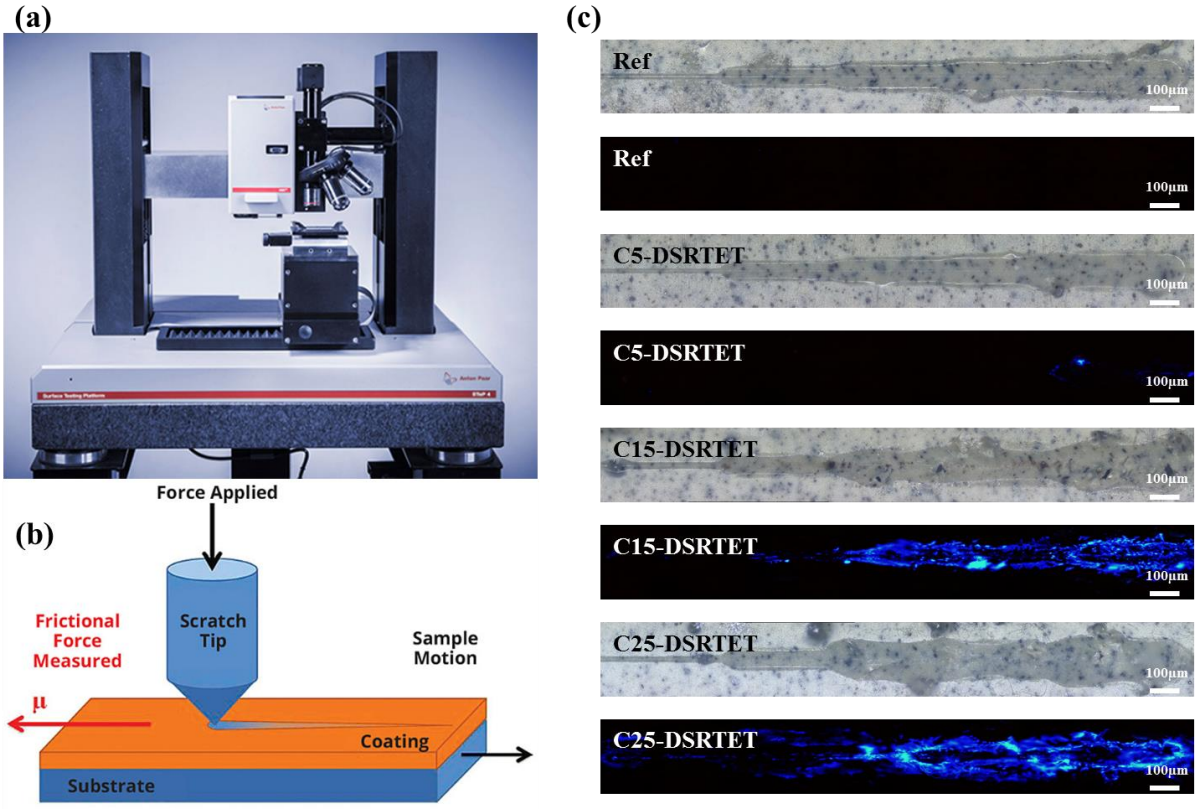

Figure 17. (a) Nanoscratch tester (NST^3, Anton Paar, Switzerland); (b) schematic diagram of a nanoscratch tester; (c) optical microscopy images obtained in progressive scratch mode.

1.4. REFERENCES

[1] C. E. Hoyle, A. B. Lowe, C. N. Bowman. Chem. Soc. Rev. 39 (2010) 1355.

[2] A. O. Kounuray, A. Ruiz, J. M. Morancho, J. M. Salla, X. F. Francos, À. Serra, X. Ramis. European Polymer Journal. 98 (2018) 39.

[3] R. K. Iha, K. L. Wooley, A. M. Nyström, D. J. Burke, M. J. Kade, C. J. Hawker. Chem. Rev. 109 (2009) 5620.

[4] S. M. Noh, J. W. Lee, J. H. Nam, K. H. Byun, J. M. Park, H. W. Jung. Prog. Org. Coat. 74 (2012) 257.

[5] J.W. Hwang, K.N. Kim, G.S. Lee, J.H. Nam, S.M. Noh, H.W. Jung. Prog. Org. Coat. 76 (2013) 1666.

[6] A.O. Konuray, F. Liendo, X.F. Francos, À. Serra, M. Sangermano, X. Ramis. Polymer. 113 (2017) 193..

[7] B. S. Chiou, R. J. English, S. A. Khan. Macromolecules. 29 (1996) 5368.

[8] B. S. Chiou, S. A. Khan. Macromolecules. 30 (1997) 7322.

[9] T.H. Lee, Y.I. Park, S.M. Noh, J.C. Kim. Prog. Org. Coat. 104 (2017) 20.

[10] K. Jin, W.H. Heath, J.M. Torkelson. Polymer. 81 (2015) 70.

[11] C. Decker, K. Moussa. Macromol. Chem. Phys. 191 (1990) 963..

[12] T. Ishimura, R. Lu, K. Yamasaki, T. Miyakoshi. Prog. Org. Coat. 62 (2008) 193.

[13] T. H. Lee, Y. K. Song, S. H. Park, Y. I. Park, S. M. Noh, J. C. Kim. Appl. Surf. Sci. 434 (2018) 1327.

[14] S. Y. Kim, T. H. Lee, Y. I. Park, J. H. Nam, S. M. Noh, I. W. Cheong, J. C. Kim. Polymer. 128 (2017) 135.

[15] S. M. Noh, J. W. Lee, J. H. Nam, J. M. Park, H. W. Jung. Prog. Org. Coat. 74 (2012) 192.

Chapter 2. In-situ visualization of the kinetics of low temperature thiol-epoxy crosslinking reactions by using a pH-responsive epoxy resin

2.1. Introduction

Thiol-epoxy click chemistry has frequently been employed to prepare thiol-epoxy polymer networks (TEPNs) for applications associated with high performance coatings and adhesives because of its rapid reaction rate at low temperatures, high degree of conversion, and multiple cross-linking pathways including nucleophilic thiol reactions such as base-catalyzed thiol-isocyanate, thiol-epoxy, and thiol-Michael addition reactions, and radical-mediated thiol reactions such as photo-initiated thiol-ene and thiol-yne reactions [1-3].

Recently, several novel TEPN systems have been reported such as hyper-branched networks, hydrogels, and hybrid networks, as well as dual curing and latent curing processes [4-13]. In these systems, control of both the cross-linking densities (v_c) and the reaction kinetics of TEPNs is recognized as the key factor determining the performance of the final products because these parameters influence processability, coating quality, thermal and mechanical properties, and chemical resistance [14-21]. In general, durable epoxy thermosets require high v_c; the facile strategies frequently used to meet this target are the employment of various types of high functionality cross-linkers and/or increasing the degree of conversion through control of the reaction temperature [22-24]. However, in some special applications, such as fast curing coatings and adhesives, low temperature curing systems that can operate near or under room temperature are required. In this case, the use of high functionality cross-linkers must be very cautious for the following reasons. First of all, there is a possibility that the degree of conversion of the curing reaction will be greatly influenced by polymer chain restriction effects since the glass transition temperatures of TEPNs in the later stages of their curing reactions are usually much higher than those at the curing temperature [25-26]. In addition, as is the case for other epoxy curing

reactions, thiol-epoxy click reactions exhibit auto-catalysis effects and the rate of the cross-linking reaction is affected by the type of the cross-linker [27]. For this reason, characterizations of both the reaction kinetics and the viscoelastic properties are very important to the design of suitable low temperature thiol-epoxy curing materials.

Several measurement techniques such as differential scanning calorimetry (DSC), Fourier transform infrared (FT-IR) spectroscopy, and Raman spectroscopy have been used to characterize the kinetics of thiol-epoxy click reactions but these methods have some drawbacks [28-31]. For example, the sample preparation and temperature control required by the DSC method before starting the measurements take considerable time. Since thiol-epoxy curing reactions are very fast even at low temperatures, the initial reaction kinetics data are usually lost when conventional DSC is used. FT-IR and Raman spectroscopy often fail to find the characteristic peaks of thiol and epoxy groups if the epoxy formulation is complex. Considerable sample preparation time is also needed in these approaches. For this reason, the development of a new analysis technique for the characterization of the reaction kinetics of thiol-epoxy curing reactions is required.

One feasible candidate is a technique for the visualization of reaction kinetics that tracks pH changes during cross-linking [32]. In general, the pH of a thiol-epoxy click reaction in the presence of a tertiary amine catalyst increases as cross-linking proceeds. If the appropriate pH indicator is employed, the reaction kinetics can be visualized as color transitions. This method has the advantage over other characterization methods that it provides simple, immediate, and in-situ visible characterization of the reaction kinetics without the loss of the initial data. In addition, no expensive equipment is required, and it can be used in both laboratory and outdoor environments.

Herein, we report our detailed testing of this visualization technique on the reaction kinetics of TEPNs. In order to track the variations in the pH during the thiol-epoxy click reactions, a small amount of the

pH indicator thymol blue was added to the TEPN formulations. Various TEPNs were prepared from multi-functional cross-linkers with different functionalities, and the color transitions during their cross-linking reactions were monitored in real-time. The experimental color transition data were compared with results obtained with the oscillation rheology, isothermal DSC, and FT-IR spectroscopy characterization techniques. The T_g and v_c values of the room temperature cured TEPNs were determined with dynamic mechanical analyzer (DMA) and DSC measurements in order to assess the chain mobility restriction effects on the reaction kinetics. In addition, mechanical and chemical resistance tests were also conducted.

2.2. Experimental

2.2.1. Materials.

Trimethylol-propane tri(3-mercaptopropionate) (TMPMP, SH3), pentaerythritol tetra(3-mercaptopropionate) (PETMP, SH4), and dipentaerythritol hexa(3-mercaptopropionate) (Di-PETMP, SH6) were purchased from Bruno Bock Thiochemicals. Diglycidyl ether bisphenol A based epoxy resin (D.E.R.) with an equivalent weight of 190-205 g eq^{-1} was obtained from Kukdo Chemical Co. 2,4,6-Tris(dimethylaminomethyl)phenol (DMP30), titanium (II) oxide (TiO_2), fumed silica (F-SiO_2), and thymol blue were purchased from Sigma-Aldrich.

2.2.2. Sample preparation.

The epoxy resin component was prepared by mixing 71.98 grams of D.E.R., 4.03 grams of thymol blue (3 wt % of the total weight of the TEPN), 19.2 grams of TiO_2 and 4.8 grams of F-SiO_2 with a planetary mixer (KM Tech, PLM-1K) at 1200 rpm for 2 hours. Polymercaptan hardeners were activated by dissolving 0.1 mol% DMP30/thiol with a high speed overhead stirrer (Ocean Science, DISPERMAT)

at 2000 rpm for 30 mins. The TEPNs were cross-linked by reacting stoichiometric amounts of epoxy groups with the thiol groups. Detailed formulations are listed in **Table 1.**

Table 1. Formulations of the TEPNs.

Polymer code	Resin Part			
	YD-128SH	TiO_2	Fumed Silica	Thymol Blue
SH3-TEPN	71.98g	19.19g	4.80g	4.03g
SH4-TEPN	72.05g	19.21g	4.80g	3.94g
SH6-TEPN	71.98g	19.19g	4.80g	4.03g

Polymer code	Hardener Part			
	SH3	SH4	SH6	DMP
SH3-TEPN	93.77g	-	-	6.23g
SH4-TEPN	-	93.26g	-	6.74g
SH6-TEPN	-	-	93.66g	6.34g

2.2.3. Characterizations

2.2.3.1. Characterizations of the Reaction Kinetics and Viscoelastic Properties during Curing.

The reactions of the epoxy groups in the polymer resins with the thiol groups in the cross-linkers were confirmed by using an FT-IR spectrometer (Thermo Fisher Scientific Inc., Nicolet 6700/Nicolet Continuum). The reaction kinetics of the TEPNs was investigated by performing isothermal DSC measurements (TA Instruments, DSC Q2000) at room temperature (25℃) under a nitrogen atmosphere. The viscoelastic properties of the TEPNs during the cross-linking reactions were characterized with a rotational rheometer (Thermo Scientific Inc., MARS III) operated at a constant frequency (1 rad s^{-1}) and strain (0.5%) at room temperature (25℃). The color transition measurements during curing were obtained in real-time by using both a video recorder and a multi-angle spectrophotometer (StellarNet, Inc., X-Rite MA98).

2.2.3.2. Characterizations of the Material Properties.

The thermal stabilities of the TEPNs were determined by carrying out TGA (TA Instruments, TGA Q500) in the range 25 – 700℃ at a rate of 10℃ min^{-1}. The T_g values of the cross-linked TEPN films were determined with DSC (TA Instruments, DSC Q2000) from the first heating ramp at 10°C/min in the range 0–100°C. The viscoelastic properties of the cured TEPNs were determined by performing DMA measurements (TA Instrument, DMA Q800) in the strain-controlled mode (5 μm) at a frequency of 2 Hz. The data were recorded by heating the samples at 10°C/min from -40 –to 140°C. The dimensions of the specimens were 60 mm x 12 mm x 3 mm. The v_c values of the TEPNs and the loss

factors (tan δ = G”/G’) were calculated from the tensile storage modulus (G’) and loss modulus (G’’) data. Tensile tests of the TEPNs were carried out by using a Universal Testing Machine (UTM) (Instron, model 5982) with constant force (5 mm/ min^{-1}) at a cross-head. The dimensions of the specimens were 60 mm× 12 mm x 3 mm. Chemical resistance tests were conducted in various chemical environments. The cured epoxy resins were cut into small pieces and kept in 100 mL amber bottles containing the aforementioned media at ambient temperature (25℃). The percentage of weight loss (eq. 1) was measured after 24 hours [8].

$$\text{Weight Loss } (\%) = \frac{intitial\ weight\ of\ TEPN\ (g) - final\ weight\ of\ TEPN\ (g)}{initial\ weight\ of\ TEPN\ (g)} \quad \text{(eq. 1)}$$

2.3. Results and Discussion

This section is divided into two main subsections. In the first section, the real-time color transitions of the TEPNs during cross-linking are correlated with the results obtained from oscillation rheometer, isothermal DSC, and FT-IR spectroscopy. In the second section, the influences of T_g and v_c on the reaction kinetics of the TEPNs are analyzed and related to experimental color coordinate data and the mechanical and chemical resistance test results. The molecular structures of the materials used in this study are presented in **Figure 1.**

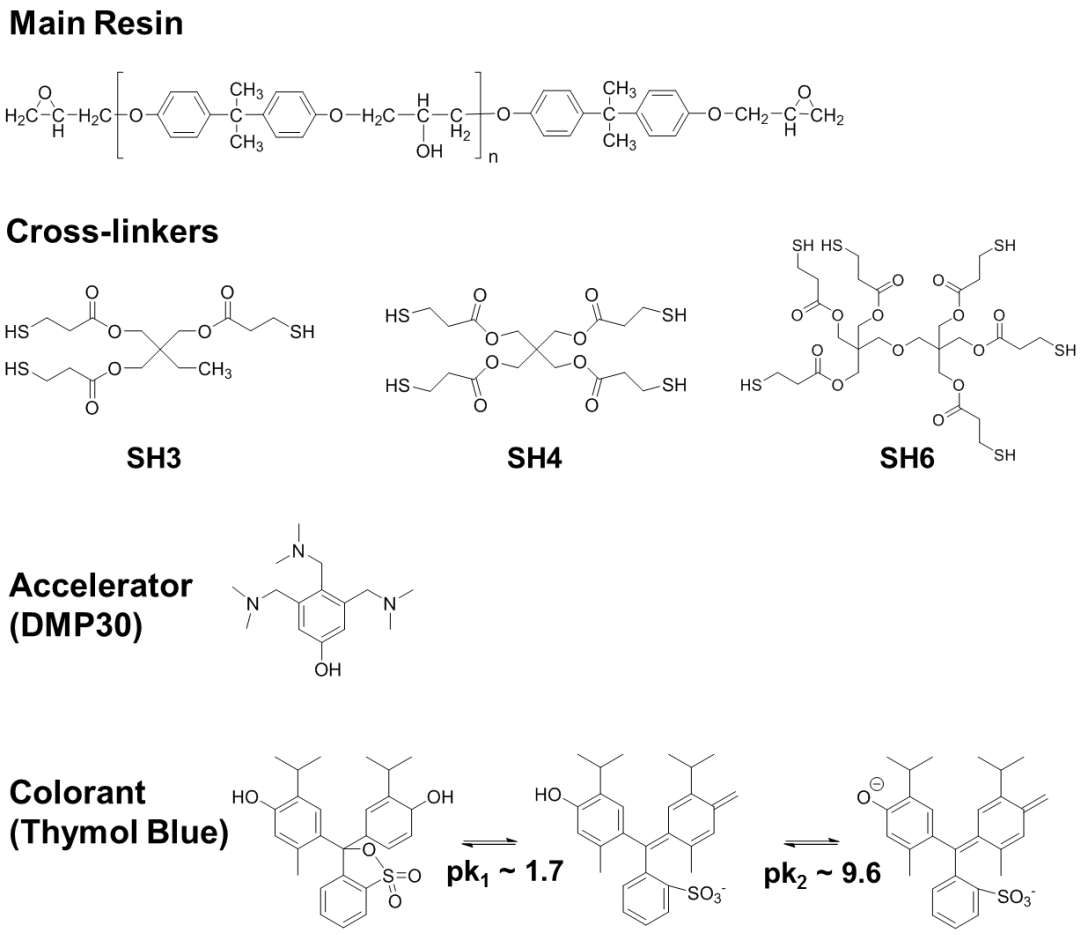

Figure 1. Chemical structures of the materials used in this study.

2.3.1. Mechanism of the Color Transition of the TEPNs.

The proposed color transition mechanism for the thiol-epoxy reactions is shown in **Scheme 1.** The thiol-epoxy coupling reactions of TEPNs are categorized as nucleophilic ring opening reactions and can be catalyzed by organic bases. In the initial stage, the reaction is fully mediated by the base catalyst, which generates thiolate anions, but as the reaction progresses, the secondary alkoxide produced by the epoxy ring opening reaction starts to participate in the thiol-activating process. This process is well known as an auto-catalysis effect of thiol-epoxy reactions [27]. During the auto-catalysis process, the pH of the system continuously increases as the number of free base catalyst molecules that no longer participate in the catalytic reaction increases [32]. In our method, this pH variation during the thiol-epoxy reactions can be tracked by mixing a small amount of the pH indicator thymol blue with the epoxy thermosets, which means that there is a transition in the color of the TEPNs from pink to blue as the crosslinking reactions progress. To control the curing process and range of color transition, the primary amine catalysts were not employed for this study due to their relatively low basicity compared to the tertiary amine catalysts.

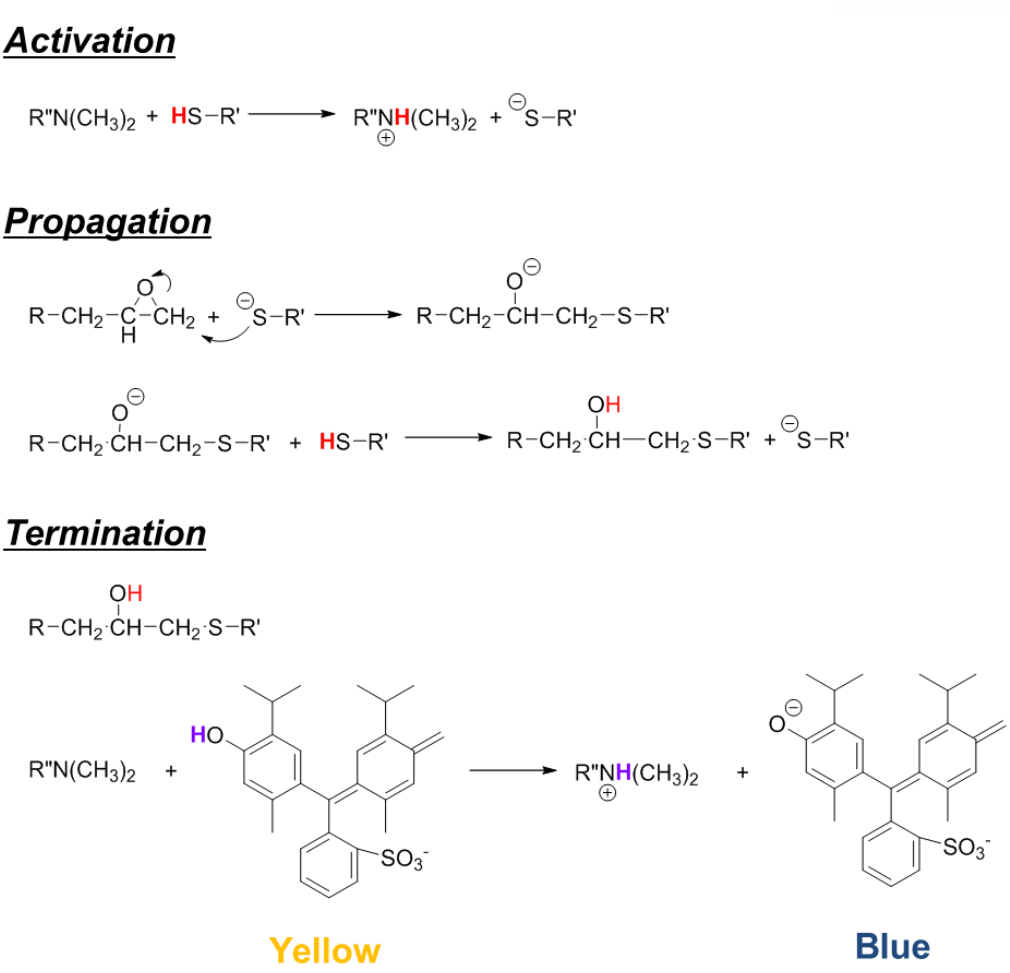

Scheme 1. The proposed mechanism of the color transition of the TEPNs.

2.3.2. Room Temperature Curing Behavior and Color Transitions of the TEPNs.

In order to investigate the curing behavior of the TEPNs, we have plotted the variations with time in the elastic modulus of the three different multi-functional cross-linkers (SH3, SH4 and SH6) under ambient conditions (**Figure 2. (a)**). As can be seen in this figure, G' gradually increases during the initial stages of the reactions but as they proceed there are steep increases in G', which indicate that the TEPNs have formed cross-linked network structures. In addition, the cross-linkers with higher functionality produce a faster increase in G' (SH6-TEPN > SH4-TEPN > SH3-TEPN).

Under the same curing conditions, the colors of the TEPNs were determined at regular time intervals (300 s). As shown in **Figure 2. (b)**, the TEPNs turn from pink to blue as the thiol-epoxy reactions progress. The cross-linkers with higher functionality produce faster color transition rates (SH6-TEPN > SH4-TEPN > SH3-TEPN). In addition, the final colors of the TEPNs are different. SH3-TEPN is deep blue whereas SH6-TEPN is pale blue. As a further investigation, the color transitions of the TEPNs were quantitatively analyzed by using a multi-angle spectrophotometer. **Figures 3. (a) and (b)** show the changes in the CIE values of each TEPN as curing proceeds. The initial color coordinates of the epoxy resin component are (0.33, 0.34). After the resin has been mixed with the cross-linkers, both the x and y values increase as the hydrogen atoms in the cross-linkers are transferred to the ketone groups in thymol blue (the first color transition region). However, as the thiol groups start to react with the epoxy groups, both the x and y values rapidly decrease and the color of the epoxy thermoset shifts from pink to blue, as described above (the second color transition region). The length of each second color transition region is inversely proportional to the curing rate of the TEPN (SH3-TEPN > SH4-TEPN > SH6-TEPN). In the third color transition region, the color changes of the TEPNs become saturated and converge. After the reactions have finished, the final coordinates of SH3-TEPN, SH4-TEPN, and SH6-TEPN are (0.22. 0.26), (0.25, 0.29), and (0.28, 0.31) respectively. The color transitions of the TEPNs are also presented in terms of their DL*, Da*, and Db* values in **Figure 3. (c)**. The dramatic decrease

in Db* arises because the colors of the TEPNs change from pink to blue. As can be seen in **Figure 3. (d)**, the rates of change in Db* of the TEPNs are proportional to the functionality of the cross-linker. On the other hand, the saturated Db* values, which indicate the degrees of conversion of the thiol-epoxy click reactions, are inversely proportional to the functionality of the cross-linker (SH3-TEPN > SH4-TEPN > SH6-TEPN).

The curing and color transition experiments both indicate that the functionality of the cross-linker influences the kinetics of the room temperature thiol-epoxy click reaction. To verify the precision of the experimental color transition results, the isothermal reaction kinetics of the TEPNs was also characterized with the DSC and FT-IR spectroscopy measurement techniques.

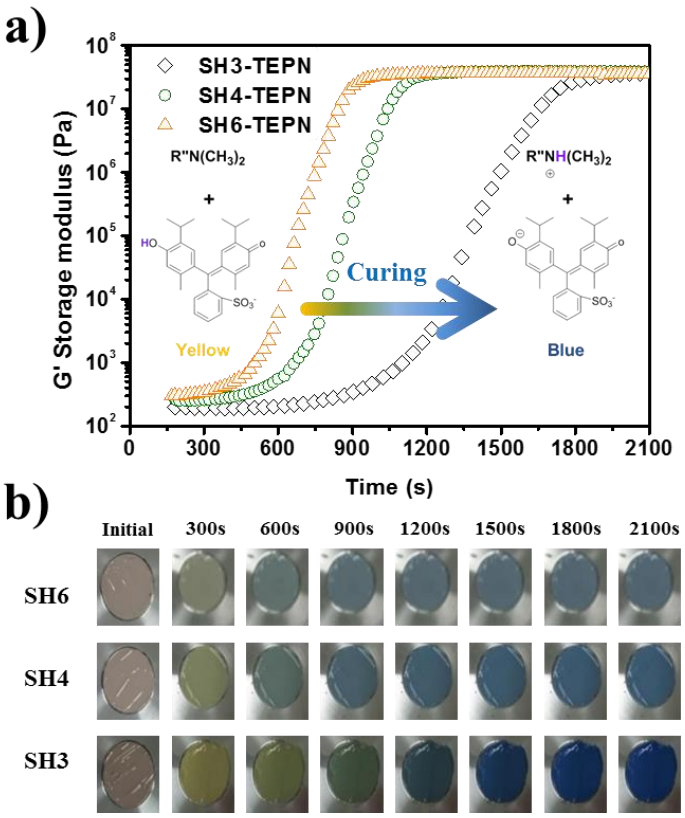

Figure 2. Curing behavior and reaction kinetics of the TEPNs: (a) G' versus time plots; (b) color transitions of the TEPNs at room temperature.

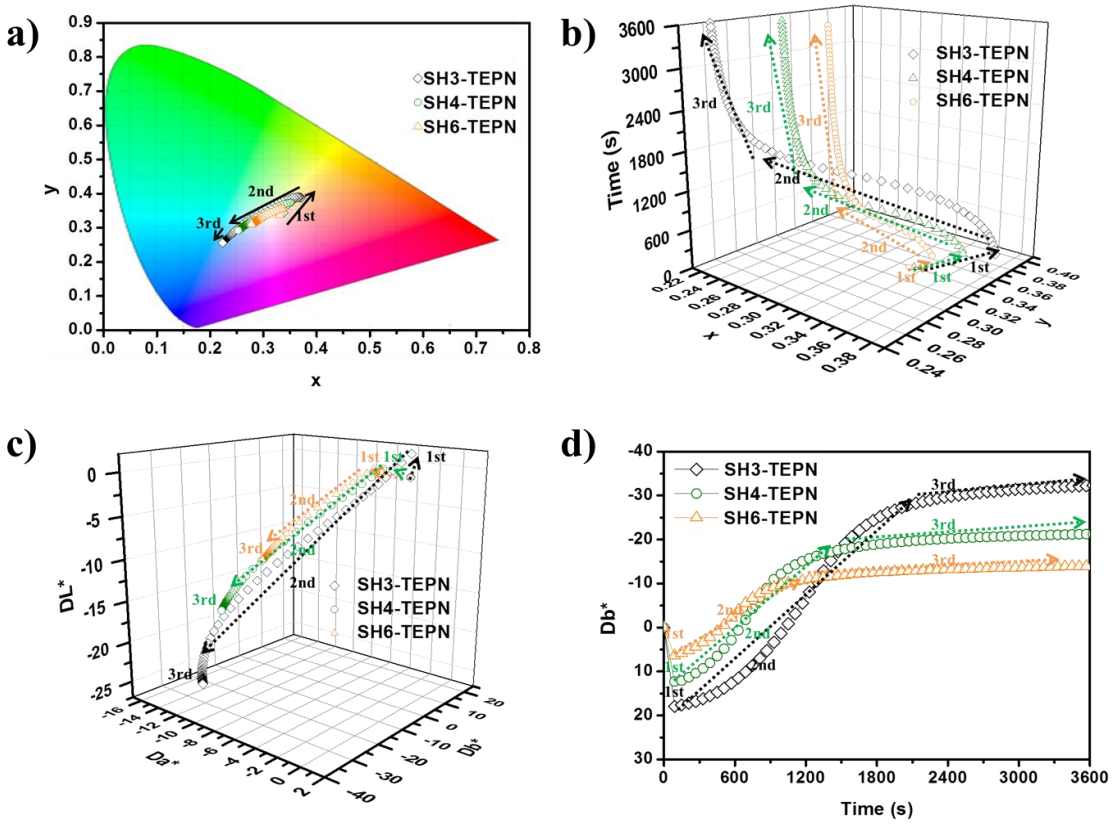

Figure 3. Color coordinate shifts of the TEPNs during curing: (a) the color transitions of the TEPNs in CIE 1931 color space; (b) color transitions in (a) as functions of time; (c) DL*, Da*, and Db* values in 3D space; (d) Db* values as functions of time.

2.3.3. Comparison of the Experimental Color Transition Results with those of Other Characterization Methods.

FT-IR spectroscopy measurements were conducted at room temperature in order to monitor the thiol-epoxy click reactions of the TEPNs. **Figure 4.** shows the variations in the ratios of the intensities of the characteristic peaks of the hydroxyl group (-OH, 3300 cm^{-1}), the thiol group (-SH, 2560 cm^{-1}), and the epoxy group (C-O-C, 915 cm^{-1}) to the intensity of the peak due to aromatic double bonds (C=C, 1608 cm^{-1}) at regular time intervals (180 s) [5,9,21]. As the thiol-epoxy reactions progress, the characteristic peak of hydroxyl groups appears and the intensities of the characteristic peaks due to thiol and epoxy groups decrease. As in the color transition results, the rate of reaction increases as the functionality of the cross-linker increases. The degree of conversion of thiol-epoxy click reaction can be calculated as the ratio of characteristic peak of SH group at 2560 cm^{-1} to C=C group at 1608 cm^{-1}. The degree of conversion of SH3-TEPN, SH4-TEPN, and SH6-TEPN were 55.4%, 45.6% and 40.4% respectively.

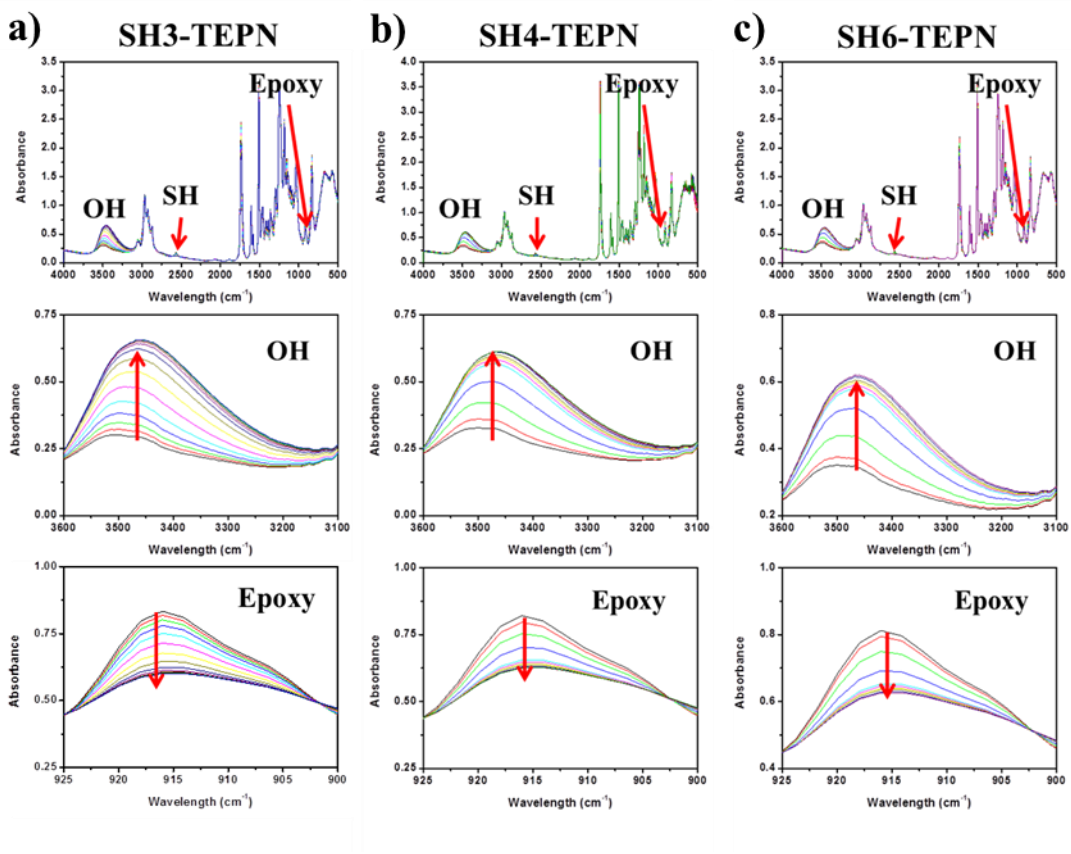

Figure 4. Variations with reaction time in the FT-IR spectra of the TEPNs at room temperature: (a) SH3-TEPN, (b) SH4-TEPN, and (c) SH6-TEPN. The data were collected at regular time intervals (180 s) after sample preparation and loading (150 s).

The isothermal reaction kinetics of the TEPNs was also studied with DSC by monitoring the heat flow evolution during the thiol-epoxy reactions. **Figure 5.** shows the isothermal heat flow curves as functions of reaction time for the TEPNs at room temperature. The shapes of the exothermic curves indicate that the thiol-epoxy click reactions follow the typical auto-catalysis reaction mechanism described above. The maximum peak positions of SH3-TEPN, SH4-TEPN, and SH6-TEPN are at 1450 s, 980 s, and 770 s, respectively, and the rates of reaction increase as the functionality of the cross-linkers increases. From these results, we conclude that the auto-catalysis effects of the epoxy-thiol reaction are enhanced by increasing the functionality of the cross-linker. The high functionality cross-linker has a high local concentration of thiol groups, so the average distance between the free thiol groups and the secondary alkoxides in the growing epoxy chain is much shorter than is the case for low functionality cross-linkers [27].

To obtain the degrees of conversion of the cross-linking reactions of the TEPNs, the total enthalpy change (ΔH_{exo}) of each thiol-epoxy click reaction was calculated by integration of the exothermic peak area; the calculated values for SH6-TEPN, SH4-TEPN, and SH3-TEPN are 222.1 J/g, 254.1 J/g, and 294.4 J/g respectively [24-25,28-30]. The degrees of conversion of the TEPNs are inversely proportional to the functionality of the cross-linkers.

In the color transition results, the rate of the color transition and the final color coordinates (or pH value) of the TEPNs reflect the rate and degree of conversion of the thiol-epoxy click reaction respectively. The rate of the color transition increases proportionally with the increase in the functionality of the cross-linkers. Similarly, the final Db* value decreases with increases in the functionality of the cross-linker. The trend in these results is in good agreement with the isothermal reaction kinetics data obtained with IR spectroscopy and the DSC measurements.

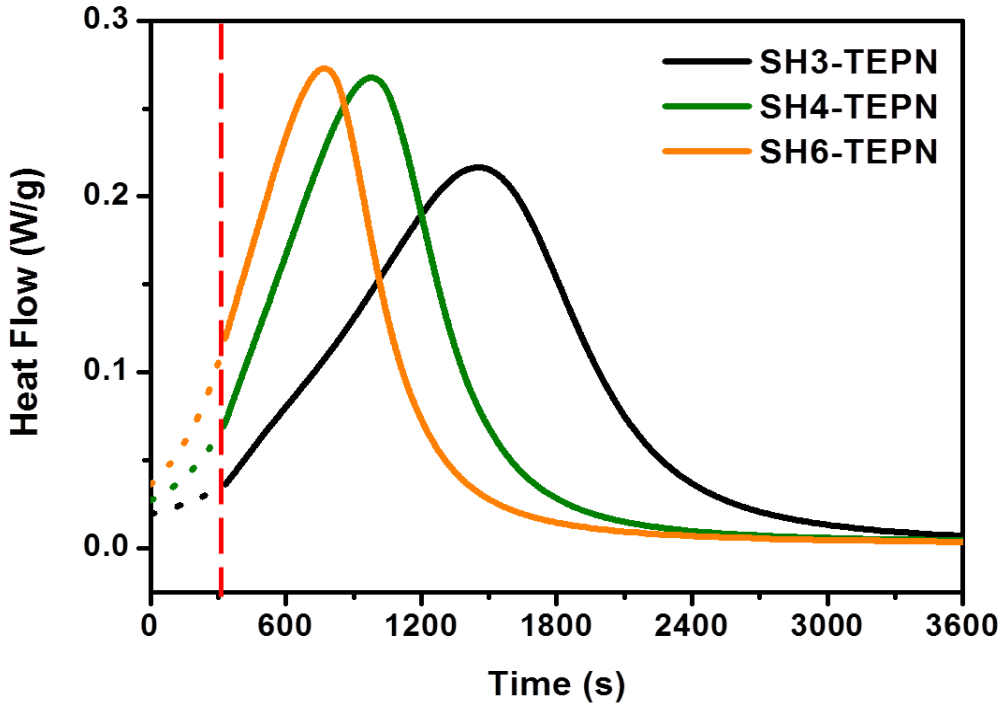

Figure 5. Isothermal DSC analyses for the thiol-epoxy click reactions of the TEPNs as functions of time at room temperature. The initial stages of the thiol-epoxy reactions up to 300 s (at the red dashed line) were not recorded because of sample preparation and the loading time. The dotted lines are predictions based on the auto-catalysis effect.

2.3.4. Thermal properties and crosslinking densities of the TEPNs.

The thermal stabilities of the TEPNs were investigated by using TGA. All the TEPNs are stable up to 300℃. The temperature dependences of the viscoelastic properties of the TEPNs were determined with DMA (**Figure 6.**). As shown in the G' vs temperature plots (**Figure 6. (a)**), the G' values of the TEPN films in a glassy state increase proportionally with the functionality of the cross-linker (SH6-TEPN > SH4-TEPN > SH3-TEPN). The G' values of the TEPNs in the glassy state are stable but as the temperature increases a steep drop in each modulus of approximately 3 orders of magnitude is observed, which indicates that the TEPNs are in a rubbery state. Plots of the loss factor vs temperature are presented in **Figure 6. (b)**. The maximum of tan δ is the temperature of α relaxation of the network and is closely related to T_g of TEPNs. The T_g values determined with DSC measurements are similar (**Figures 6. (c) and (d)**). The v_c of a cured polymer is defined as the number of moles of network chains per unit volume [15,18,22]. The v_c value of a cross-linked thermoset can be determined by performing modulus measurements in the rubbery plateau and using the equation of state for rubber elasticity (eq. 2).

$$v_c = G'/3RT \quad \text{(eq. 2)}$$

where,

G' = tensile storage modulus in the rubbery plateau

T (K) = temperature in K corresponding to the storage modulus value

R = gas constant

The calculated v_c values of the TEPNs are given in **Table 2.**: v_c increases with increases in the functionality of the cross-linker.

In general, the v_c values of the TEPNs should be proportional to the degree of conversion of the thiol-epoxy click reactions regardless of the functionality of the cross-linker if the stoichiometric ratios of the thiol groups in the cross-linker to the epoxy groups in the epoxy resin are the same. However, if the

cross-linking reaction is conducted at low temperatures, the situation is different. In this case, the reaction kinetics is greatly influenced by the polymer chain mobility restriction resulting from the cross-linking reaction because the later stages of the thiol-epoxy click reaction progress at temperatures under the T_g values of the TEPNs. Stochastically, a high functionality cross-linker provides a higher possibility of producing multi-linked points than low functionality cross-linkers. These multi-linked points increase the stiffness of the polymer chains and restrict the possibilities for reactants to meet. For this reason, the degree of conversion of thiol-epoxy reactions decreases with increases in the functionality of the cross-linker.

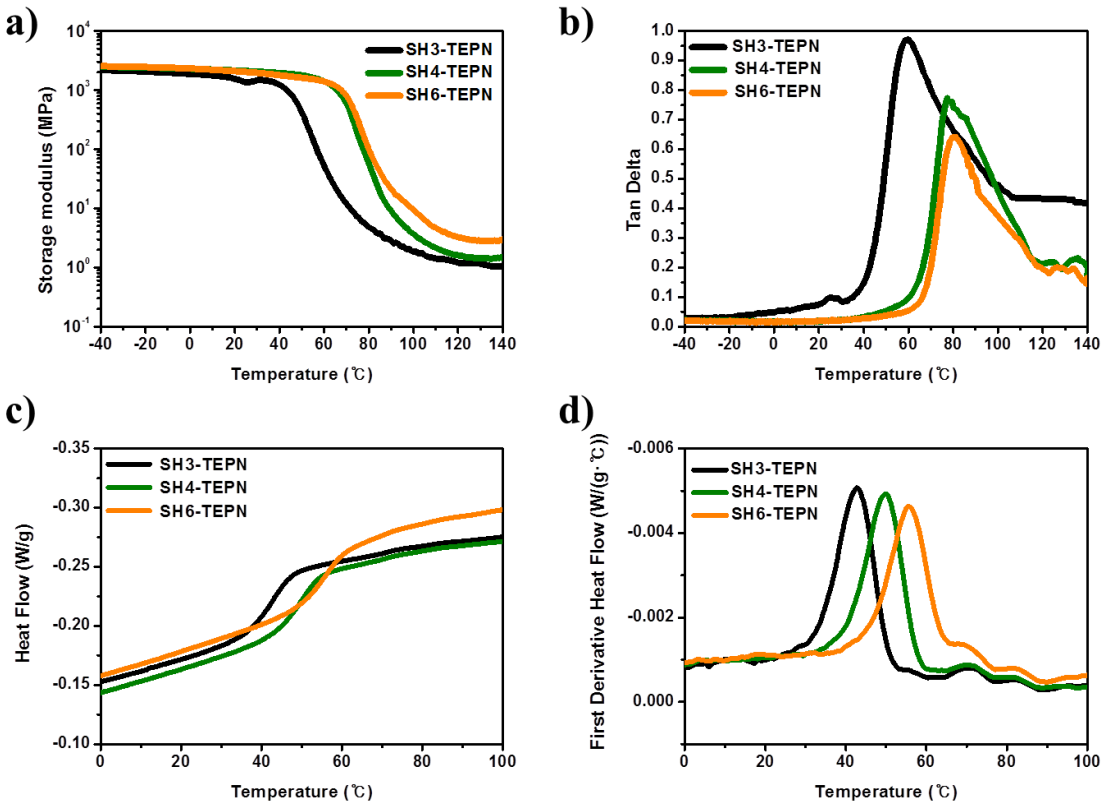

Figure 6. Thermal and viscoelastic properties of films of the TEPNs: (a) variations in G' with temperature, (b) plots of the calculated loss factors versus temperature obtained with DMA measurements, (c) heat flow curves, and (d) first derivative heat flow curves obtained from DSC measurements.

Table 2. Thermal and mechanical properties of the TEPNs.

Polymer code	T_d	T_g	V_c (at 110 °C)
SH3-TEPN	304.9 °C	59.6 °C	0.112 mol/L
SH4-TEPN	303.5 °C	77.3 °C	0.162 mol/L
SH6-TEPN	303.8 °C	81.3 °C	0.329 mol/L

2.3.5. Mechanical Properties of TEPNs.

To investigate the mechanical properties of the TEPNs, tensile tests were conducted with a UTM. The stress vs strain plots are shown in **Figure 7.** As expected, SH4-TEPN and SH6-TEPN are hard and brittle without yielding, which indicates that the thermoset has a high v_c. In contrast, SH3-TEPN exhibits low tensile strength with high yielding.

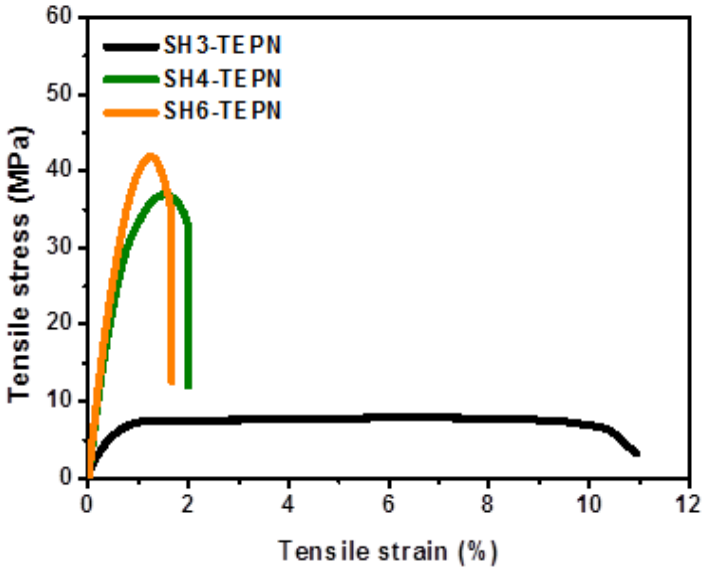

Figure 7. Tensile stress versus tensile strain plots for the TEPNs.

2.3.6. Chemical Resistances of the TEPNs.

The results for the chemical resistances of the TEPNs in various chemical environments are given in **Table 3.** The SH6-TEPN exhibits the best resistance to organic solvents (MEK and acetone), aqueous acids (HNO_3 and H_2SO_4), and base (triethyl amine) due to its high v_c. On the other hand, the chemical resistance of SH3-TEPN is much inferior to those of SH4-TEPN and SH6-TEPN despite its high degree of conversion. This result also indicates that SH3-TEPN has a lower v_c than SH4-TEPN and SH6-TEPN

Table 3. Chemical resistances of the TEPNs*.

Chemicals	Weight Loss (%)		
	SH3-TEPN	SH4-TEPN	SH6-TEPN
H_2SO_4 (10% aq.)	25.3	5.13	1.70
HNO_3(40% aq.)	7.74	0	0
MEK	6.29	2.53	0
Acetone	3.56	4.27	1.48
Triethyl amine	0	0	0

* Weight losses were calculated by using Eq. (1).

2.4. Conclusion

The reaction kinetics of the cross-linking reactions of the model TEPNs was successfully visualized by tracking their pH variations. In order to verify the precision of this technique, its results for various TEPNs prepared with different multi-functional cross-linkers were compared with those of other characterization methods, namely oscillational rheology, DSC, and FT-IR spectroscopy.

In our observations of the room temperature curing of the TEPNs, it was found that the high functionality cross-linker produces a faster rate of reaction than the low functionality cross-linker at the same stoichiometric ratio of thiol to epoxy groups because of an acceleration in the auto-catalysis effect. In addition, the degrees of conversion of the thiol-epoxy click reactions are also influenced by the functionality of the cross-linkers. However, the v_c values of the TEPNs are not proportional to the degree of conversion because a high functionality cross-linker provides a higher possibility of producing multi-linked points than low functionality cross-linkers. The trends found in the results of our mechanical property and chemical resistance tests are consistent with the results for the reaction kinetics, and with the thermal and viscoelastic property data.

Thus we have demonstrated that color transition characterization with a pH-responsive epoxy resin is a reliable and versatile technique for the study of the kinetics of room temperature thiol-epoxy cross-linking reactions.

2.5. REFERENCES

[1] D. P. Nair, M. Podgórski, S. Chatani, T. Gong, W. Xi, C. R. Fenoli, C. N. Bowman, Chem. Mater. 26 (2013) 724.

[2] C. E. Hoyle, A. B. Lowe, C. N. Bowman, Chem. Soc. Rev. 39 (2010) 1355.

[3] R. K. Iha, K. L. Wooley, A. M. Nyström, D. J. Burke, M. J. Kade, C. J. Hawker, Chem. Rev. 109 (2009) 5620.

[4] I. Gadwal, S. Binder, M. C. Stuparu, A. Khan, Macromolecules. 47 (2014) 5070.

[5] D. Zhang, C. Liu, S. Chen, J. Zhang, J. Cheng. M. Miao, Prog. Org. Coat. 101 (2016) 178.

[6] B. De, N. Karak, J. Mater. Chem. A. 1 (2013) 348.

[7] N. Cengiz, J. Rao, A. Sanyal, A. Khan, Chem. Commun. 49 (2013) 11191

[8] J. A. Carioscia, J. W. Stansbury, C.N. Bowman, Polymer 48 (2007) 1526.

[9] Y. Jian, Y. He, Y. Sun, H. Y.ang, W. Yang, J. Nie, J. Mater. Chem. C. 1 (2013) 4481.

[10] M. Sangermano, I. Roppolo, R. A. Ortiz, A. G. N. Tovar, A. E. G. Valdez, M. L. B. Duarte, Prog. Org. Coat. 78 (2015) 244.

[11] K. Suyama, M. Shirai, Prog Polym Sci 34 (2009) 194.

[12] M. Sangermano, A. Vitale, K. Dietliker, Polymer 55 (2014) 1628

[13] X. Zhang, W. Xi, C. Wang, M. Podgórski, C. N. Bowman, ACS Macro Lett. 5 (2016) 229

[14] Y. Yu, M. Nakano, A. Shishido, T. Shiono, T. Ikeda, Chem. Mater. 16 (2004) 1637.

[15] N. Zheng, G. Fang, Z. Cao, Q. Zhao, T. Xie, Polym. Chem. 6 (2015) 3046.

[16] R. Zhang, P. E. Mallon, H. Chen, C. M. Huang, J. Zhang, Y. Li, Y. Wu, T. C. Sandrezki, Y. C. Jean, Prog. Org. Coat. 42 (2001) 244.

[17] I. Giannakopoulos, A. C. Taylor, Prog. Org. Coat 78 (2015) 265.

[18] A. K. Guin, B. P. Mallik, S. Sheerpathi Prog. Org. Coat 78 (2015) 340.

[19] S. M. Noh, J. W. Lee, J. H. Nam, K. H. Byun, J. M. Park, H. W. Jung, Prog. Org. Coat. 74 (2012) 257.

[20] J. W. Yu, J. Jung, Y. M. Choi, J. H. Choi, J. Yu, J. K. Lee, N. H. You, M. Goh, Polym. Chem. 7

(2016) 36.

[21] X. Fernándes-Francos, A. -O. Konuray, A. Belmonte, S. D. L. Flor, À. Serra, X. Ramis, Polym. Chem. 7 (2016) 2280.

[22] S. Parker, R. Reit, H. Abitz, G. Ellson, K. Yang, B. Lund, W. E. Voit, Macromol. Rapid Commun. 37 (2016) 1027.

[23] T. Vidil, F. Tournilhac, Macromolecules. 46 (2013) 9240.

[24] D. Guzmán, X. Ramis, X, Fernández-Francos, A. Serra, Eur. Polym. J. 59 (2014) 377.

[25] D. Guzmán, X. Ramis, X. Fernández-Francos, A. Serra, Polymers. 7 (2015) 680.

[26] K. Jin, N. Wilmot, W. H. Heath, J. M. Torkelson, Macromolecules. 49 (2016) 4115.

[27] K. Jin, W. H. Heath, J. M. Torkelson, Polymer. 81 (2015) 70.

[28] R. Hardis, J. L. P. Jessop, F. E. Peters, M. R. Kessler, Compos Part A: Appl Sci Manuf. 49 (2013) 100.

[29] L. Merad, M. Cochez, S. Margueron, F. Jauchem, M. Ferriol, B. Benyoucef, P. Bourson, Polym. Test. 28 (2009) 42.

[30] R. M. Loureiro, T. C. Amarelo, S. P. Abuin, E. R. Soulé, R. J. J. Williams. ThermoChim. Acta. 616 (2015) 79.

[31] L. Xu, C. Li, K. Y. Simon Ng, J. Phys. Chem. A. 104 (2000) 3952.

[32] Z. Giorgio, T. Antonello, N. Monica, PCT Int Appl. WO 2013026865 (2013).

Chapter 3. Dual Stimuli Responsive Self-reporting Material for Chemical Reservoir Coating

3.1. Introduction

Polymer coatings are used extensively throughout industry and academia. Especially, polymeric coatings are used to protect against corrosion, physical, and chemical damage. In order to maximize the purpose of the polymeric coatings, a variety of coating technologies are being developed such as self-healing, self-reporting, and scratch-resistant coatings.[1–6] Especially for acid/base transfer pipes or storage tanks, the corrosion of the steel part occurred by the failure of the protective coating materials often causes a chemical spill accident which can result in an environmental catastrophe. For the reason, maintenance of damaged coating area should be carried out periodically. However, since weakening and degradation of the coating materials is rarely visible from the outside, it is necessary to develop self-reporting materials, which can report a change in performance during the application through property changes.[7–11]

Self-reporting materials developed so far can be classified into two mechanisms: intrinsic and extrinsic type. The intrinsic self-reporting materials detect the external stimuli by mechanically active materials incorporated into the polymer backbone or crosslinker units, while the extrinsic self-reporting materials are activated by the rupture of microcapsule which contains stimuli responsive materials such as fluorescence dye, pH-sensitive dye, and AIE-based materials.[7–11] Among various self-reporting mechanisms, the recent development of AIE-based extrinsic crack detection coating technology is particularly noteworthy.[8,12] The fluorescence enhancement mechanism of AIE material is exactly the opposite with the conventional fluorescence dyes which exhibit the aggregation-caused quenching (ACQ) effect.[13–15] That is, the fluorescence of the AIE materials in solid state is further enhanced than in liquid state. In the crack sensing application, an AIE material such as tetraphenylethylene (TPE)

is first diluted in a proper solvent and then encapsulated with poly(urea-formaldehyde) (UF) or polyurethane (PU) via emulsion polymerization.[8,16,17] When crack occur in matrix material containing AIE microcapsule, the microcapsule collapses and the AIE material solution come out by capillary force. After volatilization or diffusion of the solvent to matrix material, fluorescence emission of the AIE material at cracked area was enhanced and become detectable under UV light source.[8,12]

Considering its simple expression mechanism, fast response time and sensitivity, the AIE based extrinsic system could be very useful to design a high performance self-reporting coating material for a crack reporting chemical reservoir. Most importantly, this system has the potential to detect two different stimuli by placing one sensing material in the capsule and the other sensing material in the matrix. For chemical reservoirs maintenance, this dual stimuli responsive coating system is very useful because it allows the detection of the leakage occurrence at tank part as well as the crack formation at coating materials.

Herein, we designed a dual stimuli responsive self-reporting coating which can sense both crack occurrence and pH variation for chemical reservoirs coating. For crack detection, TPE containing double wall UF/PU microcapsules with different diameters were prepared via multi-step emulsion polymerization and dispersed in the thiol-epoxy thermoset (TET).[8,16,17] On the other hands, in order to detect pH variation, thymol blue was added in the matrix. The effect of capsule content in the DSRTET on their curing behavior was characterized by oscillatory rheology and rigid body pendulum test (RPT).[18–22] The relationship between the crack sensitivity and mechanical properties such as tensile strength, hardness, and elastic modulus was qualitatively analyzed with using scratch tester, universal test machine (UTM) and nano-indentation machine.[23–27] The pH detection performance of DSRTETs with different thymol blue contents was also investigated by acid or base solution drop tests. Finally, The DSRTET used in this study was coated to laboratory scale chemical reservoirs and tested the crack and pH variation detection performance.

3.2. Experimental

3.2.1 Materials.

Urea, aqueous formaldehyde solution (37 wt%), poly(ethylene-alt-maleic anhydride) (EMA), resorcinol, 1-octanol were purchased from Sigma-Aldrich. Desmodur L 75 as commercial polyurethane (PU) prepolymer was kindly donated from Bayer MaterialScience. Hexyl acetate (HA) and tetraphenylethylene (TPE) were purchased from Tokyo Chemical Industry. Ammonium chloride and sodium hydroxide were purchased from Duksan Pharmaceutical. Diglycidyl ether bisphenol A based epoxy resin (YD128SH) with an equivalent weight of 190-205 g eq^{-1} was obtained from Kukdo Chemical co. Triethylenetetramine (TETA), fumed silica (F-SiO_2), thymol blue, and titanium (||) oxide (TiO_2) were purchased from Sigma-Aldrich. Pentaerythritol tetra(3-mercaptopropionate) (SH4) was donated from Bruno Bock Thiochemicals.

3.2.2. Microencapsulation.

UF/PU double shell type microcapsule was prepared by following procedure. A 2.5 wt% EMA (5 mL) was added in distilled water (20 mL), and the urea (0.504 g), resorcinol (0.050 g), and ammonium chloride (0.050 g) were added with stirring at 25℃. The pH of the resultant solution was adjusted to 3.5 using a 10 % NaOH solution. The mixture was agitated at 600, 800, 1000, 1200, 1400, or 1600 rpm, and 12 mL of core material was added to obtain an emulsion. The core material consists of 1 wt% TPE in HA and Desmodur L 75. After adding a 37% formaldehyde (1.456 g) solution, the temperature of the mixture was raised to 60℃ and maintained for 5 h. The reaction mixture was cooled to room temperature and microcapsules were isolated by vacuum filtration. The microcapsules were washed with water and acetone, and then stored under atmospheric conditions for drying. UF single shell type

microcapsules were also obtained in similar manner to the synthetic procedure of UF/PU double shell type microcapsule expect adding Desmodur L 75.

3.2.3. Preparation of DSRTET.

The epoxy binder (a viscous liquid type) was formulated by mixing YD128SH (72 g), thymol blue (3 g), TiO2 (22 g), and F-SiO2 (3 g) with a planetary mixer (KM TECH, PLM-1K) at 1000 rpm for 3 hours. Crosslinker, SH4 was activated by adding 3 mol% of TETA prior to use. After mixing epoxy binder and activated SH4, the microcapsule was added to the mixture and well dispersed with a high speed overhead stirrer (Ocean Science, DISPERMAT) at 200 rpm for 10 min. Finally, the microcapsule containing mixture was coated on steel substrates or glass slides by doctor blade with 500 μm and cured at 25°C for 24 hours.

3.2.4. Confirmation of microcapsulation.

Mean diameter and size distribution of the synthesized micro-capsule were determined from the optical microscope images. The average values were calculated from the data set of at least 300 measurements. The surface morphology of the micro-capsules was investigated using a scanning electron microscope (SEM, SNE-3000M, SEC). The chemical structure of the micro-capsule was analyzed using FT-IR spectroscopy with attenuated total reflectance (ATR) mode. The presence of the core material in the micro-capsule was investigated by following procedure. The microcapsule and a filter paper put between a two slide glasses and were pressed. The core material was extracted from squeezed microcapsule. The broken shell materials were washed with chloroform and then dried in an oven at 60°C. The extracted core and dried shell material was mixed with KBr as pellet and measured by IR spectrometer. ^{1}H NMR spectroscopy was used to confirm that the core material was loaded inside the microcapsules. The microcapsules and $CDCl_3$ were placed in a vial, and after 30 seconds, a small amount of the $CDCl_3$ was collected. And then, the remaining microcapsules were destroyed and extracted with $CDCl_3$. The thermal characteristics were analyzed by thermogravimetric analysis (TGA)

(Q500, TA instrument), at a heating rate of 10°C/min under nitrogen atmosphere. For isothermal studies, the microcapsules were heated from 25 to 400 °C (heating rate of 10℃/min) and then at 170 °C for 5 h. The mass change was recorded through the entire experiment.

3.2.5. Curing behavior of DSRTETs.

The curing behavior of the DSRTET by the thiol-epoxy click reaction was characterized with an oscillatory rheometer (Thermo Scientific Inc., MARS III) operated at a constant frequency of 1 Hz and strain of 0.5 % using small amplitude oscillatory shear (SAOS) mode at 25 °C. The samples were placed between two 20 mm disposable upper/lower parallel plates. The gap was adjusted to 1 mm. Curing behavior of DSRTET coatings were further investigated using rigid body pendulum physical properties tester (RPT, A & D Co. Ltd, RPT-3000w). In the RPT, the test piece coating plate was mounted on the heating/cooling block and was in contact with a cylinder via a knife (FRB-300). A free vibration was applied to the pendulum and the rate and period (damping) of the motion were recorded. When the crosslinking reaction occurs, the rate of the pendulum motion was decreased.

3.2.6. Material properties of DSRTETs.

To evaluate hardness and modulus of the DSRTET coatings**,** loading, holding, and unloading indentation measurements were taken using a nano-indentation tester (Anton-Paar, NHT3) by employing a Berkovich-type indenter. During the loading step, the force imparted by the indenter was gradually increased from 0 mN to 10 mN at a rate of 20 mN min^{-1}. Then, in the holding step, the force was maintained at 10 mM for 10 s. And finally, the indenter was unloaded at the same absolute value of the rate as that of the loading. Through these three steps, the maximum displacement (h_{max}), permanent depth of penetration (final depth, h_f), elastic unloading stiffness ($S = dP/dh$), indentation hardness (H_{IT}), and indentation modulus (E_{IT}) were obtained. Micro-scratch tests were performed using

a Rockwell C indenter (tip radius 10 μm) mounted on a scratch test machine (Anton Paar, micro-scratch tester). The test was conducted using three stages; pre-scan, scratching and post-scan. First, in the pre-scan stage, the indenter was applied onto the surface with a low load of 0.4 mN to record the surface profile. Then, during the scratching stage, the force was also increased stepwise to 250, 500, 750, and 1000 mN on the coating, and scratches with lengths of 2 mm each were made at a rate of 4 mm min^{-1}. The tensile properties of the DSRTETs were determined by carrying out universal testing machine (UTM) (Instron, model 5982) with constant strain (2 mm min^{-1}). The dimension of the specimens were 50 mm × 12 mm × 1.5 mm and each samples were cured at 25°C for 24 hours. The color transition measurements during curing were obtained in real-time by using a multi-angle spectrophotometer (StellarNet, Inc., X-Rite MA98).

3.3. Results and discussion

In this study, we designed a dual stimuli responsive thiol-epoxy polymeric coating system which can visualize both the crack occurrence and pH variation by employing crack detectable AIE material and pH responsive thymol blue indicator (**Figure 1**.). The overall scheme and the materials used in this study were presented in **Figure 2.**

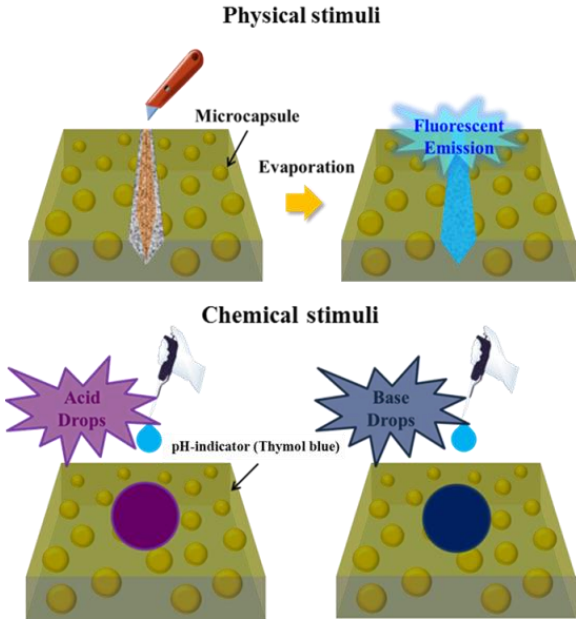

Figure 1. Self-reporting mechanism of DSRTET coatings.

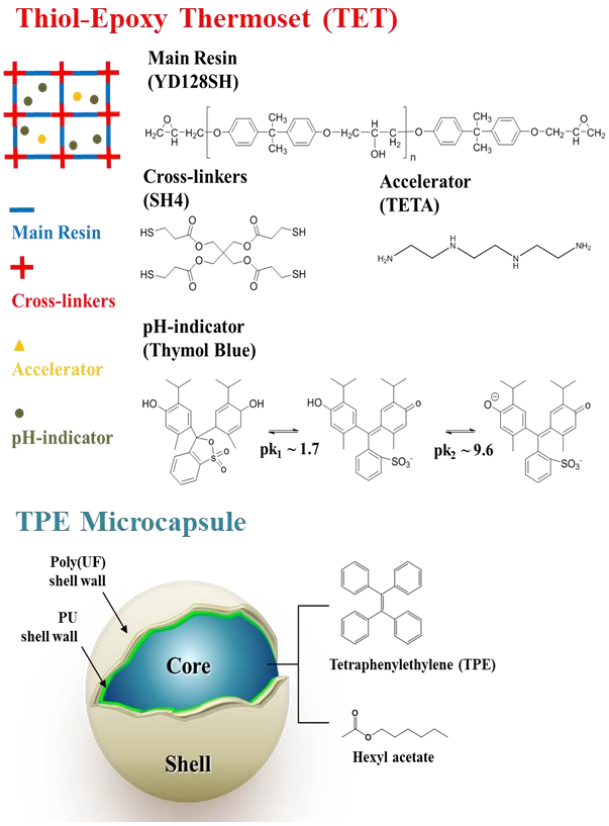

Figure 2. Schematic diagram and chemical structure of materials used in this study.

3.3.1. Microcapsules.

Durable UF and PU based double shell type microcapsule was synthesized by sequential emulsion polymerization. The Size of the UF/PU microcapsules was controlled by changing agitation rate from 600 to 1600 rpm. As can be seen in **Figure 3**., smooth and spherical microcapsules were obtained under all agitation condition. It was found that the average diameter and size distribution of the capsules were linearly decreased as increasing the agitation rate because increasing shear stress allows formation of a small and uniform emulsion droplet.

The successful formation of double wall microcapsule was confirmed by FT-IR spectroscopy (**Figure 4. (a)**). In the spectrum, broad absorbance peaks at 3660-3140 cm^{-1} were assigned to N-H and O-H stretching vibration, N-H scissoring vibration, C-O stretching vibration of urethane and urea group in PU and UF shells, respectively. In order to check successful microencapsulation of TPE solution in HA, the microcapsule was placed in two slide glasses, ruptured, and then analyzed. Characteristic absorbance peak at 1738 cm^{-1} from C=O stretching vibration in HA was observed, indicating the successful formation of the core filled microcapsules. ^{1}H-NMR spectroscopy was also support the successful emulsion polymerization of the core filled microcapsule. The successful formation of the double wall microcapsule was proven by TGA data obtained from dynamic scanning experiment and isothermal analysis. The UF/PU double wall microcapsule showed superior thermal stability to that of PU single wall microcapsule.

To verify the expression of AIE phenomenon from TPE, the microcapsule was placed between two glass slides, ruptured by pressing the glasses, and then analyzed using optical microscope (OM) with UV light source (**Figure 4. (b)**). As can be seen in the figure, intensive blue fluorescence was emitted from the ruptured microcapsule under UV light. On the other hand, no light emission was detected from the undamaged microcapsule, indicating that AIE phenomena was successfully suppressed by HA solvent.

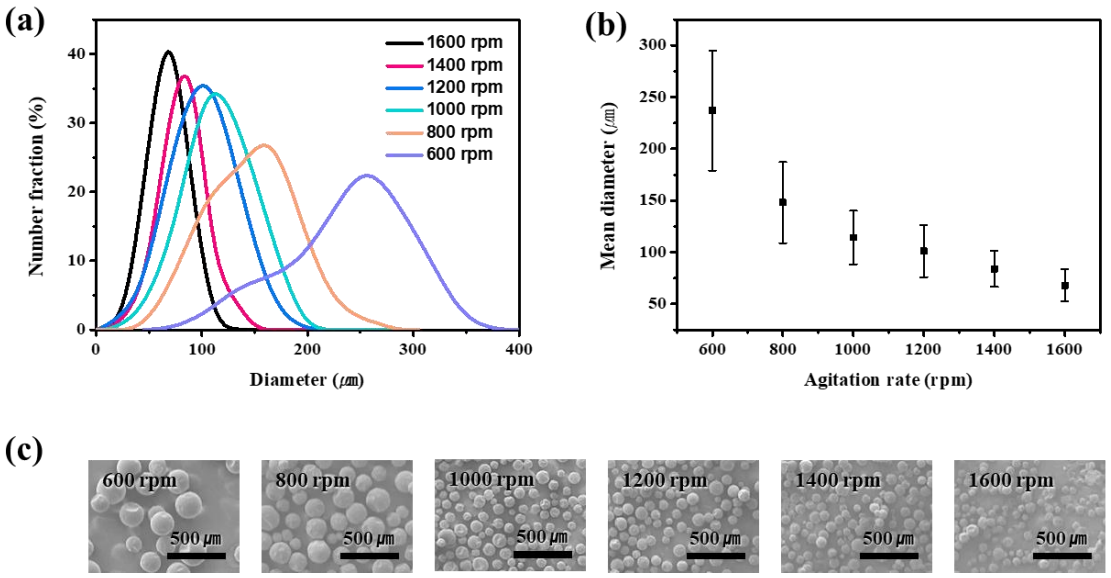

Figure 3. Effect of agitation rate on diameter and size distribution of the microcapsule: (a) size distribution, (b) mean diameter, and (c) optical microscope images of the synthesized microcapsules.

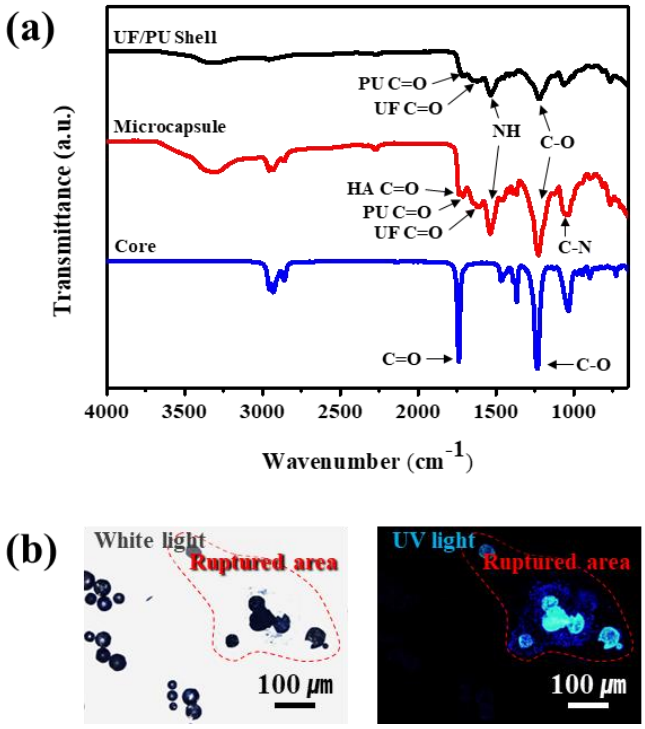

Figure 4. Confirmation of the microcapsule formation: (a) FT-IR spectra of core material, UF/PU shell, and synthesized microcapsule and (b) optical microscope images of the undamaged and ruptured microcapsules obtained under white or UV light sources.

3.3.2 Curing behaviors of DSRTETs.

To investigate effect of the microcapsule contents on the curing behaviors of DSRTETs, various epoxy thermosets with different microcapsule contents were prepared. The detailed formulation was summarized in Table 1. The viscoelastic property changes during thiol-epoxy crosslinking reaction of DSRTETs were characterized using oscillatory rheometer operated at room temperature. As shown in time vs *E'* plot in **Figure 5. (a)**, the storage modulus of all DSRTETs increased according to time evolution, indicating that the polymer formed the network structure. It was also found that the slopes in time vs *E'* of DSRTETs were decreased with increasing microcapsule contents. This delayed curing time is attributed to lower thiol and epoxy group concentration per unit volume of DSRTETs which have higher microcapsule contents. Curing behavior of DSRTETs was further investigated using RPT method (**Figure 5. (b)**). As shown in time vs frequency plot, the steep decrease in frequency was observed, indicating that the polymer formed the network structure. In addition, it is observed that increase in the microcapsule contents of DSRTETs lead to decrease the rate of curing and the result is well consistent with the rheology data.

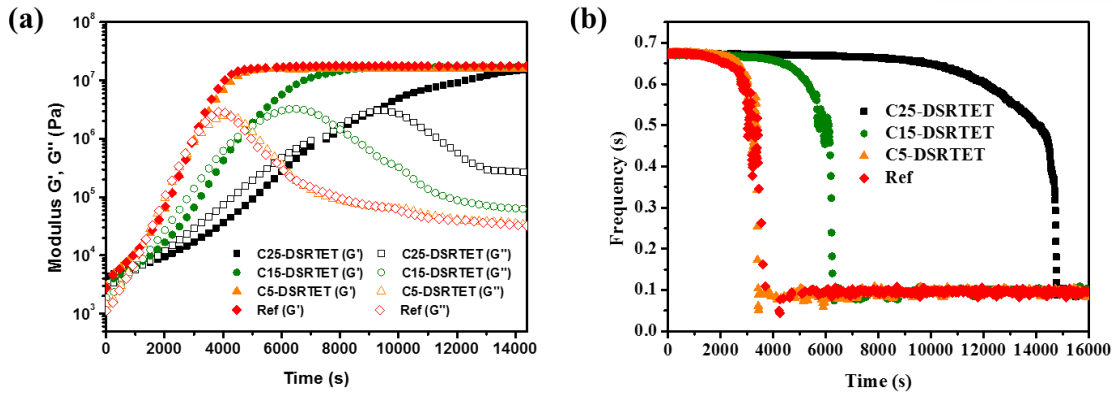

Figure 5. Curing behaviors of the DSRTETs: (a) time versus storage modulus plot of DSRTETs measured using the oscillatory rheometer and (b) time versus frequency plot of DSRTETs obtained from the RPT measurement.

3.3.3 Effect of microcapsule content on material properties.

Figure 6. (a) shows typical load–displacement curves for nano-indentation tests carried out on the DSRTET coatings. All DSRTET coatings exhibited plastic deformation in response to applied normal forces. The H_{IT} and E_{IT} of the DSRTETs can be calculated by following equations.

$$H_{\mathrm{IT}} = F_{max} \ / \ A_p \quad (eq.1)$$

$$E_{\mathrm{IT}} = E^* \cdot (1 - \upsilon_s^2) \quad (eq.2)$$

Where, F_{max}, E^*, A_p, and ν_s indicate maximum indentation normal force, plane strain modulus, the pressed area by perfect berkovich type indenter, and poisson's ratio respectively.

Figure 6. (b) shows the microcapsule contents vs H_{IT} and E_{IT} value plot. As the microcapsule contents in the coatings was increased, the h_{max}, h_f, and S (in the unloading step values) gradually decreased because high concentration of microcapsule decreased the crosslinking density of the DSRTET coatings.

Figure 7. shows tensile strain versus stress curve of DSRTET films measured using UTM. There shows the clear difference in the stress-strain curves depending on the microcapsule content. As increasing the microcapsule content, the model shifted to soft and tough from hard and brittle. The result is also attributed to different crosslinking density of the DSRTET specimens. The number of linked point of the polymer chains per unit volume decreased with increasing the microcapsule content.

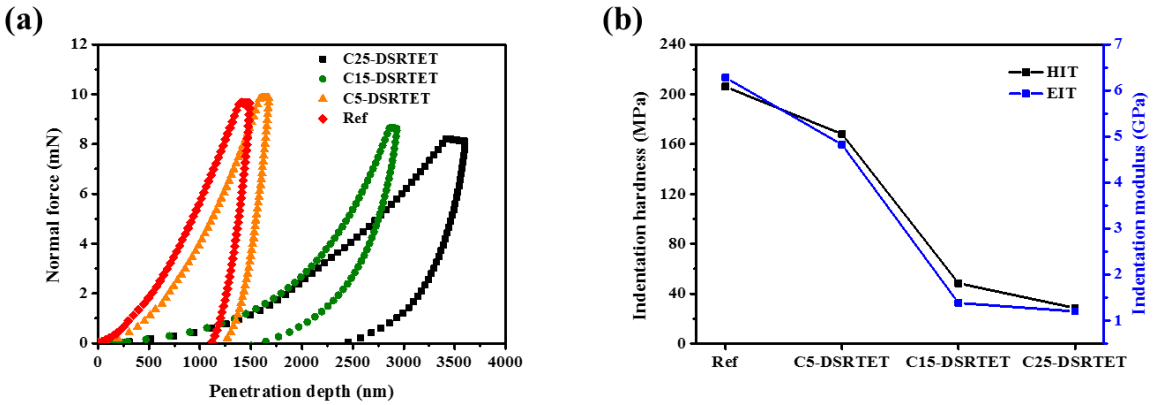

Figure 6. The result of nano-indentation test of DSRTET coatings: (a) Load-displacement curve and (b) changes in H_{IT} and E_{IT} values according to microcapsule contents.

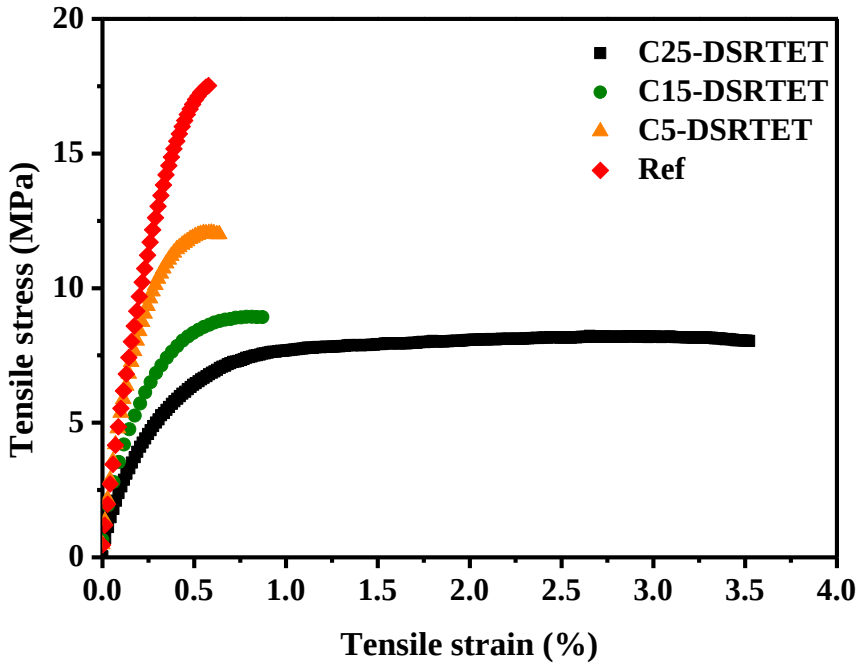

Figure 7. Tensile stress versus tensile strain plots for the DSRTET coatings.

3.3.4. Effect of microcapsule content on the crack sensitivity.

The scratch test of the DSRTET coatings in response to a step-wise increase in the deforming load was conducted using the scratch tester to exert four sequentially increasing loads from 250 to 1000 mN and initiate formation of the fracture on the coating surface. As shown in panoramic images in **Figure 8. (a)**, the surface of all DSRTET coatings begun to be scratched from 250 mN. The crack sensitivity of DSRTET coatings was investigated by exposing the scratched coating to 365 nm UV light. No florescence emission was observed from the C5-DSRTET coating since the concentration of microcapsule was too low. However, C15 and C25-DSRTET coatings showed clear and bright AIE effect from the ruptured microcapsules. In addition, the scratched surface of C15-DSRTET coating emitted the blue florescence from 250 mN, while the crack of the C25-DSRTET coatings was detected form 500 mN. The result is closely related to the H_{IT} as well as microcapsule contents of the DSRTET coatings. As can be seen in **Figure 8. (b)**, the penetration depth of the DSRTET coatings in response to the applied load was proportionally increased with increasing the microcapsule contents because of their low the H_{IT} values. The higher penetration depth leads to the more microcapsules break. Note that the intensity of the blue florescence is proportional to the number of ruptured microcapsules.

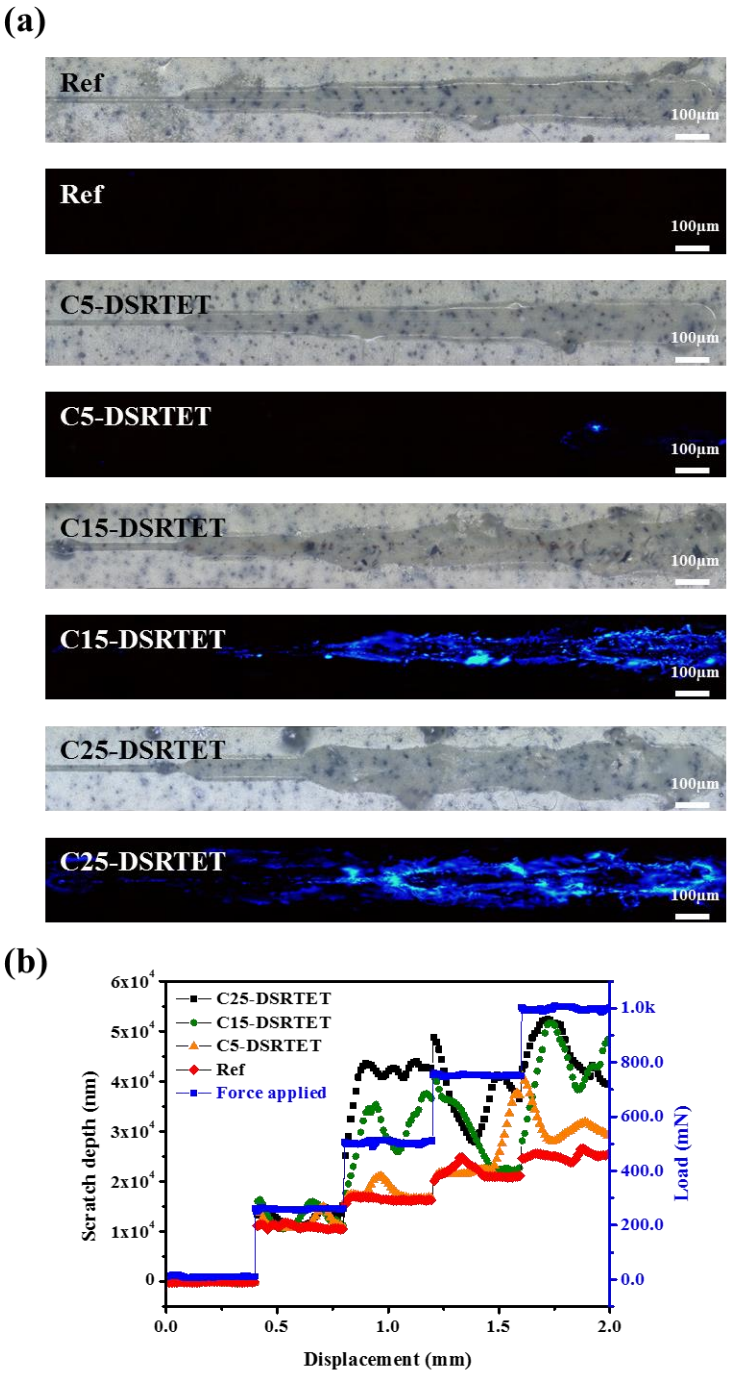

Figure 8. Effect of microcapsule content on the crack sensitivity of DSRTET coatings subjected to step-wise-increasing deforming load from 250 mN to 1000 mN: (a) optical microscope image of the cracked surface of DSRTET coatings under UV light (365 nm) and (b) penetration depths profiles as a function of lateral position of a line of the DSRTET coatings.

3.3.5. Effect of thymol blue contents on pH sensitivity.

In order to optimize the color transition range, various epoxy thermosets with different thymol blue contents were prepared and their color transition in response to the chemical stimuli such as organic acid and base were investigated using solution drop test. As shown in **Figure 9. (a)**, the color of the thiol-epoxy thermosets changed from pale green to red or blue after contact with aqueous 35 wt% HCl or 10 wt% NaOH solutions as expected. It is also observed that the contrast between the changed and original color of the thiol epoxy thermosets was increasing with increasing thymol blue contents. For further investigation, the color transition of the thiol epoxy thermosets was quantitatively analyzed using a multi-angle spectrophotometer. **Figure 9. (b)** shows the changes in the CIE values of each epoxy thermoset after dropping corresponding acid or base solution. Initially, the range of color transition of the thiol-epoxy thermoset was increased as increasing the thymol blue contents but gradually saturated at the concentration of 3.0%. Considering the color transition range and the contrast values, we can conclude that the optimized thymol concentration in this system is 3.0%.

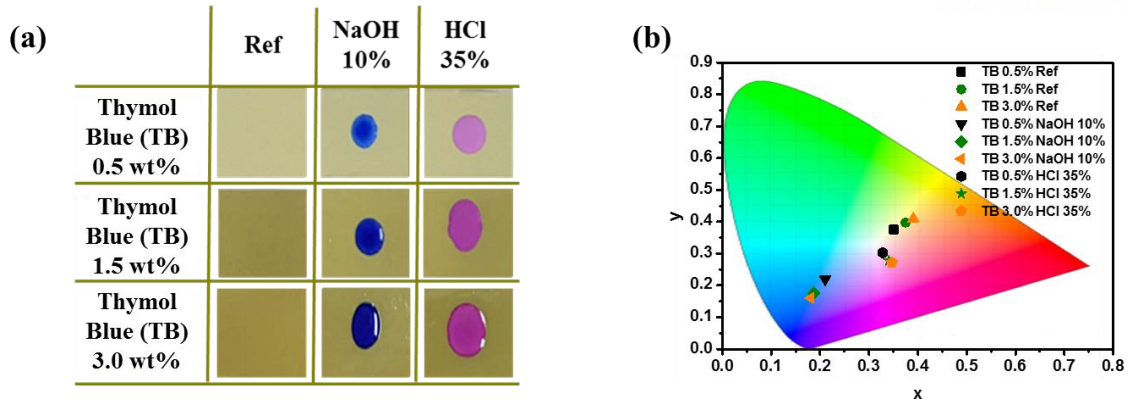

Figure 9. Color transition of DSRTET coatings in response to acid or base solutions: (a) optical microscope images of DSRTET coatings and (b) the color transitions of the DSRTET coatings in CIE 1931 color space before/after solution drop test.

3.3.6. Application of DSRTET coatings to the chemical container.

In order to demonstrate the dual stimuli response crack reporting system, the C15-DSRTET was applied to a laboratory scale model chemical reservoir. As shown in Figure 10., both cracks on coating and reservoir were successfully detected by AIE effect and pH variation respectively.

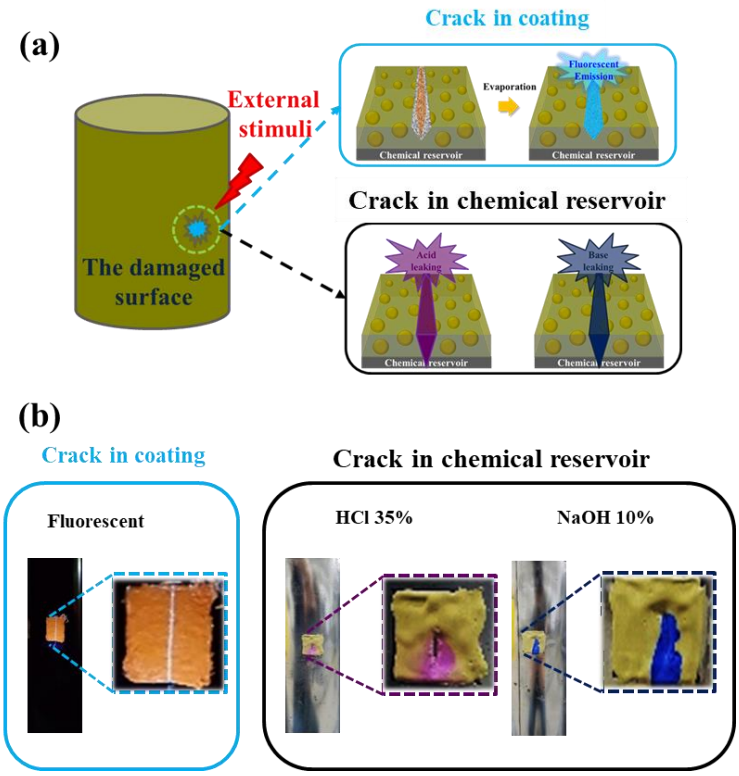

Figure 10. Application of the DSRTET coatings to the laboratory scale chemical reservoirs : (a) illustration of chemical reservoir design and dual stimuli responsive self-reporting mechanism and (b) actual crack test.

3.4. Conclusion

The DSRTET coatings which can detect both crack occurrence and pH variation were successfully prepared by employing a double wall microcapsule containing core TPA solution in HA and thymol blue as a pH indicator.

The curing behavior of the DSRTETs was characterized by oscillatory rheometer and RPT. In the both measurements, it was found that the rate of curing of DSRTETs was decreased with increasing microcapsule contents. This delayed curing time is attributed to lower thiol and epoxy group concentration per unit volume of DSRTETs which have higher microcapsule contents.

The effect of microcapsule content on material properties of DSRTET coatings was investigated using nano-indentation and tensile tests. In nano-indentation test, all DSRTET coatings exhibited the plastic deformation, and both H_{IT} and E_{IT} were decreased with increasing the microcapsule content. In tensile test, as the microcapsule content in DSRTET coatings increases, the shape of the stress vs strain curve was shifted from hard and brittle to soft and tough model. The results are mainly attributed to different crosslinking density of the DSRTET films. The number of linked point of the polymer chains per unit volume decreased with increasing the microcapsule content.

In order to optimize the AIE effect of DSRTET coatings in response to formation of crack in coating layer, the scratch patterns of various DSRTET coatings with different microcapsule contents were investigated using the scratch tester. It was revealed that the crack sensitivity of the DSRTET coatings is closely related to the H_{IT} as well as microcapsule contents.

The pH variation of DSRTET coatings with different thymol blue concentration was quantitatively analyzed using the multi-angle spectrometer. The color of DSRTET coatings was changed from pale

green to red for the acidic HCI solution and to blue for basic NaOH solution as expected. Considering color transition range and contrast values, we canclude that the optimum concentration of thymol blue in DSRTET coatings was 3.0 wt%.

Finally, in order to demonstrate the dual stimuli response crack reporting system, the C15-DSRTET was coated on a laboratory scale model chemical reservoir. The detection of both crack occurrence at the DSRTET coating and acid/base chemicals spill caused by the leak at damaged container were successfully detected by AIE mechanism and pH variation.

3.5. REFERENCES

[1] S.M. Noh, J.W. Lee, J.H. Nam, J.M. Park, H.W. Jung, Analysis of scratch characteristics of automotive clearcoats containing silane modified blocked isocyanates via carwash and nano-scratch tests, Prog. Org. Coat. 74 (2012) 192–203. doi:10.1016/j.porgcoat.2011.12.009.

[2] H. Yari, M. Mohseni, M. Messori, A scratch resistant yet healable automotive clearcoat containing hyperbranched polymer and POSS nanostructures, RSC Adv. 6 (2016) 76028–76041. doi:10.1039/C6RA07824A.

[3] G. Bahlakeh, B. Ramezanzadeh, M.R. Saeb, H. Terryn, M. Ghaffari, Corrosion protection properties and interfacial adhesion mechanism of an epoxy/polyamide coating applied on the steel surface decorated with cerium oxide nanofilm: Complementary experimental, molecular dynamics (MD) and first principle quantum mechanics (QM) simulation methods, Appl. Surf. Sci. 419 (2017) 650–669. doi:10.1016/j.apsusc.2017.05.070.

[4] J. Zhou, Z. Tan, Z. Liu, M. Jing, W. Liu, W. Fu, Preparation of transparent fluorocarbon/TiO2-SiO2 composite coating with improved self-cleaning performance and anti-aging property, Appl. Surf. Sci. 396 (2017) 161–168. doi:10.1016/j.apsusc.2016.11.014.

[5] X. Liu, X. Lu, P. Wen, X. Shu, F. Chi, Synthesis of ultrasmall silica nanoparticles for application as deep-ultraviolet antireflection coatings, Appl. Surf. Sci. 420 (2017) 180–185. doi:10.1016/j.apsusc.2017.05.124.

[6] E.B. Caldona, A.C.C. de Leon, B.B. Pajarito, R.C. Advincula, Novel anti-corrosion coatings from rubber-modified polybenzoxazine-based polyaniline composites, Appl. Surf. Sci. 422 (2017) 162–171. doi:10.1016/j.apsusc.2017.05.083.

[7] Frederico Maia, João Tedim, Alexandre C. Bastos, Mário G. S. Ferreira and Mikhail L. Zheludkevich, Active sensing coating for early detection of corrosion processes, RSC Adv. 4 (2014) 17780-17786. DOI: 10.1039/c4ra00826j

[8] Rudolph G Buchheit, Hong Guan, Suhakar Mahajanam, FariatyWong, Active corrosion protection and corrosion sensing in chromate-free organic coatings, Prog. Org. Coat. 47 (2003) 174–182. DOI:10.1016/j.porgcoat.2003.08.00

[9] S.-Y. Cho, J.-G. Kim, C.-M. Chung, A fluorescent crack sensor based on cyclobutane-containing crosslinked polymers of tricinnamates, Sens. Actuators B Chem. 134 (2008) 822–825. doi:10.1016/j.snb.2008.06.042.

[10] M.J. Robb, W. Li, R.C.R. Gergely, C.C. Matthews, S.R. White, N.R. Sottos, J.S. Moore, A Robust Damage-Reporting Strategy for Polymeric Materials Enabled by Aggregation-Induced Emission, ACS Cent. Sci. 2 (2016) 598–603. doi:10.1021/acscentsci.6b00198.

[11] W. Li, C.C. Matthews, K. Yang, M.T. Odarczenko, S.R. White, N.R. Sottos, Autonomous Indication of Mechanical Damage in Polymeric Coatings, Adv. Mater. 28 (2016) 2189–2194. doi:10.1002/adma.201505214.

[12] Y.-K. Song, K.-H. Lee, W.-S. Hong, S.-Y. Cho, H.-C. Yu, C.-M. Chung, Fluorescence sensing of microcracks based on cycloreversion of a dimeric anthracene moiety, J. Mater. Chem. 22 (2012) 1380–1386. doi:10.1039/C1JM13709C.

[13] S.A. Odom, A.C. Jackson, A.M. Prokup, S. Chayanupatkul, N.R. Sottos, S.R. White, J.S.

Moore, Visual Indication of Mechanical Damage Using Core–Shell Microcapsules, ACS Appl. Mater. Interfaces. 3 (2011) 4547–4551. doi:10.1021/am201048a.

[14] Y.K. Song, B. Kim, T.H. Lee, J.C. Kim, J.H. Nam, S.M. Noh, Y.I. Park, Fluorescence Detection of Microcapsule-Type Self-Healing, Based on Aggregation-Induced Emission, Macromol. Rapid Commun. 38 (2017) n/a-n/a. doi:10.1002/marc.201600657.

[15] J. Huang, Y. Jiang, J. Yang, R. Tang, N. Xie, Q. Li, H.S. Kwok, B.Z. Tang, Z. Li, Construction of efficient blue AIE emitters with triphenylamine and TPE moieties for non-doped OLEDs, J. Mater. Chem. C. 2 (2014) 2028–2036. doi:10.1039/C3TC32207F.

[16] C. Liu, H. Luo, G. Shi, J. Yang, Z. Chi, Y. Ma, Luminescent network film deposited electrochemically from a carbazole functionalized AIE molecule and its application for OLEDs, J. Mater. Chem. C. 3 (2015) 3752–3759. doi:10.1039/C4TC02475C.

[17] Y. Hong, J.W.Y. Lam, B.Z. Tang, Aggregation-induced emission: phenomenon, mechanism and applications, Chem. Commun. (2009) 4332–4353. doi:10.1039/B904665H.

[18] H. Jin, C.L. Mangun, A.S. Griffin, J.S. Moore, N.R. Sottos, S.R. White, Thermally Stable Autonomic Healing in Epoxy using a Dual-Microcapsule System, Adv. Mater. 26 (2014) 282–287. doi:10.1002/adma.201303179.

[19] M.M. Caruso, B.J. Blaiszik, H. Jin, S.R. Schelkopf, D.S. Stradley, N.R. Sottos, S.R. White, J.S. Moore, Robust, Double-Walled Microcapsules for Self-Healing Polymeric Materials, ACS Appl. Mater. Interfaces. 2 (2010) 1195–1199. doi:10.1021/am100084k.

[20] T.H. Lee, Y.I. Park, S.M. Noh, J.C. Kim, In-situ visualization of the kinetics of low temperature thiol-epoxy crosslinking reactions by using a pH-responsive epoxy resin, Prog. Org. Coat. 104 (2017) 20–27. doi:10.1016/j.porgcoat.2016.11.007.

[21] K. Jin, W.H. Heath, J.M. Torkelson, Kinetics of multifunctional thiol-epoxy click reactions studied by differential scanning calorimetry: Effects of catalysis and functionality, Polymer. 81 (2015) 70–78. doi:10.1016/j.polymer.2015.10.068.

[22] D.G. Lee, S.Y. An, M.S. Um, W.J. Choi, S.M. Noh, H.W. Jung, J.K. Oh, Photo-induced thiol-ene crosslinked polymethacrylate networks reinforced with Al2O3 nanoparticles, Polymer. 101 (2016) 119–126. doi:10.1016/j.polymer.2016.08.049.

[23] J.W. Hwang, K.N. Kim, G.S. Lee, J.H. Nam, S.M. Noh, H.W. Jung, Rheology and curing characteristics of dual-curable automotive clearcoats using thermal radical initiator derived from O-imino-isourea and photo-initiator, Prog. Org. Coat. 76 (2013) 1666–1673. doi:10.1016/j.porgcoat.2013.07.019.

[24] Y.-J. Park, D.-H. Lim, H.-J. Kim, H.-S. Joo, H.-S. Do, Curing Behavior and Adhesion Performance of UV-Curable Styrene–Isoprene–Styrene-Based Pressure-Sensitive Adhesives, J. Adhes. Sci. Technol. 22 (2008) 1401–1423. doi:10.1163/156856108X309549.

[25] W.C. Oliver, G.M. Pharr, Measurement of hardness and elastic modulus by instrumented indentation: Advances in understanding and refinements to methodology, J. Mater. Res. 19 (2004) 3–20. doi:10.1557/jmr.2004.19.1.3.

[26] H. Jiang, R. Browning, J.D. Whitcomb, M. Ito, M. Shimouse, T.A. Chang, H.-J. Sue, Mechanical Modeling of Scratch Behavior of Polymeric Coatings on Hard and Soft Substrates, Tribol. Lett. 37 (2010) 159–167. doi:10.1007/s11249-009-9505-8.

[27] A.M. Díez-Pascual, M.A. Gómez-Fatou, F. Ania, A. Flores, Nanoindentation in polymer nanocomposites, Prog. Mater. Sci. 67 (2015) 1–94. doi:10.1016/j.pmatsci.2014.06.002.

[28] M.K. Mishra, G.R. Desiraju, U. Ramamurty, A.D. Bond, Studying Microstructure in Molecular Crystals With Nanoindentation: Intergrowth Polymorphism in Felodipine, Angew. Chem. Int. Ed. 53 (2014) 13102–13105. doi:10.1002/anie.201406898.

[29] H. Liu, J. Xu, B. Guo, X. He, Preparation and performance of silica/polypropylene composite separator for lithium-ion batteries, J. Mater. Sci. 49 (2014) 6961–6966. doi:10.1007/s10853-014-8401-2.

Chapter 4. A Crack Repair Patch Based on Acrylated Epoxidized Soybean Oil

4.1 Indroduction

The safe transport and storage of chemicals are very important in the chemical industry. The majority of chemical spill accidents are caused by leaks from chemical transfer pipes or tanks, so the periodical maintenance of chemical facilities is vital. If cracks are found in transfer or storage units during such inspections, it is very important to block them rapidly using an emergency crack repair patch prior to crack recovery process in order to prevent the further spread of toxic chemicals.[1,2]

The crack repairing materials developed so far can be classified into two categories: putties and patches. Putty-type repair materials are mostly fast-curing epoxy thermosets.[3–5] The advantages of such materials include excellent adhesion to steel substrates and resistance to toxic chemicals, but considerable time is required to mix the main resin and curing agent prior to use and it is difficult to apply them to a wet surface. On the other hand, patch-type repair materials consist of a pressure sensitive adhesive (PSA) coated onto a polymer film that can be immediately applied to damaged areas without any preparation steps.[6] However, one disadvantage of this approach is that leaking chemicals can degrade the surface adhesion of the repair material by swelling or dissolving the PSA. Thus, we aimed in this study to develop a new type of repair material with the advantages of both types described above.

Soybean oil is a good candidate material for such a crack repairing system because it can easily be functionalized with various types of reactive groups such as acrylate,[7] epoxy,[8] and carboxylic acid groups,[9] it is suitable for UV-thermal dual-curing systems that involve sequential polymer network formation,[10–13] and by controlling its crosslinking density it can be used in many applications such as adhesives, pressure sensitive adhesives (PSAs), and coatings.[14–18]

Herein, we propose a novel UV-curable patch system with high chemical resistance and adhesion properties for the rapid blocking of cracks in chemical reservoirs. The basic procedure of its application is shown in **Figure 1**. In the first step, the patch is quickly attached to the damaged area in order to prevent further chemical spillage. In the second step, the attached patch is cured with a portable UV source in order to improve its adhesion properties and chemical resistance. Crosslinked acrylated epoxidized soy bean oil (AESO) samples with various compositions and crosslinking densities were prepared by reacting AESO with the triethylenetetramine (TETA) crosslinker, and tested as UV-curable PSA materials. In the UV-curing reaction, 2-hydroxy-2-methylpropiophenone (HDA) and 2,4,6-trimethylbenzoyl-diphenyl phosphine (TBDP) were employed as photo-initiators. The curing behaviors and PSA performances of the UV- curable patch systems (AESO-PSAs) were quantitatively analyzed by using an oscillatory rheometer, a universal test machine (UTM), and a probe tack and shear strength tester. Finally, the optimized patch was applied to a laboratory scale chemical reservoir in order to assess its performance as a UV-curable leak repairing patch system for the prevention of chemical spills from cracked reservoirs.

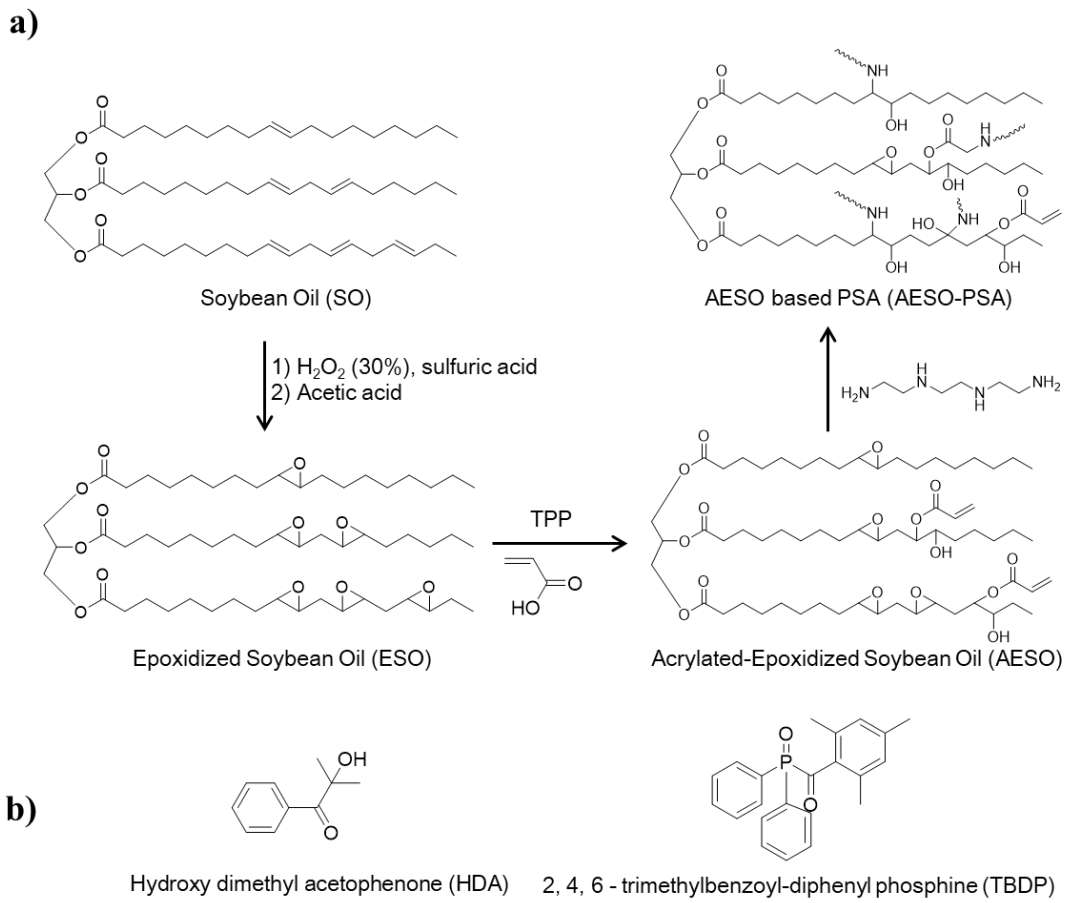

Scheme 1. a) The synthesis of AESO-PSAs from renewable sources and b) the UV-radical initiators used in this study.

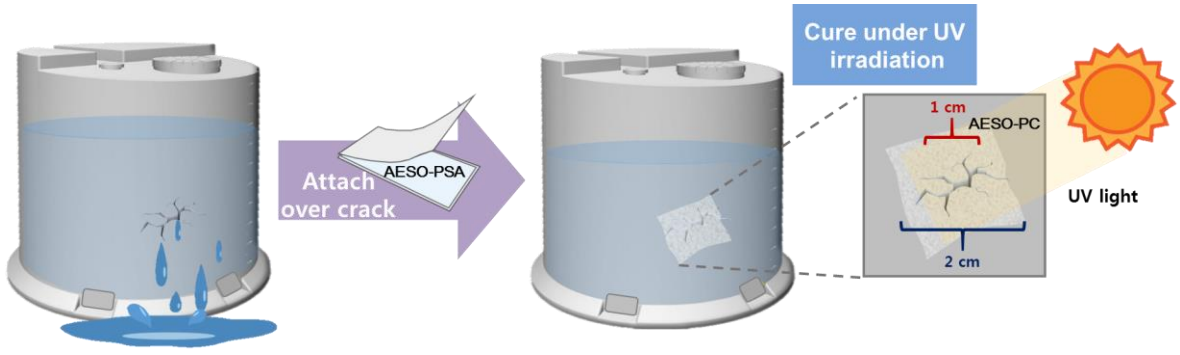

Figure 1. Schematic overview of the UV-curable crack repair patch system.

4.2 Experimental

4.2.1. Materials

2-hydroxy-2-methylpropiophenone (HDA) and 2,4,6-trimethylbenzoyl-diphenyl phosphine (TBDP) were kindly donated by Miwon Specialty Chemical Co. Triethylenetetramine (TETA) and acrylated epoxidized soybean oil (AESO) were prepared as described in the literature.

4.2.2. Preparation of AESO

[19] Epoxidized soybean oil (ESO) was synthesized via the reaction of SO (8.5 g) with peroxyacetic acid (was prepared in situ by reacting 3.5 g of 99.5% glacial acetic acid and 16.5 g of 30% H_2O_2 in the presence of catalytic amount of concentrated sulfuric acid) at 65℃ for 13.5. AESO was synthesized from the reaction of acrylic acid with ESO. The molar ratio of epoxy groups of ESO and acrylic acid is 1 : 1.05. Triphenyl phosphine was used as catalyst and the concentration was 1.5wt% of the ESO and acrylic acid. Small amount of hydroquinone was added due to prevention of radical formation. The reaction mixture was stirred at 110℃ for 2 h. After the completion of reaction, the product was diluted in ethyl ether and washed with aqueous $NaHCO_3$ and brine for several times. The oil phase was dried with Na_2SO_4 and concentrated by using a rotary evaporator at 50℃. ^{1}H-NMR spectra of synthesized ESO and AESO were recorded using a 300 MHz NMR spectrometer (Bruker, Ultrashield) at ambient condition (**Figure 2**). The tetramethyl silane (TMS) singlet at 0 ppm was selected as the reference standards. Epoxy group contents of synthesized AESO was 2054 mmol/kg (determined by ASTM D-1652).

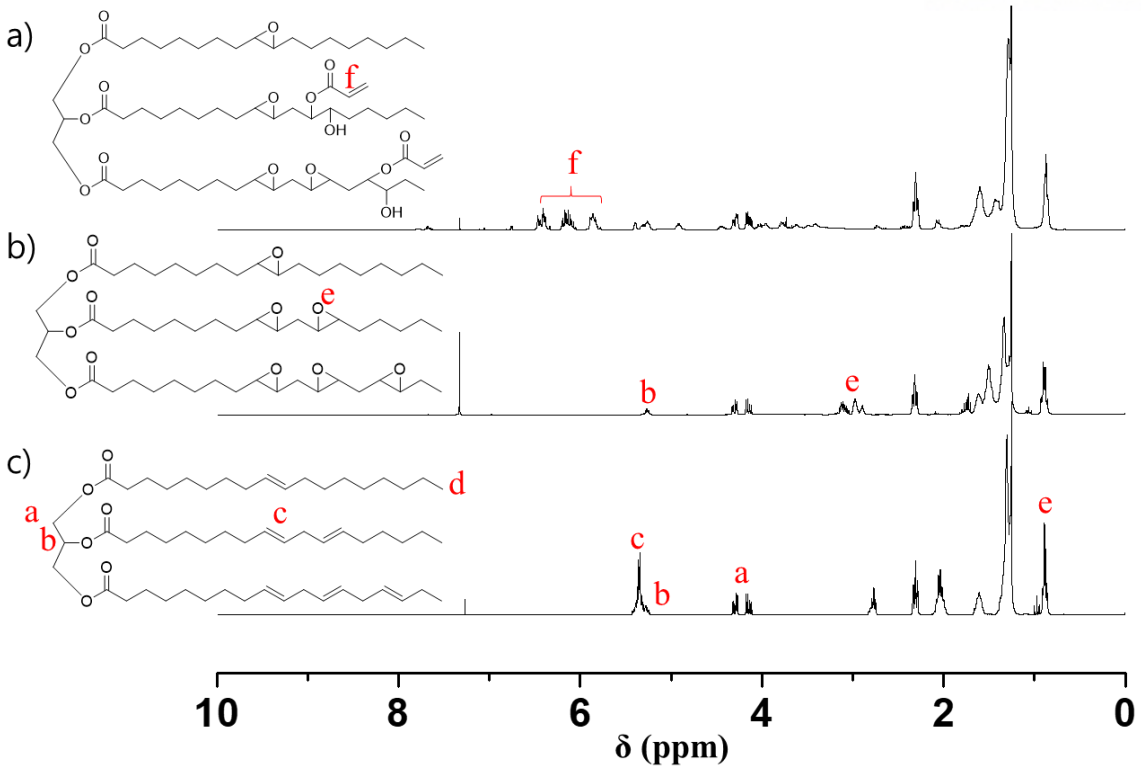

Figure 2. ^{1}H-NMR spectra of (a) acrylated epoxidized soybean oil (AESO), (b) epoxidized soybean oil (ESO) and (c) soybean oil (SO).

4.2.3. Preparation of the AESO-PSAs and PC-PSAs.

The formulations of the AESO-PSAs are presented in detail in **Table 1.** The appropriate quantities of AESO, TETA, HDA, and TBDP were placed in plastic containers and mixed with a spatula at room temperature for 5 minutes. The mixtures were coated with a thickness of 100 μm onto PET films by using a micrometer-adjustable film applicator. The coated PET films were cured at 80°C for 2 hours and attached to a corona-treated PET film by using a 2 kg rubber roller. Competitive epoxy-amine and epoxy-acrylate reaction of AESO with TETA was monitored using FT-IR spectroscopy as shown in Figure 3 (Thermo Fisher Scientific Inc., Nicolet 6700/Nicolet Continuum). The UV-cured PSAs (PC-PSAs) were obtained by UV-curing each AESO-PSA. The power of the UV source used in this experiment is 10.6 W/cm^2. Degree of conversion of the curing reaction was calculated from the characteristic peak intensity ratio of stretching band at 1615 cm^{-1} and 1635 cm^{-1} of C=C group to carbonyl group band at 1712 cm^{-1} using FT-IR spectroscopy **(Figure 4).**

Table 1. Formulations of the ASEO-PSAs.

Polymer Code	AESO (g)	TETA (g)	HDA (g)	TBDP (g)
ASEO-PSA1	100	1.5	0.75	0.75
ASEO-PSA2	100	2.0	0.75	0.75
ASEO-PSA3	100	2.5	0.75	0.75
ASEO-PSA4	100	3.0	0.75	0.75

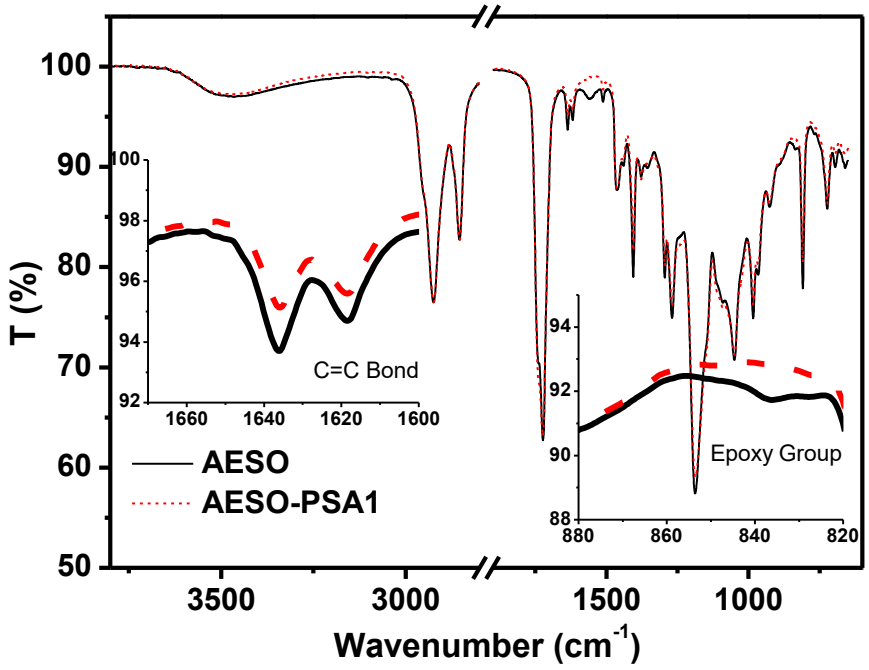

Figure 3. The FT-IR spectra of (a) AESO and (b) AESO-PSA1.

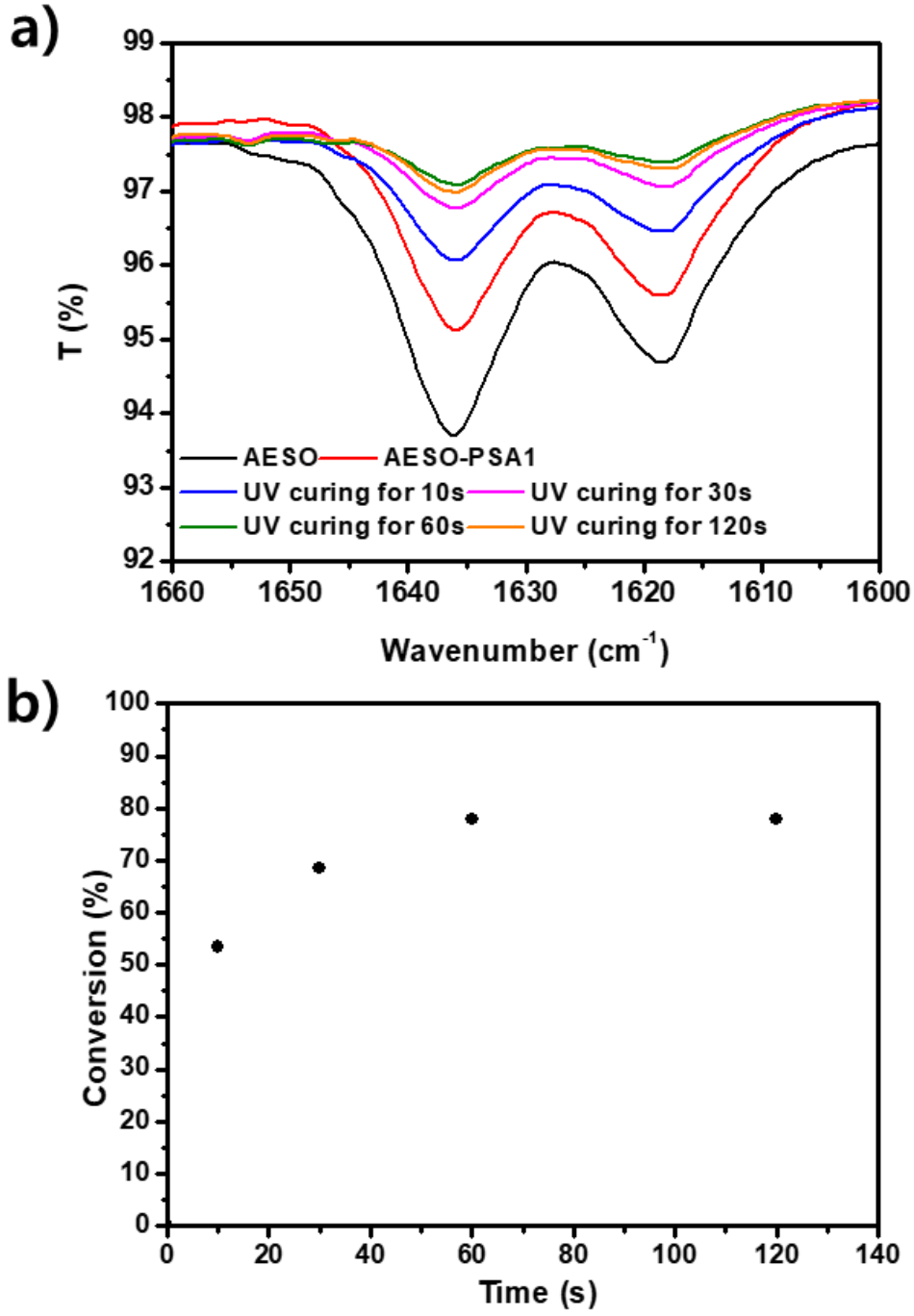

Figure 4. a) Variation in FT-IR C=C band of AESO-PSA1 as a function of UV curing time b) time versus conversion curve of UV curing reaction of AESO-PSA1.

4.2.1. Thermal/UV Curing behaviors of the AESO-PSAs and PC-PSAs.

The crosslinking reactions of the AESO-PSAs and PC-PSAs were characterized with an oscillatory rheometer (Thermo Scientific Inc., MARS Ⅲ) operated at a constant frequency of 1 Hz and a strain of 0.5% by using the small amplitude oscillatory shear (SAOS) mode at 80°C. The samples were placed between parallel plates, i.e., an 8 mm disposable aluminum upper plate and a 20 mm quartz lower plate. The temperature was adjusted by using a controlled test chamber (CTC) and UV light was supplied in a downward direction onto the sample, as shown in **Figure 5.**

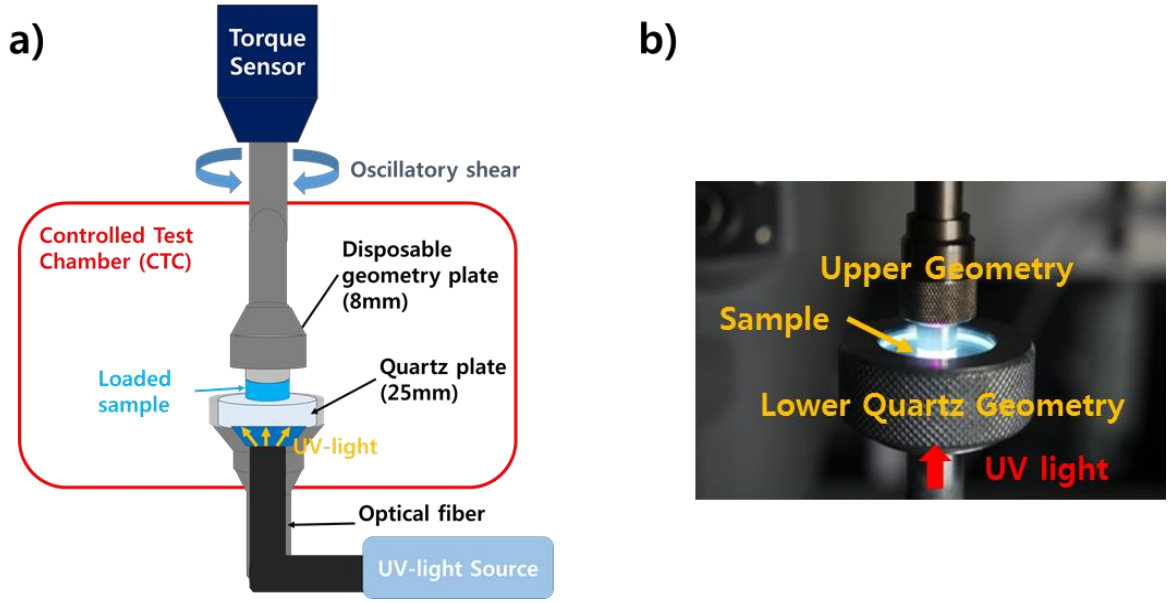

Figure 5. a) Schematic diagram of a photo-curable device in an oscillatory rheometer; b) photograph of UV photo-curing within an oscillatory rheometer.

4.2.5. Material properties of the AESO-PSAs and PC-PSAs.

To evaluate the viscoelastic properties of the AESO-PSAs, an oscillatory rheometer (Thermo Scientific Inc., MARS III) was used in the frequency sweep mode. The PET films of the AESO-PSAs were applied to a stainless steel substrate by using a 2 kg rubber roller. The peel strength was determined after 2.54 cm of the film peeled away from the surface of 305 mm min^{-1}, and the average obtained from at least five tests for each sample is reported. An inverted probe machine with Polyken Probe Tack (PT-1000, ChemInstruments, Inc.) was used to determine the tack strength of each AESO-PSA. The thermal stabilities of the AESO-PSAs and PC-PSAs were determined by performing TGA (TA Instruments, TGA Q500) in the range 25–600°°C at a rate of 10°C/min^{-1}. The glass transition temperatures (T_g) of the crosslinked AESO-PSAs and PC-PSAs were determined with differential scanning calorimetry (DSC) (TA Instruments, DSC Q2000). In the DSC measurements, T_g was determined during the second heating ramp at 10°C/min in the range -60–20°C. The lap shear tests were carried out by using a Universal Testing Machine (UTM) (Instron, model 5982) with constant speed (1.3 mm/min^{-1}) at the cross-head. The AESO-PSAs were positioned (25.4 mm * 12.7 mm) between plastic and iron specimens (25.4 mm * 101.6 mm) as shown in **Figure 6.** The specimens for the lap shear tests were cured thermally and with UV light. To evaluate the gel content, pieces of the AESO-PSAs and PC-PSAs (approximately 100 mg, W_d) were placed in toluene (2 mL) for over 48 hours. The toluene was evaporated and the samples were dried (W_{ex}) in a vacuum oven for 6 hours. The gel content was calculated with the formula (W_{ex}/W_d) * 100%.

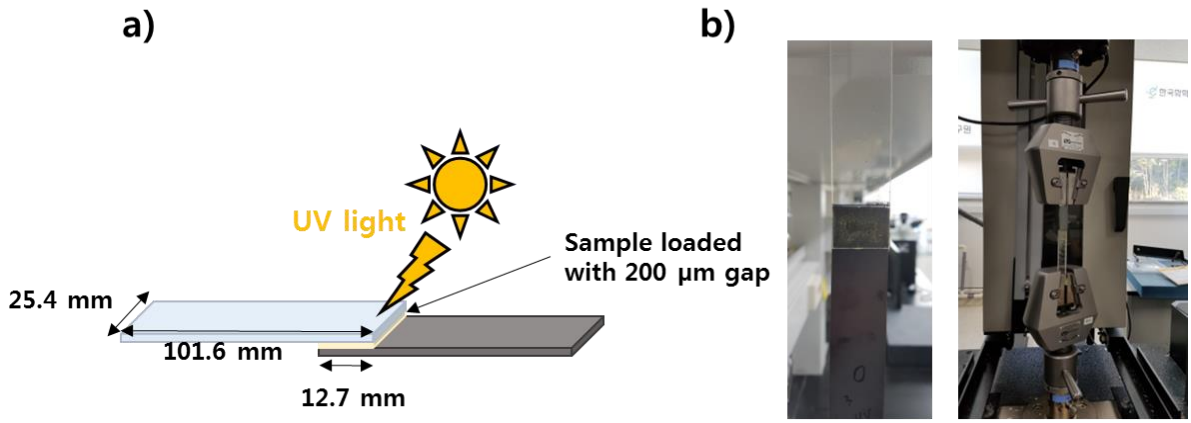

Figure 6. a) Schematic illustration of the lap shear test; b) photographs of a lap shear test specimen in the UTM.

4.2.6. Performances of the UV-Curable Repair Patch systems.

The performance of each UV-curable crack repair patch system was evaluated by applying the patch to the cracked surface of a laboratory scale chemical tank. In this experiment, a circular crack (diameter 1 cm) was generated on the side of the chemical reservoir. The volume of the liquid chemical in the reservoir was 1 L. The fluid pressure (P) and force (F) on the cracked area (A) can be calculated with the following equations:

$$P = P_{atm} + \rho g h \quad \text{(eq. 1)}$$

$$F = PA \quad \text{(eq. 2)}$$

where P_{atm}, ρ, g, and h are the atmospheric pressure, the density of the chemical, gravitational acceleration, and the height of the cracked area in the chemical reservoir, respectively.

The calculated P and F values are approximately 100 kPa and 8 N respectively. The calculations are described in detail in the supporting information (**Figure 7**). Crack repair patches with sizes varying from 2.25 cm^2 to 12.25 cm^2 were applied to the damaged area in the chemical reservoir tank and then cured by using a portable UV source and then a liquid chemical was poured into the chemical reservoir tank. The performances of the crack repair patches were quantified for several liquid chemicals by measuring the maximum leak prevention times.

In order to demonstrate the crack repair patch system, AESO-PSA1 was applied to a cracked chemical reservoir (crack size is approximately 0.01cm^2) filled with a liquid chemical and then cured by using a UV light source.

*Assumptions

1. Steady flow
2. Incompressible flow
3. Frictionless flow
4. Uniform flow at each section
5. Hydrostatic pressure distribution (at each location, pressure increases linearly with depth)

The pressure of dichloromethane on the cracked area can be calculated from assumption 5 as follows:

$$\mathrm{P} = P_{atm} + \rho gh = 101{,}325\ Pa + \frac{1330kg}{m^3} * \frac{9.8m}{s^2} * 0.08\ m = 101{,}937\ Pa$$

$$\mathrm{F} = \mathrm{P}A_{Cracked\ Area} = 101{,}937\ Pa * 2.5 * 10^{-5} * \pi = 8.01\ N$$

The Bernoulli equation was used to calculate the velocity of the flow through the cracked area.

$$\frac{P_1}{\rho} + \frac{V_1^2}{2} + gh_1 = \frac{P_2}{\rho} + \frac{V_2^2}{2} + gh_2$$

$$P_1 = P_{atm} + \rho gh_1 \text{ and } P_2 = P_{atm} + \rho gh_2$$

$$\frac{P_{atm} + \rho gh_1}{\rho} + \frac{V_1^2}{2} = \frac{P_{atm} + \rho gh_2}{\rho} + \frac{V_2^2}{2}$$

$$\frac{V_1^2}{2} + gh_1 = \frac{V_2^2}{2} + gh_2$$

Since $V_1^2 \approx 0, h_2 \approx 0$,

$$V_2 = \sqrt{gh_1} = \sqrt{2 * \frac{9.8m}{s^2} * 0.08m} = 1.25m/s$$

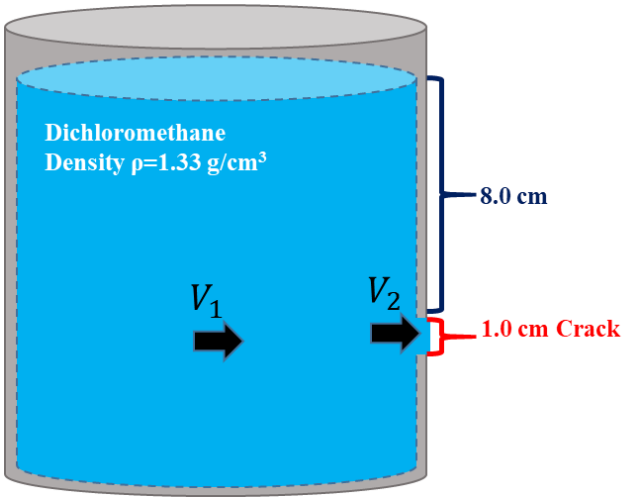

Figure 7. Calculation of the pressure and force on a cracked area due to dichloromethane. The velocity of the flow through the cracked area was estimated with the Bernoulli equation.

4.3. Results and Discussion

4.3.1. Thermal and UV-curing behaviors.

The thermal and UV-curing behaviors of the AESOs were investigated by using an oscillatory rheometer equipped with a CTC and a UV-source. **Figure 8. (a)** shows the thermal curing behaviors of the AESO-PSAs at 80℃. As shown in the plots of the storage modulus (G') versus time, the G' value increases as the epoxy-amine and acrylate-amine reaction progresses, which indicates that the polymers form crosslinked network structures. The progress of the reaction was monitored by the characteristic peak ratio of the intensity of the FT-IR band at 842 cm^{-1} corresponding to epoxy group and 1615 and 1635 cm^{-1} corresponding to C=C group in acrylate moiety to the FT-IR band at 1750 cm^{-1} corresponding to carbonyl group in AESO. It was also found that the rate of the curing reaction and the saturated G' values of the AESO-PSAs increase with increases in their TETA content. The AESO-PSAs with higher TETA contents exhibit a higher storage modulus as well as faster amine-epoxy ring opening and acrylate-amine reactions due to their higher amine group concentrations per unit volume. The UV-curing behaviors of the AESO-PSAs were monitored under UV irradiation at 25℃ (**Figure 8. (b)**). As in the thermal curing experiments, the rapid increases in G' during UV-curing with UV irradiation indicate that the AESO-PSAs form additional crosslinked structures during the UV-radical polymerization of the acrylate moieties. In this case, the rate of curing of the PC-PSAs is almost independent of their TETA contents due to the high UV-crosslinking reaction rate. However, it was found that the saturated G' values of the PC-PSAs decrease with increases in their TETA content. Thus the AESO-PSAs with lower crosslinking densities have a higher polymer chain mobility and thus exhibit higher conversion efficiency in the UV-curing process. The gel content measurement data and the T_g values of the AESO-PSAs also support this trend (**Tables 2, 3**).

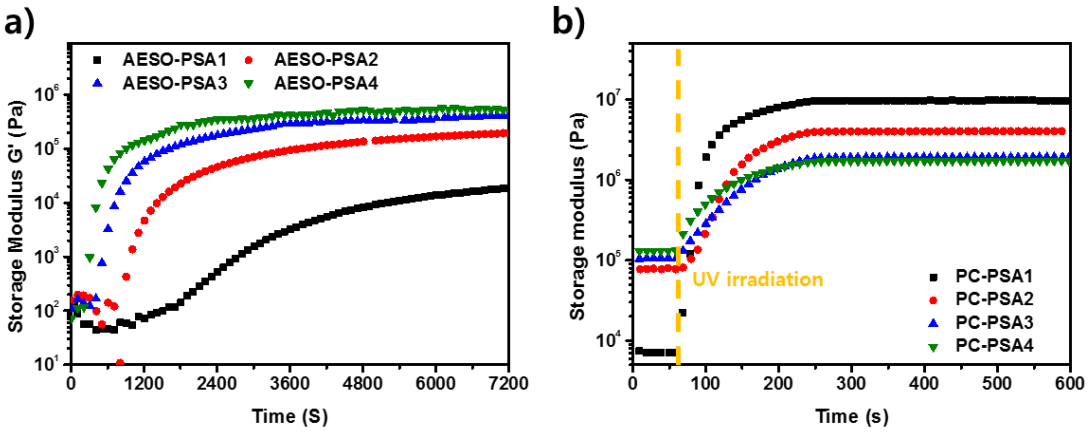

Figure 8. Curing behaviors of the AESOs measured with an oscillatory rheometer: a) epoxy-amine curing behaviors of the AESO-PSAs at 80 ℃ and b) the UV-curing behaviors of the PC-PSAs.

Table 2. Material properties of the AESO-PSAs and PC-PSAs.

Polymer Code	T_d (℃)	T_g (℃)	Gel Contents (%)
ASEO-PSA1	275.8	-29.5	56
ASEO-PSA2	298.3	-27.4	57
ASEO-PSA3	299.7	-25.3	64
ASEO-PSA4	300.0	-25.2	73
PC-PSA1	308.3	-6.4	92
PC-PSA2	305.1	-14.5	91
PC-PSA3	304.9	-17.1	88
PC-PSA4	302.2	-17.4	83

Table 3. Adhesion properties of the PC-PSAs.

Polymer Code	Lap Shear (KPa)	Polymer Code	Lap Shear (KPa)
AESO-PSA1	4.45	**PC-PSA1**	222.4
AESO-PSA2	6.19	**PC-PSA2**	164.15
AESO-PSA3	5.38	**PC-PSA3**	93.9
AESO-PSA4	4.05	**PC-PSA4**	88.15

4.3.2. Thermal properties of the AESO-PSAs and PC-PSAs.

The thermal stabilities of the AESOs were investigated by using TGA (**Figure 9.**). As can be seen in **Figures 9. (a) and (c)**, both the T_d and T_g values of the AESO-PSAs decrease linearly with increases in the TETA content (AESO-PSA1 < AESO-PSA2 < AESO-PSA3 < AESO-PSA4). This trend is attributed to the different crosslinking densities of the different ASEO-PSAs. In general, a polymer network with a higher crosslinking density exhibits a higher T_d value and a higher T_g value. Similarly, both the T_d and T_g values of the PC-PSAs increase after the UV-crosslinking reaction when compared to those of the corresponding ASEO-PSAs (**Figures 9. (b) and (d)**). However, in the case of the PC-PSAs, both T_d and T_g decrease with increases in the TETA content. Thus the crosslinking densities of the PC-PSAs are inversely proportional to their TETA contents.

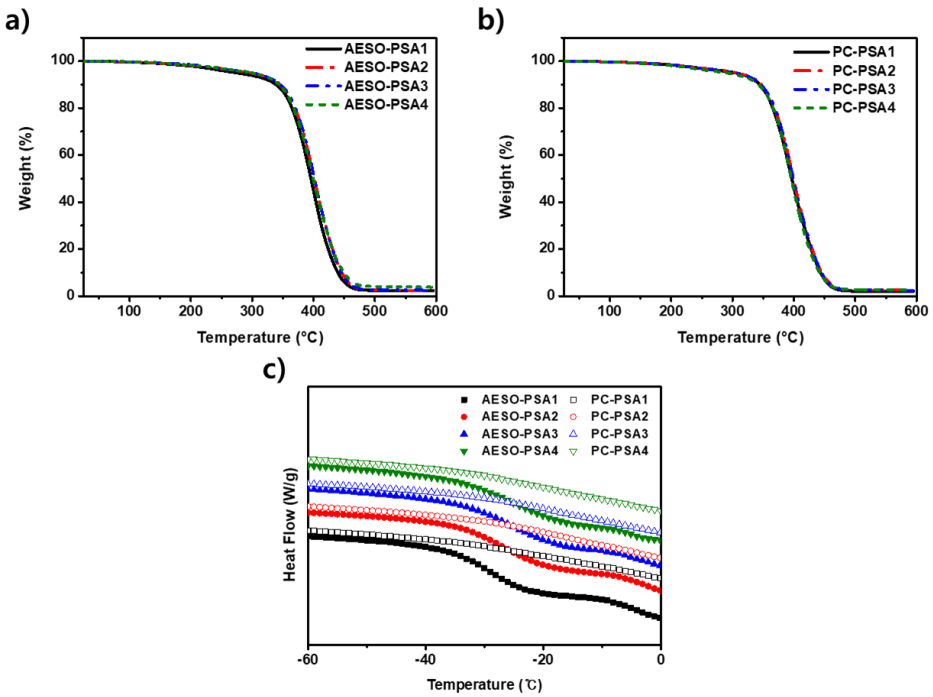

Figure 9. Thermal properties of the AESOs: TGA pyrograms of a) the AESO-PSAs and b) the PC-PSAs, and DSC thermograms of c) the AESO-PSAs and PC-PSAs.

4.3.3. Performances of the AESO-PSAs.

The performances of the AESO-PSAs were characterized by using a peel and probe tack tester. As shown in **Figure 10. (a)**, both the peel and the tack strength of the AESO-PSAs decrease with increases in their crosslinking densities (AESO-PSA1 < AESO-PSA2 < AESO-PSA3 < AESO-PSA4). In general, the performance of a PSA is closely related to its viscoelastic properties. It is known that the ideal PSA requires a low bonding plateau modulus (G' and G'') at low (bonding) frequencies and high energy dissipation (high G") at high (de-bonding) frequencies. We demonstrated with rheology experiments that both the G' and G'' values of the AESO-PSAs increase with increases in the crosslinking density at bonding frequencies, whereas the G'' and tan δ values are inversely proportional to the crosslinking densities of the PSAs at de-bonding frequencies (**Figures 10. (b) - (d)**). AESO-PSA1 has the lowest bonding plateau modulus and the highest energy dissipation at high frequencies and so exhibits the best PSA performance. The trends in these results are in good agreement with the general PSA performance-viscoelastic properties relationship described above.

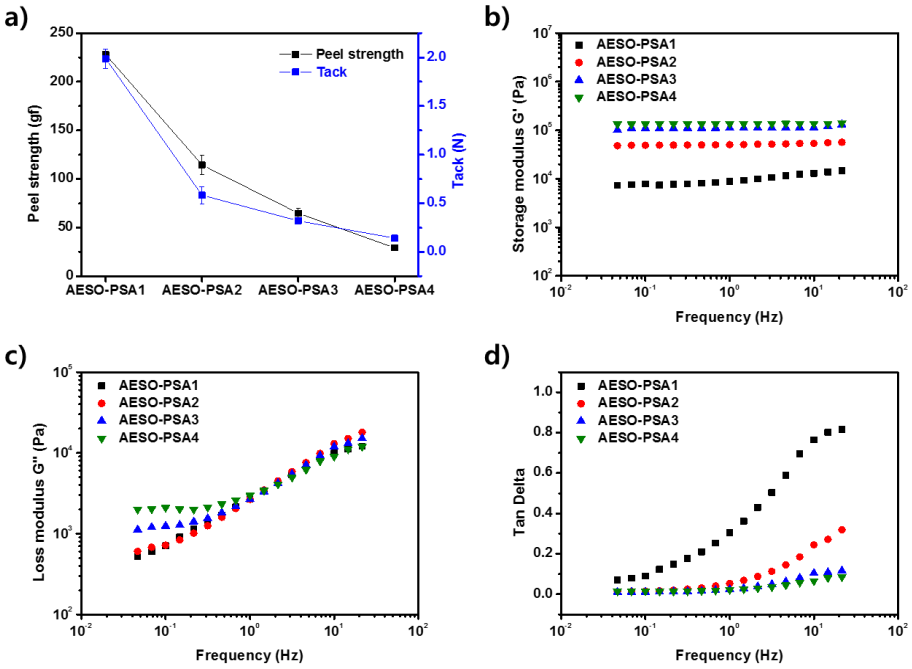

Figure 10. Adhesion properties and viscoelastic responses of the AESO-PSAs: a) peel and tack strengths, b) frequency versus storage modulus plots, c) frequency versus loss modulus plots, and d) frequency versus tan δ plots.

4.3.4. The adhesion properties of the PC-PSAs.

The lap shear strengths of the PC-PSAs were tested within a PE and steel interface by using a UTM. As shown in **Figure 11.** and **Table 3**, the lap shear strength values decrease with increases in the crosslinking density of the AESO-PSAs (AESO-PSA1 < AESO-PSA2 < AESO-PSA3 < AESO-PSA4). An AESO-PSA with a lower crosslinking density enables the conversion of the acrylate moiety to a higher degree as well as a higher rate of diffusion into the steel substrate due to the higher polymer chain mobility. The results of the PSA performance and adhesion property tests confirm that AESO-PSA1 is the most suitable formulation for the UV-curable crack repairing patch system.

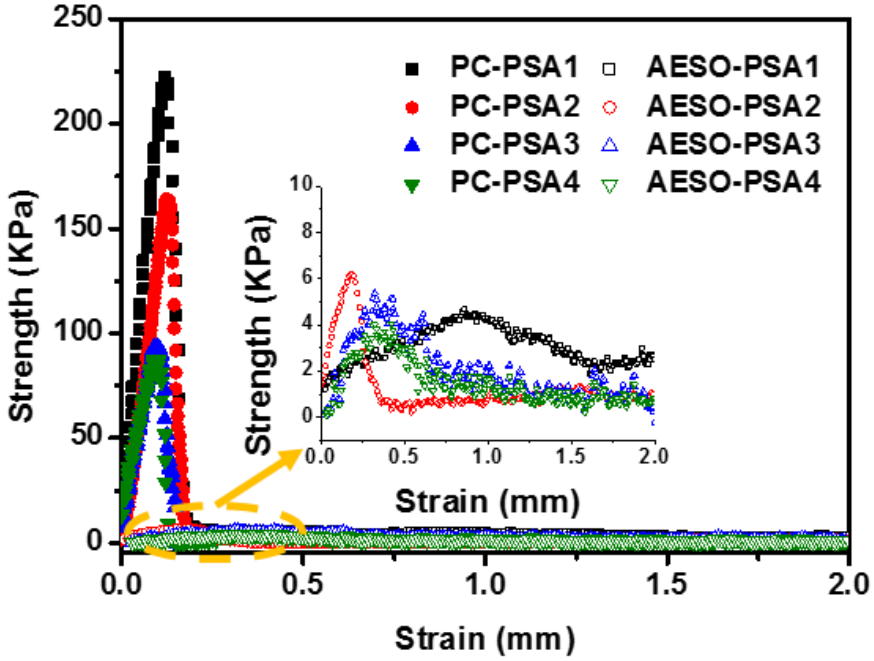

Figure 11. Strength versus strain curves for the PC-PSAs and AESO-PSAs.

4.3.5. Assessment of the UV-curable crack repair patch system.

In order to assess the performance of the UV-curable crack repair patch system, UV-curable crack repair patches based on AESO-PSA1 with a size of 2.5 cm x 2.5 cm were patched onto the cracked surfaces of laboratory scale chemical reservoirs containing various chemicals such as acids, bases, and organic solvents, and then cured under the portable UV source. In this experiment, the mean crack size in the chemical reservoir and the fluid pressure on the cracked area were adjusted to 0.79 cm^2 and 100 kPa respectively. As shown in **Table 4**, the breaching of most chemicals was successfully inhibited for 48 h by patching the crack with the repair patch. However, it was found that the performance of the patch system was inferior for the organic solvents acetone, chloroform, dichloromethane, and diethyl ether. These results can be interpreted in terms of the thermodynamics of the polymer solution.

Table 4. Crack repair performances of AESO-PSA1 and PC-PSA1 (2.5 cm x 2.5 cm).

Chemicals	Hansen Solubility Parameter δ ($MPa^{1/2}$)	Holding Time (s)	
		AESO-PSA1	PC-PSA1
n-Hexane	14.9	> 50,000	> 50,000
Triethyl amine	15.2	> 50,000	> 50,000
Diethyl ether	15.4	623	4380
Dichloromethane	19.0	87	627
Acetone	19.9	329	6156
Chloroform	20.2	73	1423
Acetonitrile	24.4	> 50,000	> 50,000
Ethanol	26.5	> 50,000	> 50,000
Methanol	29.6	> 50,000	> 50,000
Sulfuric acid (10% aq.)	N/A	> 50,000	> 50,000
Hydrochloric acid (10% aq.)	N/A	> 50,000	> 50,000
Sodium hydroxide (10% aq.)	N/A	> 50,000	> 50,000

Thermodynamics requires that the free energy of mixing (ΔG_{mix}) must be zero or negative for a solution process to occur spontaneously.[20] The free energy change for a solution process is given by the equations:

$$\Delta G_{mix} = \Delta H_{mix} - T\Delta S_{mix} \quad \text{(eq. 3)}$$

$$\Delta H_{mix} = \emptyset_p \emptyset_s \, V_m \left(\delta_p - \delta_s\right)^{1/2} \quad \text{(eq. 4)}$$

where ΔG_{mix}, ΔH_{mix}, T, and ΔS_{mix} are the free energy change of mixing, the enthalpy change of mixing, the absolute temperature, and the entropy change of mixing, and $\emptyset_p$, $\emptyset_s$, V_m, δ_p, and δ_s are the volume fractions of the polymer and solvent respectively, the volume of the polymer solution, and the Hansen solubility parameters of the polymer and solvent, respectively.[21]

Equation 4 yields only zero or positive values for ΔH_{mix} and predicts that mixing becomes more favorable as the difference between the volume fractions of the two components decreases, with $\Delta H_{mix} = 0$ when $\delta_p = \delta_s$. Since the Hansen solubility parameter of AESO is approximately 21 $MPa^{1/2}$, which is very similar to those of diethyl ether (15.4 $MPa^{1/2}$), dichloromethane (19.0 $MPa^{1/2}$), acetone (19.9 $MPa^{1/2}$), and chloroform (20.2 $MPa^{1/2}$), these solvents can effectively dissolve or swell the AESO adhesive.[19]

The UV-crosslinked AESO-PC1 patch was found to exhibit a leak repair performance superior to that of the AESO-PSA1 patch due to its higher crosslinking density and adhesion strength. In addition, it was found that the crack repair performances of the AESO-PSA1 and AESO-PC1 patches improve with increases in the patch size from 2.25 to 12.25 cm^2 (**Figure 12.**).

Finally, the repair patches were applied to actual cracks in chemical tanks (**Figure 13.**). In this

case, the fluid pressure value and the crack size were much smaller than in the assessment described above. Both the AESO-PSA1 and AESO-PC1 patches were found to exhibit good crack repair performance but as expected the chemical resistance of the UV-crosslinked AESO-PC1 patch is much higher than that of the AESO-PSA patch.

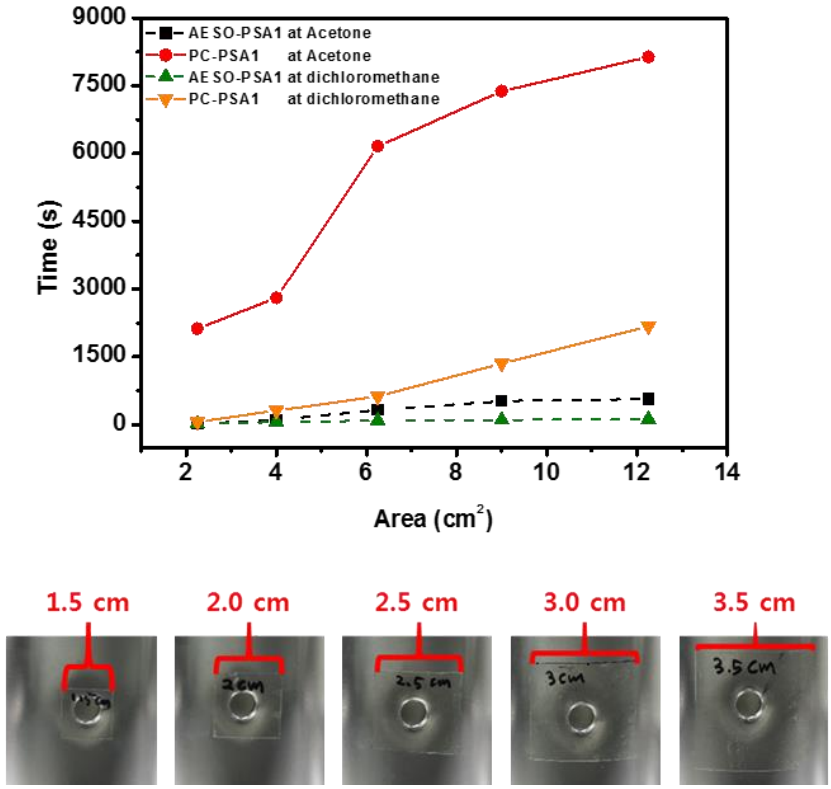

Figure 12. The variation with patch size in crack repair performance.

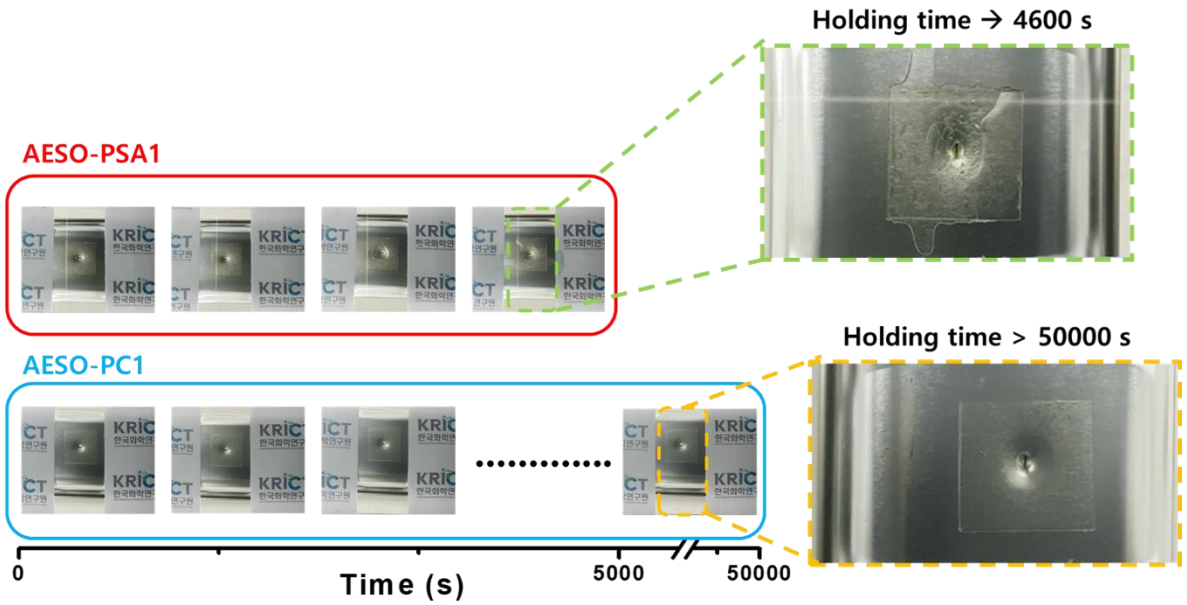

Figure 13. Application of repair patches to cracks in the surface of a laboratory scale chemical tank (contained chemical: chloroform).

4.4. Conclusion

In this study, a novel UV-curable crack repair patch with high chemical resistance and adhesion properties was successfully prepared by employing AESO, TETA, HDA, and TBDP.

The curing behaviors of the AESOs were characterized with an oscillatory rheometer. The rate of curing and the saturated G' values of the AESO-PSAs increase with increases in their TETA content due to the resulting increase in the local concentration of amine groups per unit volume. On the other hand, the saturated G' values of the PC-PSAs decrease with increases in their TETA content because the PC-PSAs with a lower crosslinking density exhibit higher chain mobility during the UV-curing process.

The performances of the AESO-PSAs were assessed by using peel testing and probe tack measurements. It was found that the peel and tack strength of the AESO-PSAs decrease with increases in the TETA content. These results are mainly due to the variation in the G' and G'' values at bonding and de-bonding frequencies. The adhesion properties of the PC-PSAs were characterized by using tensile testing and it was found that their adhesion decreases with increases in the crosslinking density of the AESO-PSAs due to the resulting variation in polymer chain mobility.

Finally, the UV-curable crack repair patch was applied to a cracked area on the surface of a laboratory scale model chemical reservoir to assess its crack repair performance and it was demonstrated that this system is very effective in the prevention of chemical spill accidents caused by the formation of cracks in chemical reservoirs and transfer pipes.

4.5. REFERENCES

[1] K. Lee, H. Kwon, S. Cho, J. Kim, I. Moon, Improvements of safety management system in Korean chemical industry after a large chemical accident, J. Loss Prev. Process Ind. 42 (2016) 6–13. doi:10.1016/j.jlp.2015.08.006.

[2] G. He, L. Zhang, Y. Lu, A.P.J. Mol, Managing major chemical accidents in China: Towards effective risk information, J. Hazard. Mater. 187 (2011) 171–181. doi:10.1016/j.jhazmat.2011.01.017.

[3] D.B. Lytton, Formulations and process for effecting stoppage of leaks of liquid from tanks, pipes and the like, US4195001A, 1980. https://patents.google.com/patent/US4195001/en (accessed July 30, 2018).

[4] T.H. Lee, Y.I. Park, S.M. Noh, J.C. Kim, In-situ visualization of the kinetics of low temperature thiol-epoxy crosslinking reactions by using a pH-responsive epoxy resin, Prog. Org. Coat. 104 (2017) 20–27. doi:10.1016/j.porgcoat.2016.11.007.

[5] T.H. Lee, Y.K. Song, S.H. Park, Y.I. Park, S.M. Noh, J.C. Kim, Dual stimuli responsive self-reporting material for chemical reservoir coating, Appl. Surf. Sci. 434 (2018) 1327–1335. doi:10.1016/j.apsusc.2017.11.219.

[6] EP 3273132 A1 20180124 - FLUID LEAK REPAIR, (n.d.). https://data.epo.org/gpi/EP3273132A1-FLUID-LEAK-REPAIR (accessed July 30, 2018).

[7] Y. Li, X.S. Sun, Synthesis and characterization of acrylic polyols and polymers from soybean oils for pressure-sensitive adhesives, RSC Adv. 5 (2015) 44009–44017. doi:10.1039/C5RA04399A.

[8] D.P. Pfister, Y. Xia, R.C. Larock, Recent Advances in Vegetable Oil-Based Polyurethanes, ChemSusChem. 4 (n.d.) 703–717. doi:10.1002/cssc.201000378.

[9] Facile functionalization of soybean oil by thiol-ene photo-click reaction for the synthesis of polyfunctional acrylate, (n.d.). doi:10.1016/j.porgcoat.2014.01.018.

[10] X. Zhang, W. Xi, S. Huang, K. Long, C.N. Bowman, Wavelength-Selective Sequential Polymer Network Formation Controlled with a Two-Color Responsive Initiation System, Macromolecules. 50 (2017) 5652–5660. doi:10.1021/acs.macromol.7b01117.

[11] K. Dean, W.D. Cook, Effect of Curing Sequence on the Photopolymerization and Thermal Curing Kinetics of Dimethacrylate/Epoxy Interpenetrating Polymer Networks, Macromolecules. 35 (2002) 7942–7954. doi:10.1021/ma020628p.

[12] J.A. Carioscia, J.W. Stansbury, C.N. Bowman, Evaluation and control of thiol–ene/thiol–epoxy hybrid networks, Polymer. 48 (2007) 1526–1532. doi:10.1016/j.polymer.2007.01.044.

[13] D. Guzmán, X. Ramis, X. Fernández-Francos, A. Serra, Preparation of click thiol-ene/thiol-epoxy thermosets by controlled photo/thermal dual curing sequence, RSC Adv. 5 (2015) 101623–101633. doi:10.1039/C5RA22055F.

[14] C. Zhang, T.F. Garrison, S.A. Madbouly, M.R. Kessler, Recent advances in vegetable oil-based polymers and their composites, Prog. Polym. Sci. 71 (2017) 91–143. doi:10.1016/j.progpolymsci.2016.12.009.

[15] A. Li, K. Li, Pressure-Sensitive Adhesives Based on Epoxidized Soybean Oil and Dicarboxylic

Acids, ACS Sustain. Chem. Eng. 2 (2014) 2090–2096. doi:10.1021/sc5003853.

[16] A. Li, K. Li, Pressure-sensitive adhesives based on soybean fatty acids, RSC Adv. 4 (2014) 21521. doi:10.1039/c4ra03557g.

[17] H. Liu, W. Lu, S. Liu, Development of acrylated soybean oil-based UV-curable coatings with high impact strength from low viscosity oligomer, J. Appl. Polym. Sci. 135 (n.d.) 45698. doi:10.1002/app.45698.

[18] S. Ma, Y. Jiang, X. Liu, L. Fan, J. Zhu, Bio-based tetrafunctional crosslink agent from gallic acid and its enhanced soybean oil-based UV-cured coatings with high performance, RSC Adv. 4 (2014) 23036–23042. doi:10.1039/C4RA01311E.

[19] J.S. Choi, W.H. Park, Effect of biodegradable plasticizers on thermal and mechanical properties of poly(3-hydroxybutyrate), Polym. Test. 23 (2004) 455–460. doi:10.1016/j.polymertesting.2003.09.005.

[20] Introduction to Polymers, CRC Press. (2011). https://www.crcpress.com/Introduction-to-Polymers-Third-Edition/Young-Lovell/p/book/9780849339295 (accessed July 30, 2018).

[21] Hansen Solubility Parameters: A User's Handbook, Second Edition, CRC Press. (2007). https://www.crcpress.com/Hansen-Solubility-Parameters-A-Users-Handbook-Second-Edition/Hansen/p/book/9780849372483 (accessed July 30, 2018).

Acknowledgement

학위기간 동안 저를 응원해주신 많은 분들께 이 기회를 통해서 감사의 인사를 전하고자 합니다. 앞으로 사회로 진출하여 그 은혜 있지 않고 열심히 보답하며 살 수 있도록 노력하겠습니다. 학위 중간 중간 고비도 많았고 극복해야 할 순간들도 많았지만 이렇게 학위를 마치고 보니 그 모든 과정들 또한 이제는 추억으로 돌이켜 보곤 합니다. 운 좋게 주변에 좋은 사람들을 많이 만나 이 과정들을 현명하게 극복 할 수 있었습니다.

항상 어떠한 어려움이 있어도 저의 편에서 저를 응원해준 가족 어머니 아버지 정말 큰 감사를 드립니다. 제가 어떠한 말로 표현해도 감사를 표현하기 힘들지만 정말 낳으시고 키워주신 은혜 평생 갚으며 살겠습니다. 그리고 항상 어린아이 생각 하듯이 챙겨주는 누나 내가 말로 잘 표현을 못하지만 항상 고맙게 생각합니다.

석사학위부터 저를 따뜻한 마음과 높은 지식으로 지도해 주신 UNIST 백충기 교수님 정말 감사합니다. 교수님께서 제가 학위 기간 동안 힘들어 할 때 교수님께서 시간을 주시며 기다려 주셔서 정말 감사합니다. 앞으로 사회에 나아가 교수님에게 도움이 되는 제자가 되겠습니다. 박사학위기간 저를 한국화학연구원에서 실험을 할 수 있도록 도와주신 노승만 센터장님 함께한 3년 6개월 간의 시간 잊지 못 할 것 같습니다. 때로는 엄하게 제가 잘못하는 부분을 지적해 주시고 정이 많으셔서 항상 마지막에는 다독여주시고 항상 새로운 도전 하는 것을 도와주셔서 정말 감사합니다. 한국화학연구원 김진철 박사님과 함께 연구 할 수 있어서 영광이었습니다. 제가 부족한 부분이 많아도 항상 격려해 주시고 기다려 주시고 도와주셔서 힘든 과정을 잘 이겨나갈 수 있었습니다. 학문적으로 발전한 모습으로 기대에 부응하도록 하겠습니다. 수업 조교로 인연을 맺어 석사학위 논문과 본 논문 지도를 해주신 UNIST 김소연 교수님 정말 감사합니다. 학위기간 아주 힘들 때 교수님의 따뜻한 말씀들이 정말 많은 도움이 되었습니다. 바쁘신 와중에도 본 논문을 지도하여 주신 UNIST 고현협 교수님과 고려대학교 정현욱 교수님께도 깊은 감사의 말씀을 올립니다.

또한 저의 인생의 멘토이신 최경창 선생님 감사합니다. 울산에 있으면서 자주 찾아 뵙지 못하여 죄송합니다. 그리고 초등학교 때 저를 바른 길로 이끌어주신 류춘희 선생님 감사합니다. 꼭 다시 찾아 뵙겠습니다. 제가 처음 반장을 했던 경신고등학교 2학년 6반 석민 선생님 좋은 추억을 만들어 주셔서 항상 감사합니다. 그리고 오랜 시간 함께한 나의 소중한 친구 성엽이 항상 옆에 든든하게 있어주어 고맙다.

UNIST 대학원생활을 함께 시작하면서 큰 의지가 되었던 동지들 정말 고맙다. 나와 함께 같은 주제를 잠깐 연구한 진성이 빨리 마무리 잘하여 좋은 결과 얻길 바라고 많은 부분 도와주어 고맙다. 동생이지만 인생에 대한 지혜가 있는 수원이 어려울 때 많이 도와주어 고맙다. 4차원의 매력을 가진 승흠이 요즘 너무 사회화 되어서 매력을 잃고 있지만 항상 도와주어 고맙다. 처음 대학원 들어왔을 때 모르는 부분을 많이 알려준 정하와 소담이 정말 고맙다. 정하는 졸업 마무리 잘하고

소담이는 LG화학가서 적응 잘하자 화이팅. 미란, 은정이 남은 학위 마무리 잘하길 바랍니다. 욱중이와 태용이는 함께 이야기 한 시간이 적었지만 연구에 대한 열정 보기 좋았습니다. 마지막으로 저의 대학원생활이 기틀을 만들어주신 김준모 박사님께 감사의 말을 전합니다.

한국화학연구원에서 제가 있는 동안 많은 사람들이 나가고 들어왔습니다. 가장 먼저 4층 실험실에서 함께 실험한 송영규 박사님 정말 감사합니다. 마음으로 많은 의지를 주시고 연구적으로 모범이 되어주셔서 감사합니다. 항상 인자하고 온화한 미소로 따뜻하게 대해주신 남준현 센터장님 은혜 잊지 않겠습니다. 처음 화학연구원에 왔을 때 많은 도움을 주신 박영일 박사님 감사합니다. 인간적인 매력이 넘치는 이상호 박사님 많은 조언 주셔서 감사합니다. PPT 발표의 실력자 성수진 박사님 꼼꼼하고 세심하게 챙겨주셔서 정말 감사합니다. 양현지 박사님 많은 시간 함께하진 못하였지만 행복에너지 정말 좋았습니다. 저와 이야기를 많이 나눠 주신 이규철 박사님 인생의 조언들 정말 감사합니다. 전문연구요원 생활을 함께한 문현씨 그 동안 감사하였습니다. 실험실 초창기 맴버 순천 선희 소영 혜원 기영 정말 잊지 못할 것 같습니다. 그리고 서연 예설 수빈 영진 유진 은별 정은 다해 유림 준의 모두 좋은 결과 있기를 희망합니다. 유변학 실험 관련해서 도움을 준 고려대학교 이동근, 정인조 연구원 감사합니다.

대학교 입학과 동시에 같은 방에 살면서 친해진 친구들 성현 용진 진솔 진수 민 영규 그리고 명준 이름 치만 UNIST방송부를 함께하면서 친해진 창윤이형 호석 종환 상필 영수 영오 재경 상윤 한얼 너희들이 있어서 대학교 생활이 지루하지 않았다. 좋은 친구가 되어주어 항상 감사하고 고맙다.

마지막으로 박사학위 기간 든든한 응원자 항상내편 2019년 10월 19일 아내가 될 박선희 항상 감사하고 사랑합니다.

이제 저의 박사학위 이후 새로운 시작을 앞에 두고 설렘과 두려움을 가지고 사회생활을 시작하고자 합니다. 저의 학위기간 동안 도움을 주신 모든 분들께 이렇게 짧게나마 감사의 인사를 전하고 싶습니다. 다시 한 번 감사합니다.

2019년 7월

이 태 희 올림

■ Publication list

1. Lee, T.-H.; Park, Y.-I.; Noh, S.-M.; Kim, J.-C., "In-situ visualization of the kinetics of low temperature thiol-epoxy crosslinking reactions by using a pH-responsive epoxy resin.", ***Prog. Org. Coat.,*** 2017**,** 104, 20-27

2. Lee, T.-H.; Park, Y.-I.; Lee, S.-H.; Shin, J.-H.; Noh, S.-M.; Kim, J.-C., "A crack repair patch based on acrylated epoxidized soybean oil.", ***Appl. Surf. Sci.,*** 2019**,** 476, 276-282

3. Lee, T.-H.*.; Song, Y.-K.*; Park, S.-H.; Park, Y.-I.; Noh, S.-M.; Kim, J.-C., "Dual Stimuli Responsive Self-reporting Material for Chemical Reservoir Coating.", ***Appl. Surf. Sci.,*** 2018**,** 434, 1327-1335

- ***These authors contributed equally to this work.**

4. Kim, S.-Y.*; **Lee, T.-H.*** ; Park, Y.-I.; Nam, J.-H.; Noh, S.-M.; Kim, J.-C., "Influence of material properties on scratch-healing performance of polyacrylate- graft -polyurethane network that undergo thermally reversible crosslinking", ***Polymer,*** 2017**,** *128*, 135-146.

- ***These authors contributed equally to this work.**

5. Park, S.-H.*; **Lee, T.-H.***; Park, Y.-I.; Noh, S.-M.; Kim, J.-C., "Effect of the n-butyl acrylate/2-ethylhexyl acrylate weight ratio on the performances of waterborne core–shell PSAs.", ***J. Ind. Eng. Chem.,*** 2017**,** 53, 111-118

- ***These authors contributed equally to this work.**

6. Song, Y.-K.; Kim, B.-J.; **Lee, T.-H.**; Kim, J.-C.; Nam, J.-H.; Noh, S.-M.; Park, Y.-I., "Fluorescence Detection of Microcapsule-Type Self-Healing, Based on Aggregation-Induced Emission.", ***Macromol. Rapid Commun.,*** 2017**,** 38, 1600657

7. Sung, S.-J.; Kim, S.-Y.; **Lee, T.-H.**; Favaro, G.; Park, Y.-I.; Lee, S.-H.; Ahn, J.-B.; Noh, S.-M.; Kim, J.-C., "Thermally reversible polymer networks for scratch resistance and scratch healing in automotive clear coats", ***Prog. Org. Coat.,*** 2019**,** 127, 37-44

8. Jung, I.-J.; Kim, B.-J.; Lee, D.-G.; **Lee, T.-H.**; Choi, S.-Y.; Kim, J.-C.; Noh, S.-M.; Park, Y.-I.; Jung, H.-W., "Characteristics of dual-curable blocked isocyanate with thermal radical initiator for low-temperature curing of automotive coatings.", ***Prog. Org. Coat.,*** 2018**,** 125, 160-166

9. Lee, K.-C.; Jeong, S.-B.; Kim, D.-Y.; **Lee, T.-H.**; Kim, S.-C.; Kim, J.-C.; Lee, S.-H.; Noh, S.-M.; Park, Y.-I., "Synthesis and radical polymerization properties of thermal radical initiators based on o-imino-isourea: The effect of the alkyl side chain on the radical initiation temperature.", ***J. Polym. Sci. A***. 2018**,** 56, 1749-1756

10. Song, Y.-K.; Kim, B.-J.; **Lee, T.-H.**; Kim, S.-Y.; Kim, J.-C.; Noh, S.-M.; Park, Y.-I., "Monitoring Fluorescence Colors to Separately Identify Cracks and Healed Cracks in Microcapsule-containing Self-healing Coating.", ***Sens. Actuator B-Chem.,*** 2018**,** 257, 1001-1008

11. Park, J.-I.; Choe, A.-Y.; Kim, M.-S.; Ko, H.-H.; **Lee, T.-H.**; Noh, S.-M.; Kim, J.-C.; Cheong, I.-W., "Water-adaptive and repeatable self-healing polymers bearing bulky urea bonds.", ***Polym. Chem.,*** 2018**,** 9, 11-19

12. Song, Y.-K.; **Lee, T.-H.**; Kim, J.-C.; Lee, K.-C.; Lee, S.-H.; Noh, S.-M.; Park, Y.-I., "Dual Monitoring of Cracking and Healing in Self-healing Coatings using Microcapsules Loaded with Two Fluorescent Dyes.", ***Molecules.,*** 2019**,** 24, 1679

13. Jeong, C.-Y.; **Lee, T.-H.**; Noh, S.-M.; Park, Y.-B., "Real-time in situ monitoring of manufacturing process and CFRP quality by relative resistance change measurement.", ***submitted***

■ Patents

1. "Temporary epoxy restoring composition having hazardous chemical detection function" Korea Patent No. 1017916120000 (2017.10.24)

2. "Oxime carbamate compound as a polymerization initiator and composition containing the same" Korea Patent No. 1018155780000 (2017.12.29)

3. "Thermoreversible self-healable polyacrylate networks using Diels-Alder/Retro Diels-Alder reaction and use thereof" Korea Patent No. 1019141870000 (2018.10.26).